applied sciences

# The State of the Art of Thermo-Chemical Heat Storage

Edited by
Salvatore Vasta

Printed Edition of the Special Issue Published in *Applied Sciences*

www.mdpi.com/journal/applsci

MDPI

# The State of the Art of Thermo-Chemical Heat Storage

# The State of the Art of Thermo-Chemical Heat Storage

Editor

**Salvatore Vasta**

MDPI • Basel • Beijing • Wuhan • Barcelona • Belgrade • Manchester • Tokyo • Cluj • Tianjin

*Editor*
Salvatore Vasta
Consiglio Nazionale delle Ricerche (CNR)
Istituto di Tecnologie Avanzate per l'Energia "NicolaGiordano" (ITAE)
Italy

*Editorial Office*
MDPI
St. Alban-Anlage 66
4052 Basel, Switzerland

This is a reprint of articles from the Special Issue published online in the open access journal *Applied Sciences* (ISSN 2076-3417) (available at: https://www.mdpi.com/journal/applsci/special_issues/Thermo-Chemical_Heat_Storage).

For citation purposes, cite each article independently as indicated on the article page online and as indicated below:

LastName, A.A.; LastName, B.B.; LastName, C.C. Article Title. *Journal Name* **Year**, *Volume Number*, Page Range.

**ISBN 978-3-0365-1373-7 (Hbk)**
**ISBN 978-3-0365-1374-4 (PDF)**

Cover image courtesy of Salvatore Vasta.

# Contents

# About the Editor

**Salvatore Vasta** was born in Catania (Italy) on March 2, 1976. He studied Mechanical Engineering (Energy branch) at the University of Catania and graduated in 2001. He completed his PhD in Materials and Chemical Engineering at the University of Messina in 2011. He achieved a National Academic Qualification as an Associate Professor, sector 09/C2—Engineering physics and Nuclear Engineering, in 2013 and 2019 (the latter is valid from 09/09/2019 to 09/09/2028). He joined as a fellow researcher at the Italian National Council of Research—Institute for Advanced Energy Technologies (CNR-ITAE)—Messina in 2001. Since 2011, he has been a Full Researcher at CNR ITAE, carrying out research and project development and management in the field of energy technologies, with special regard to thermally driven heat pumps, solar cooling and heat storage systems. Since 2016, he has been leading the research group on thermal technologies at CNR-ITAE. Within his activity, he has developed extensive knowledge about advanced systems for energy production and use, renewable sources, trigeneration systems, alternative systems for the production of cold, both for mobile as well as stationary applications. The skills acquired allowed him to hold positions of responsibility within research projects in the fields of thermally driven systems, thermal energy storage, renewables and trigeneration. Dr. Salvatore Vasta is regularly publishing in peer-reviewed scientific journals, contributing to books and various other publications. Specifically, he is the author of four book chapters, about 80 papers on scientific journals and conference proceedings and about 100 technical reports. About 50 papers are indexed in the Scopus database, with 1100 citations and a H-Index of 18. Dr. Salvatore Vasta has been reviewing numerous papers and articles for international journals and he is a member of the editorial staff of international journals in the field of energy and renewables. As part of his research activities, he is also involved in the supervision of students at different levels (PhD, MSc, BSc), and lectures at CNR-ITAE and University of Messina. In 2019, in Prague, Czech Republic, he received the best paper award from the International Society for Terrain Vehicle Systems (ISTVS), in recognition of his exceptional research paper titled: "An Innovative Prototype of Adsorption Chiller for Air Conditioning for Industrial and OFF-ROAD vehicles". In 2007, in Kyoto, Japan, he won the Best Poster Award at IMPRES—International Symposium on Innovative Materials for Processes in Energy Systems, for the poster titled "Performance of a novel Functional Adsorbent Material for automotive adsorption air conditioning". He regularly presents his research activity at international conferences and meetings. In 2018, he held a keynote lecture as an invited speaker in Stockholm, Sweden, at European Advanced Energy Materials and Technology Congress, AEMC-2018, with a speech titled "Adsorption Heat Storage: state of the art and future perspectives". In 2017, he held a keynote lecture as an invited speaker in Doha, Qatar, at SUSTAINABILITY SUMMIT 2017, on behalf of Task 53 of IEA/SHC, addressing a presentation on the "Solar Cooling: Worldwide Overview and New Technological Opportunities". In 2009, he was invited as a speaker at 3rd European Workshop MOBILE AIR CONDITIONING, VEHICLE THERMAL SYSTEMS AND AUXILIARIES, held in Torino, presenting the work titled "An innovative prototype of adsorption chiller for mobile air conditioning". He has been the scientific coordinator of several research projects, including H2020 project contracts with private national and international companies. He is currently leading specific subtasks within his participation to the TASK 65, "Solar cooling for sun-belt regions" and ANNEX 36, "Carnot Batteries" of SHC and ECES programs of IEA. He participated as expert within the TASK 48, "Quality assurance and support measures for solar Cooling", TASK53, "New Generation Solar Cooling & Heating Systems" and ANNEX 30,

"TES for Energy Management and CO2 mitigation" of SHC and ECES programs of IEA. As a nominated expert of the Department of Engineering, ICT and Technologies for Energy and Transport (DIITET) of the Italian National Council of Research (CNR), he participated (2011–2014) in the Joint Programme Energy Storage of European Energy Research Alliance (EERA), and since 2020, he has been coordinating Sub-Programme 3, Thermal Energy Storage.

applied sciences

MDPI

*Editorial*

# Special Issue: The State of the Art of Thermochemical Heat Storage

**Salvatore Vasta**

Istituto di Tecnologie Avanzate per l'Energia "Nicola Giordano", (ITAE-CNR), Via S. Lucia Sopra Contesse n 5, 98126 Messina, Italy; salvatore.vasta@itae.cnr.it

Nowadays, thermal energy storage (TES) is gaining a crucial role in the development of highly efficient thermal energy systems [1]. This topic is stimulating a growing interest in the scientific community, in many cases by borrowing and using, in a new and profitable way, the research results obtained in the field of heat pumps and thermally driven systems [2,3]. The proper use of TES systems can facilitate the effective exploitation of renewable energies, allowing the mismatch between energy production and demand for discontinuous energy sources and/or variable loads to be overcome. Moreover, special classes of TES systems, based on sorption or chemical reactions, can enable the long-term storage of renewable heat. The thermochemical technology is based on a reversible reaction occurring between two components, and it is associated with higher amounts of energy stored with respect to systems based on sensible heat [4]. Furthermore, it can effectively support the operation and integration of renewables in local smart grids. To prove this interesting feature, in [5] the authors reviewed the state of the art of theoretical, experimental and numerical studies available in the literature on thermochemical thermal energy storage systems and their use in power-to-heat applications, with a focus on applications with renewable energy sources to serve energy grids. The authors highlighted the advantages of the technology: flexibility, load management, power quality, continuous power supply and enhanced use of variable renewable energy sources. Such features are considered crucial elements to increase the commercial profitability of these storage systems. Eventually the authors introduced specific challenges, i.e., life span and stability of storage material, and high cost of power-to-heat/thermochemical systems, as aspects to increase the technology readiness level.

Thermochemical TES systems, especially those based on sorption processes, can allow the design and implementation of unprecedented solutions for mobile applications. In [6] we demonstrated, through an experimental activity, the feasibility of a compact system for cold storage for mobile commercial applications. In our work, we described the realization and testing of two different types of cold storage based on two innovative adsorbent reactors: a pelletized adsorber filled with commercial FAM Z02 zeolite, and a composite adsorber based on an aluminum porous structure and a SAPO-34 coating. The application of the specific testing procedure allowed the characterization of the prototypes under cold storage mode for mobile refrigeration purposes. Results showed that the prototypes can store up to 580 Wh, with an average power during the discharging phase that ranges from 200 to 820 W and an energy efficiency of 0.3, thus revealing promising opportunities for future further developments.

However, such future developments must be supported by proper research carried out at material and system levels. For instance, solving issues related to adsorbent material or the investigation of new classes of zeolites can support research on more efficient, compact and lightweight sorption TES. To this aim, the authors of [7] proposed a novel silicone–SAPO34 composite material obtained through a mold foaming process activated by a dehydrogenative coupling reaction between siloxane compounds, for application in adsorption TES systems. A series of analyses and measurements of the mechanical properties demonstrated quite a homogeneous open-cell structure and good structural stability of



**Citation:** Vasta, S. Special Issue: The State of the Art of Thermochemical Heat Storage. *Appl. Sci.* **2021**, *11*, 1956. https://doi.org/10.3390/app11041956

Received: 11 February 2021
Accepted: 19 February 2021
Published: 23 February 2021

the foam. Moreover, the authors demonstrated that the presence of the polymeric fraction does not affect the adsorption capacity of the composite adsorbent. Finally, the authors compared the properties of the foam with those of other adsorbent materials, confirming its possible use in thermal energy storage systems.

Research at the system level provides useful information about achievable performance by integrating adsorption TES in real contexts, such as buildings and solar systems for domestic or residential purposes.

The authors of [8] investigated the theoretical limits of sorption TES, first facing the classification of thermochemical heat storages, then studying their thermodynamics. They observed that the reaction enthalpy value only varies slightly for one mole of water, thus deriving the following conclusions on the energy efficiency of closed and open TES: (i) the energy required for evaporation of water is, at least, 65% of the available energy of the reaction; (ii) the maximum theoretical energy efficiency of the system is about 1.8. Based on those results, they calculated that a perfect thermochemical heat storage system would store up to 12 times more energy compared with conventional water storage with a temperature difference of 50 °C, thus confirming that this solution is definitely competitive.

In [9], the authors presented a numerical study on the performance of a solar domestic sorption TES module operating in seven different world locations. The authors optimized the TES configuration for the Portuguese climate and then calculated its performance by varying latitude, operating conditions and solar collector tilt angle. They proved the effectiveness of the system by implementing a dynamical model and numerical simulations and by using the reduction in the annual energy consumption of a backup heater as a benchmark. The results showed that the best performances were obtained in locations where winter and summer are clearly defined, especially locations where winters are colder, and with the inclination angles of solar collectors being larger than the local latitude, except for locations with low latitudes, where the inclination angles of solar collectors are not so relevant to the system performance.

Finally, in [10] the authors proposed a novel adsorption TES system based on water and zeolite 13X for industrial applications. Their unconventional scheme was conceived so that steam production and condensation, during adsorption and desorption processes, occur in the same vacuum reactor, where the zeolite is heated and cooled. They also attempted to preliminarily assess the energy performance using numerical simulations and experiments. To this aim, they constructed a reduced-scale prototype: the limited experimental campaign produced data for the validation of the simplified model of the adsorption/desorption processes. However, the experimental campaign and the simulative activities carried out by the authors highlighted some critical issues of their system, thus indicating a lack of a suitable preliminary experimental activity, and a deep comprehension of the phenomena involved.

**Funding:** This research received no external funding.

**Institutional Review Board Statement:** Not applicable.

**Informed Consent Statement:** Not applicable.

**Conflicts of Interest:** The authors declare no conflict of interest.

## References

1. Borri, E.; Zsembinszki, G.; Cabeza, L.F. Recent developments of thermal energy storage applications in the built environment: A bibliometric analysis and systematic review. *Appl. Therm. Eng.* **2021**, 116666. [CrossRef]
2. Freni, A.; Maggio, G.; Vasta, S.; Santori, G.; Polonara, F.; Restuccia, G. Optimization of a solar-powered adsorptive ice-maker by a mathematical method. *Sol. Energy* **2008**. [CrossRef]
3. Palomba, V.; Dawoud, B.; Sapienza, A.; Vasta, S.; Frazzica, A. On the impact of different management strategies on the performance of a two-bed activated carbon/ethanol refrigerator: An experimental study. *Energy Convers. Manag.* **2017**, *142*, 322–333. [CrossRef]
4. Zhang, Z.; Wang, J.; Feng, X.; Chang, L.; Chen, Y.; Wang, X. The solutions to electric vehicle air conditioning systems: A review. *Renew. Sustain. Energy Rev.* **2018**, *91*, 443–463. [CrossRef]

5. Airò Farulla, G.; Cellura, M.; Guarino, F.; Ferraro, M. A Review of Thermochemical Energy Storage Systems for Power Grid Support. *Appl. Sci.* **2020**, *10*, 3142. [CrossRef]
6. Vasta, S.; Palomba, V.; La Rosa, D.; Bonanno, A. Adsorption Cold Storage for Mobile Applications. *Appl. Sci.* **2020**, *10*, 2044. [CrossRef]
7. Calabrese, L.; De Antonellis, S.; Vasta, S.; Brancato, V.; Freni, A. Modified Silicone-SAPO34 Composite Materials for Adsorption Thermal Energy Storage Systems. *Appl. Sci.* **2020**, *10*, 8715. [CrossRef]
8. Kuznik, F.; Johannes, K. Thermodynamic Efficiency of Water Vapor/Solid Chemical Sorption Heat Storage for Buildings: Theoretical Limits and Integration Considerations. *Appl. Sci.* **2020**, *10*, 489. [CrossRef]
9. Fernandes, M.S.; Costa, V.A.F.; Brites, G.J.V.N.; Gaspar, A.R.; Costa, J.J. Performance Analysis of a Solar DHW System with Adsorption Module Operating in Different World Locations. *Appl. Sci.* **2019**, *9*, 5480. [CrossRef]
10. di Palo, M.; Sabatelli, V.; Buzzi, F.; Gabbrielli, R. Experimental and Numerical Assessment of a Novel All-In-One Adsorption Thermal Storage with Zeolite for Thermal Solar Applications. *Appl. Sci.* **2020**, *10*, 8517. [CrossRef]

applied sciences

MDPI

*Review*

# A Review of Thermochemical Energy Storage Systems for Power Grid Support

**Girolama Airò Farulla [1,*], Maurizio Cellura [1,2], Francesco Guarino [1] and Marco Ferraro [2]**

[1] Dipartimento di Ingegneria, Università degli Studi di Palermo, Viale delle Scienze Ed.9, 90128 Palermo, Italy; maurizio.cellura@unipa.it (M.C.); francesco.guarino@unipa.it (F.G.)

[2] Consiglio Nazionale delle Ricerche, Istituto di Tecnologie Avanzate per l'Energia "Nicola Giordano", via S. Lucia sopra Contesse 5, 98126 Messina, Italy; marco.ferraro@itae.cnr.it

* Correspondence: girolama.airofarulla@unipa.it

Received: 26 March 2020; Accepted: 17 April 2020; Published: 30 April 2020

**Abstract:** Power systems in the future are expected to be characterized by an increasing penetration of renewable energy sources systems. To achieve the ambitious goals of the "clean energy transition", energy storage is a key factor, needed in power system design and operation as well as power-to-heat, allowing more flexibility linking the power networks and the heating/cooling demands. Thermochemical systems coupled to power-to-heat are receiving an increasing attention due to their better performance in comparison with sensible and latent heat storage technologies, in particular, in terms of storage time dynamics and energy density. In this work, a comprehensive review of the state of art of theoretical, experimental and numerical studies available in literature on thermochemical thermal energy storage systems and their use in power-to-heat applications is presented with a focus on applications with renewable energy sources. The paper shows that a series of advantages such as additional flexibility, load management, power quality, continuous power supply and a better use of variable renewable energy sources could be crucial elements to increase the commercial profitability of these storage systems. Moreover, specific challenges, i.e., life span and stability of storage material and high cost of power-to-heat/thermochemical systems must be taken in consideration to increase the technology readiness level of this emerging concept of energy systems integration.

**Keywords:** thermochemical storage; sorption heat storage; power-to-heat; power grid support

## 1. Introduction

Decarbonization of the power sector, increase of energy efficiency and energy security are the major focus of several policies to achieve ambitious climate targets in the next years [1,2]. In the evolution of the energy systems, renewable energy sources (RES) play a major role towards the achievement of environmental sustainability [3–5]. Due to their stochastic nature, however, renewable energies are not programmable so their energy generation is usually not adjusted in order to match electricity demands [6,7]. To guarantee the stability of the power grids, the instant balance of temporal and spatial mismatch between generation and loads can be achieved introducing flexible elements in the power networks [8–13]. Flexibility is defined as the capability to balance rapid changes in power generation according to Bertsch et al. [14] or variation and uncertainty in net load according to Denholm et al. [15]. Several definitions of flexibility can be found in the literature [15–18].

Power-to-heat (PtH), based on the conversion of electricity into heat and its reverse process Heat-to-Power (HtP), are well recognized processes among the most mature demand-side management (DSM) options [19–21].

These techniques are particularly promising to provide renewable energy integration, power grid flexibility [12,13,22,23] and power sector decarbonization contributing to a better utilization of existing assets supporting the RES penetration into the electricity supply mix [24–29].

Thermal energy storage systems (TESs) can be effective in improving the mismatch between energy generation and use in terms of time, temperature, power or site leading to an increase of the overall efficiency and reliability [30–34]. Reduced investment and running costs, lower pollution and less greenhouse gases (GHG) emissions are some of the advantages connected to the use of these technologies [35,36] including: sensible, latent and thermochemical storage [37–41].

Coupling thermal energy storage to a PtH technology to provide flexibility to the power system is a promising option of the demand-side management strategies currently investigated [42,43]. In particular, turning surplus of variable renewable electricity (VRE) into heat to be stored as thermal energy offers a significant additional flexibility with a great potential in stabilizing the grid voltage [42,44]. In particular, during off-peak times, heating or cooling can be generated by thermal energy and then used during peak-hours flattening the customer's load profile [45]. In this way, customers can have a more efficient system and also be cost-efficient. They can take advantage of different electricity prices during peak and off-peak hours and for utilities that can spread the demand over the whole day [46,47].

Several studies examine the coupling of thermal storage with power-to-heat systems (PtHs) for several purposes, e.g., buffering, heating and cooling, transport of residual heat [48–50]. In general, small-scale PtH and TES applications can be applied in the residential and commercial sectors while large scale are mainly focus on industrial applications such as district heating grids [51,52].

Storage devices have great advantages not only in terms of flexibility of the entire power system [53,54] but also in terms of economic profitability with higher efficiency and cost effectiveness of the power grid as shown in the studies of Christidis et al. [55] and Jamshid et al. [56]. In a recent study (2020) Meroueh and Chen [57] provided a detailed analysis on the potential from TESs to provide a cost-effective solution for grid level integration in the near term for renewable-based plants. Several studies show the potential of heat pumps and thermal energy storages in terms of load shifting, energy consumption and increasing self-sufficiency [58–62].

This work is focused on thermochemical thermal energy storage (TCTES) systems coupled with PtH technologies. In particular, the aim is to provide a comprehensive review on the state of art of thermochemical thermal energy storage systems (TCTESs) and their applications in PtH technologies, including theoretical, experimental and numerical studies. Recent advancements and their potential perspectives will be discussed.

This review is structured as follows. In Section 2 a classification of storage system is reported. Section 3 is a review of the state of art of both sorption and chemical reaction TCES processes and the related main operation processes. Section 4 includes a general description of PtH technologies and an analysis of recent case studies on the application of TCTES systems. Section 5 presents the conclusions of this paper.

*Power-to-Heat Technologies: Classification*

Power-to-heat (PtH) is the classification including all devices that perform the conversion of electricity into heat. It is one of the most relevant flexibility options of the DSM [63,64]. With the aim to ensure the integration of the renewables, PtH technologies (PtHs) are considered crucial sources of system flexibility [65]. PtHs contribute to both a better utilization of existing assets and use of temporary renewable surplus generation [65]. When there is an excess of generation, electricity is converted into heat, in this way, additional power in the situations of increased load, is provided contributing, in the same time, to peak shaving, load shifting and energy conservation [66]. Turning surplus of electricity into heat, including thermal energy storage, offers a significant additional flexibility with a great potential in stabilizing the power grid [67,68]. The conversion into thermal energy can be performed through centralized and decentralized options. According to Olsthoorn et al. [69] in the centralized option the electricity is converted into heat at a location far from the point of actual heat demand. By

district heating systems (DHS) heat is distributed through pipelines to its use. In contrast, according to Lund et al. [70] in the decentralized approach the conversion is in a point right or very close the location of heat demand. Heat is distributed without districting networks. A schematic example of the power-to-heat concept is shown in Figure 1:

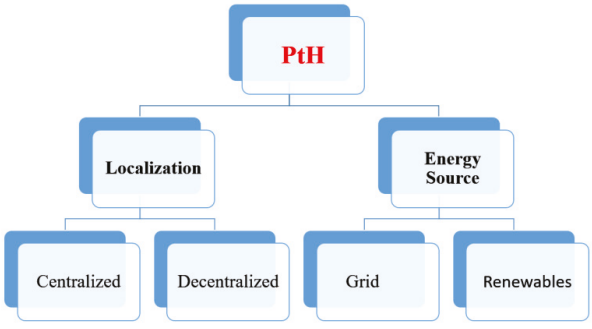


**Figure 1.** Schematic concept of power-to-heat technologies.

DHS are considered particularly promising due to several advantages in energy production, distribution and consumption, especially for space heating applications [71,72]. In particular, the systems using RES have the advantage that renewable technologies can be placed on the energy supplier side in the actual distribution network or be installed on individual buildings [73–75]. In literature, district heating networks are commonly described as one of the most effective solution towards a low-carbon feature [76–81]. Lund et al. [12] in a review of nearly four hundred studies on energy flexibility showed that the interaction between the electricity and district heating sectors is a promising option for increasing energy system flexibility. Heat pumps (HPs) and resistive heaters are the main centralized technologies to draw electricity from the grid to generate heat to be connected to the thermal storage [73].

According to Lund et al. [70] in the decentralized approach the conversion occurs at a site very close to the location of heat demand without networks, grids and piping. The decentralized technologies have several advantages in energy production, distribution and consumption, in particular, providing a sustainable, economical and future-proof solution for heating large spaces [82,83]. A common classification of the decentralized options is among technologies combined with thermal energy, referred as thermal energy storage coupled heating, and technologies without energy storage, referred as direct heating [26]. Heat pumps, resistive boilers, smart electric thermal storage, fans, radiators are examples of the more widely used decentralized power-to-heat technologies [63,84–87]. Electric boilers are the cheapest alternative due to their low investment costs and can be switched on and off at low cost [88]. HPs enable flexibility in smart grid operations [59,85,89]. However, HPs usually function as a base load technology due to their higher efficiencies [90–92]. To further reduce energy use during operation, waste heat from industrial processes or renewable heat sources can be used as heat source with the advantage that they are not dependent from weather conditions and temperature fluctuations, like for example solar and ground sources. In this way heat generation is more stable and better suited as input for HPs [93,94].

HPs used for power-to-heat applications are electrically driven because electricity is used to lift low exergetic heat to a higher temperature and consequently higher exergy level by running a vapor compression cycle [89,95,96]. Electricity renewable is an option to reduce the use of fossil fuel [97,98]. During periods of low demand and high renewable energy generation, the excess of electricity can be converted into heat and stored in TESs [99]. In contrast, the stored energy is released when demand is high and renewable power production is low [100–102]. In this way, HPs contribute to peak shaving, load shifting and energy conservation with benefits not only to the decarbonizing of

the heating sector but also in the improving the capacity utilization of renewable power generation infrastructures [87,103]. In literature several examples of heat pumps coupled to TES systems, mainly sensible storage systems, are proposed [104–108]. These devices can both provide flexibility to the power system and increase the use of electricity from renewables plants [108–110]. The capacity of the thermal storage is limited by the maximum condenser temperature of the heat pump coupled. Thus, the maximum state of charge is attained when a predefined temperature in the storage is reached [87].

## 2. Classification of Thermal Storage Systems

Storage technologies can be classified with respect to underlining heat storage principle into: sensible, latent and thermochemical [82,111].

Sensible thermal energy storage (STES) is based on storing thermal energy by cooling or heating of a liquid/solid storage medium. Sensible heat determines a temperature linear change (increase or decrease) in the thermal storage material, without changing its chemical composition or phase. Sensible heat $Q_s$ depends on the temperature change and the specific heat capacity of the storage material. The amount of energy stored (J) is as followed (1):

$$Q_s = mc_p\Delta T \quad (1)$$

where:

- $m$ is the mass of the storage medium (kg);
- $c_p$ is the heat capacity of the storage medium (J/(kg K));
- $\Delta T$ is the temperature difference (°C).

It is important for sensible heat storage systems to use a heat storage material having high specific heat, good thermal conductivity, long-term stability under thermal cycling, compatibility with its containment, recyclability, a low $CO_2$ footprint and low cost [112]. Sensible heat storage is most widely used in building applications [30].

Latent thermal energy storage (LTES) is based on storing heat into a storage medium undergoing a phase transition [113]. Thermal storage materials store their latent heat during phase change from solid to liquid. The latent heat is stored without a temperature change. The amount of energy stored (J) is as followed (2):

$$Q_l = m\Delta h \quad (2)$$

where:

- $\Delta h$ is the melting or phase change enthalpy (J/kg).

Micro-encapsulated paraffin based phase change materials PCMs or water-based ice-storage are among methods most suitable can be used [114].

Thermochemical or sorption thermal energy storage (TCTES) recovers the reaction enthalpy involved in a reversible chemical/adsorption reaction [115]. According to Scapino et al. [36] the chemical reaction takes place between a sorbent, which is typically a liquid or solid, and a sorbate, which is, e.g., a vapor. During the charging process, a heat source is used to induce an endothermic reaction, the sorbent and sorbate are separated. The chemical/physical energy of the two components can then be stored separately. During the discharging process, an exothermic reaction occurs and heat stored is recovered.

*Characteristics of Thermal Storage Systems*

The following features can be used to characterize an energy storage system [21,116,117]:

- Storage period defines how long the energy is stored (i.e., hours, days, weeks);

- Power defines how fast the energy stored in the system can be charged and discharged. In particular, power capacity (W) is the maximum amount of power that can be delivered by the storage system during discharging while Power density (W/l) is the ratio between the power capacity and the capacity of the energy storage system;
- Energy storage capacity or energy capacity is defined as the amount of energy absorbed in the storage system during the charging process under nominal conditions. The quantity of stored energy in the system after it is charged depends on the storage process, storage medium and size of the system;
- Energy density or volumetric heat capacity is defined as the ratio between the stored energy and the volume of the energy storage system;
- Charge and discharge time defines how much time is needed to charge or discharge the system. The maximum number of charge-discharge cycles in the specified conditions is defined as the cycling capacity or number of cycles;
- Self-discharge is the amount of energy initially stored and dissipated over a specified non-use time;
- Efficiency is the ratio of the energy provided to the user to the energy needed to charge the storage system. It accounts for the energy losses during the storage period and the charge/discharge cycle;
- Response time is defined as the speed with which the energy is absorbed or released [h];
- Cycle life refers to how many times the storage system releases the energy after each recharge;
- Costs are indicators to define the overall cost normalized on the total amount of capacity (€/kWh) or power (€/kW). They are capital costs, and operation and maintenance costs of the storage equipment during its lifetime;
- Cost per output (useful) energy is the ratio of the cost per unit energy divided by the storage efficiency;
- Cost per cycle is defined as the cost per unit energy divided by the cycle life.

Typical values of the above-cited parameters for thermal energy storage technologies are reported in Table 1. With respect to the storage period, TES methods are referred as short-term when heat input and output occur within an interval of several hours or days and, instead, as long-term if the time frame is within an interval of few months or even a whole season [118]. In contrast to STES and LTES, TCTES are particularly suitable for long term storage [119]. The reason is that during the storage phase there are no significant energy losses (no self-discharge) [23]. STES and LTES require insulation systems during storage and thus, to avoid thermal losses, heat cannot be stored for a long time [21]. Despite its seasonal storage potential, TCTES for hot/cold demand is still in early development with few prototype set-ups [120].

Storage energy density is a crucial factor to select a thermal energy storage system for a particular application [121]. Because of its potentially higher energy storage density—5 to 10 times higher than latent heat storage system and sensible heat storage system respectively [112]—TCTES is receiving an increasing attention in several domains [122]. High energy density makes thermochemical thermal energy storage systems (TCTESs) such more compact energy systems so their use, reducing the volume of the system, could be very effective in the situations whereas space constraints are significant [123].

**Table 1.** Parameters of thermal energy storage systems (TESs) [122,123].

| TES System | Capacity (kWh/t) | Power (MW) | Efficiency (%) | Storage Period | Cost (€/kWh) |
|---|---|---|---|---|---|
| Sensible | 10–50 | 0.001–10.0 | 50–90 | days/months | 0.1–10 |
| Latent | 50–100 | 0.001–1.0 | 75–90 | hours/months | 10–50 |
| Thermochemical | 120–250 | 0.01–1.0 | 75–100 | hours/days | 8–100 |

A further simplified economic comparison shows that STES is less expensive than LTES and TCTES. High capital costs are among disadvantages that make TCTESs not widely available in the market [119].

## 3. Thermochemical Heat Storage: Description of Materials and Processes

A schematic classification of thermochemical heat storage principles is shown in Figure 2. With respect to type of reaction, thermochemical processes are divided into reversible chemical reactions and sorption processes [124]. The fixation or capture of a gas or a vapor by a sorbent is referred as sorption (adsorption and absorption) [125]. In contrast, chemical reactions (solid–gas, solid–liquid) are characterized by a change in the molecular configuration of the compound involved [125].

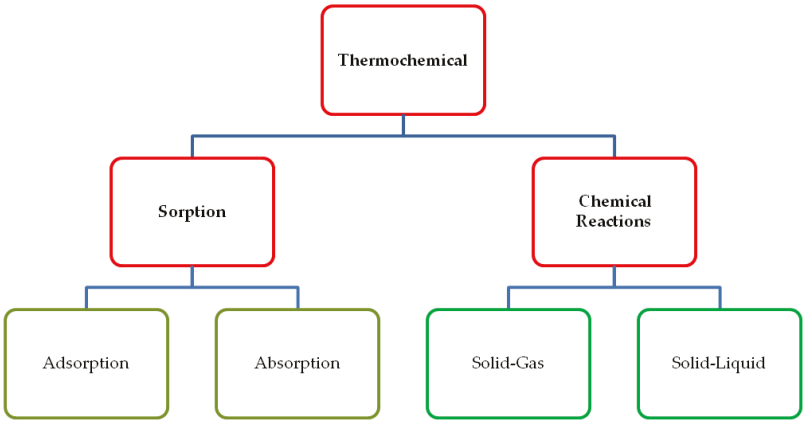


**Figure 2.** Thermochemical Heat Storage principles classification.

Some authors, e.g., Yu et al. [126], use the definition sorption storage to indicate both reversible chemical reactions and sorption processes.

The thermochemical process consists of desorption, storage and sorption [127]. Desorption is the charging process during which heat, supplied to the storage material, is stored in the form of chemical potential by breaking the binders between the sorbent and the sorbate [128]. Storage is the phase in which the sorbent and the sorbate are separated [129]. Sorption is the discharging process aimed at recovering heat by contacting the sorbent and the sorbate [130].

For desorbing the storage material, any system can be used as heat source. Solar energy [131–133] or micro combined heat and power (CHP) [134,135] are examples of heat sources.

As an example, Lass-Seyoum et al. [136] used industrial waste heat and heat from CHP systems, Helden et al. [137] thermal collectors, Zondag H. et al. [138] exhaust air from buildings. Li et al. [139] developed a thermochemical (sorption) storage system based on use of methanol to recover the heat from photovoltaic (PV) panels.

### *3.1. Thermochemical Processes and Materials*

According to Y. Ding [125], sorption is the phenomenon of fixation or capture of a gas or a vapor by a substance in a condensed state. As shown in Figure 2, sorption processes are classified into absorption and adsorption [140]. According to Nic et al. [141] absorption is defined as "the process of one material (absorbate) being retained by another (absorbent)". According to Yu et al. [126], adsorption is defined as "a phenomenon occurring at the interface between two phases, in which cohesive forces act between the molecules of all substances irrespective of their state of aggregation". An important difference is that absorption occurs at the sorbent molecular level by altering its composition and morphological structure, adsorption occurs at the surface of the adsorbent [34,142]. As shown in Figure 2, solid/gas and liquid/gas systems are example of working pairs used for sorption processes.

These processes are used to store both low-grade heat (<100 °C) and medium-grade heat (100–400 °C) [143–145]. High kinetics at low temperatures make the sorption processes particularly

attractive for low-temperature applications such as space heating, domestic hot water preparation or other low-grade and medium-grade heat uses [7,146–152]. Usually sorption materials are liquid, solid and composite sorbents [35,153]. Example of working pairs are:

- LiBr solution/$H_2O$ [154,155];
- LiCl solution/$H_2O$ [156–158];
- LiCl/activated alumina [159,160];
- LiCl/expanded graphite [161];
- $LiCl_2$ solution/$H_2O$ [162];
- $CaCl_2$ solution/$H_2O$ [163–165];
- Binary sales [166–174];
- Zeolite 13X [175–182], Zeolite 4A [183–189], Zeolite 5A [190,191];
- Aluminophosphates (ALPOs) [192] and Silico-aluminophosphates (SAPOs) [193–195];
- Composite materials made up by the combination of a salt hydrate and an additive with a porous structure and high thermal conductivity (expanded graphite [196,197], metal foam [198], carbon fiber [199] and activated carbon [199]).

(ALPOs) and (SAPOs) are among promising examples of sorption materials, in particular, for low temperature heat storage [200,201]. Among zeolites, Zeolite 13X is one of the most common thermochemical material in current research due to its hydrothermal and mechanical stability and corrosion behavior [190]. Example of composite materials are $CaCl_2$-Silica gel/$H_2O$ [202], $CaCl_2$-$FeKIL_2$/$H_2O$ [203,204], LiBr-Silica gel/$H_2O$ [205], $MgSO_4$-Zeolite/$H_2O$ [206,207], $MgSO_4$-$MgCl_2$-/$H_2O$ [208,209].

Chemical reactions are used to store medium (100–400 °C) and high (>400 °C) grade heat [210–212]. Example of chemical reactions are:

- dehydration of metal hydroxides [213–218];
- dehydration of metal hydrides [219–224];
- dehydration of salt hydrates [151,225–230];
- deammoniation of ammonium chlorides [172,231–233];
- decarboxylation of metal carbonates [121,234–239];
- methane steam reforming [240–242];
- catalytic dissociation [243–245];
- metal oxide redox [246–248].

The interest towards dehydration of metal hydroxides is not recent, e.g., the hydration of MgO has been extensively studied as early as 1960 [249,250], the dehydration of $Ca(OH)_2$ has found wide attention as early as 1988. In particular, under support of the National Energy Administration, the American Pacific Northwest National Laboratory started the research on $Ca(OH)_2$/CaO as energy storage system [251]. In this context, Liu et al. [251] developed an experimental set up to investigate thermal cycling stability of the $Ca(OH)_2$/CaO system laying the foundation of applying this system to practical. A similar experimental set up was developed by Schaube et al. [252].

$Ca(OH)_2$/CaO is among more used systems in chemical processes [253–256]. This system has numerous advantages, e.g., efficient reaction kinetics [257] and high reaction enthalpy (104.4 KJ/mol) [258]. It is a very suitable material in thermal storage systems [259], in particular for high-temperatures (400–600 °C) applications [260]. In the context of power-to-heat applications the usage of $Ca(OH)_2$/CaO thermochemical systems coupled to heat pumps is arousing great investigation with a particular focus on heat and mass transfer process [261–263].

Also the interest towards metal hydrides is not recent, these thermochemical storage systems were explored since the mid-1970s [264]. Several applications and different metal hydrides systems were explored for thermochemical heat storage [265–269]. Among metal hydrides, Mg-based systems

are promising as thermochemical storage materials owing to high reaction enthalpy as shown in the studies of Gigantino et al. [223] and Shkatulov et al. [53]. Mg-based metal systems show cyclic stability over a temperature range from 250 °C to 550 °C in which high thermal energy densities of up to 2257 kJ/kg are reached [130]. The abundance of metal hydrides, low cost, high reaction enthalpy, high storage density are among characteristics attracting extensive investigations [219]. These systems, are suitable for both low and high temperature applications [270]. As an example, Sheppard et al. [270] investigated the potential of metal hydrides for low temperature applications while Ronnebro et al. [220] investigated their use for high temperatures applications, in particular based on experimental and modelling results they designed and fabricated a prototype to store both hydrogen and heat with solar technologies. In accordance to other studies, they showed that metal hydrides show both good reversibility and cycling stability combined with high enthalpies. A study about the future perspectives of thermochemical storage based on use of metal hydrides for solar technologies have been developed by Manickam et al. [271].

High energy density and desorption temperatures make salt hydrates fitting with the use of power-to-heat technologies, waste heat sources, solar thermal collectors, particularly investigated and proposed for seasonal heat storage of solar energy in the built environment [150,272,273]. N'Tsoukope et al. [274] investigated 125 salt hydrates for low temperatures heat storage and found that $SrBr_2 \cdot 6H_2O$ and $MgCl_2 \cdot 6H_2O$ are among the most promising choices for thermochemical storage applications. To investigate the potential energy storage density and the storage efficiency of salt hydrates, a micro-combined heat and power system was developed for the storage of heat generated. They found that for applications requiring lower discharging temperatures like 35 °C, the expectable efficiency and net energy storage density was low. Their results are in accordance to [275–279]. Salt hydrates are considered the most suitable materials for residential applications owing to their high energy density (400-870 $kWh \cdot m^{-3}$) and low turning temperature [280].

Metal carbonates have several advantages, e.g., high energy density, nontoxicity, low costs and widespread availability. All these properties make them suitable for thermochemical storage applications [281–284]. Among suitable alternatives, the combined use of $CaO/CaCO_3$ (density 0.49 kWh/kg), proposed by Barker in 1973 [283], is largely investigated. In a recent study Fernandez et al. [235] used the working pair $CaO/CaCO_3$ to develop a system referred as Photovoltaic-Calcium looping (PV-CaL) as large scale storage system. They showed that the high turning temperatures of the exothermic carbonation reaction allows using high-efficiency power cycles. $CaCO_3$ is one of the most abundant materials in nature. Its use circumventing the risk of resource scarcity may not compromise the economic and technical viability of a thermochemical storage system [236].

The performances of a storage system based on chemical reactions or sorption processes are strongly dependent on the nature of the storage material chosen [125,285,286]. High heat storage capacity and good heat transfer are important characteristics affecting the performance of the heat storage systems. In the choice of the storage materials, parameters such as the cost, environmental impact, and safety conditions should be also taken into account [54,287,288]. Despite many materials being widely investigated, research is always under development to increase material performance with respect to storage density and heat transfer properties [288,289].

Note that among the various thermochemical storage materials described in this section, only few of them have been used so far in power-to-heat applications, as will be shown in more detail in Section 4.1.

### 3.2. Thermochemical Heat Storage Systems

Thermochemical heat storage systems with respect to system configuration can be divided in open and closed systems [274,290,291]. Open systems work at atmospheric pressure in contact with the environment while closed ones work with pure vapor, circulating in hermetically closed loops, at vacuum pressure [292]. A schematic sketch of a closed and open system is shown in Figure 3.

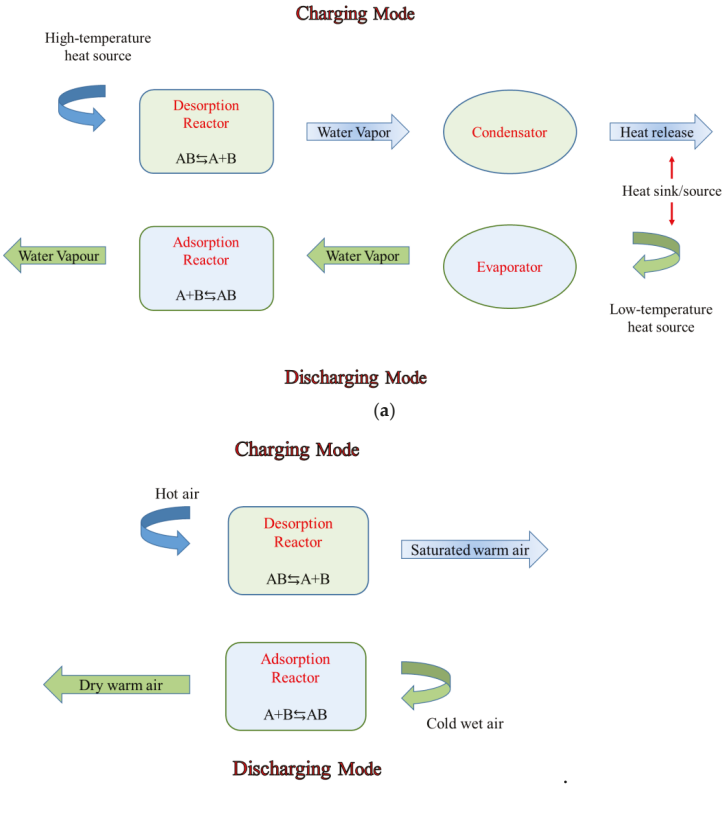


**Figure 3.** Schematic sketch of (**a**) closed and (**b**) open thermochemical system.

A closed system is usually based on a sorption reactor (heat exchanger), a condenser and an evaporator. During the charge process (desorption), heat must be supplied to the storage material at high temperature in the sorption reactor. Desorbed water vapor, released from the sorbent, is condensed at low temperature. The liquid is stored in the reservoir while the heat of condensation can be used either as a low-temperature source or rejected to the environment. After the accomplishment of the charging mode, the storage materials and components will cool down to ambient temperature so during storage no further energy losses occurs. When heat is needed, the valve between the evaporator and sorption reactor is turned on and discharging mode occurs. During the discharging process (adsorption), heat is supplied to the liquid stored in the evaporator at low temperature; the resulting steam is adsorbed in the adsorber releasing heat. Adsorption is a completely reversible process so heat supplied for desorption is equal to the heat gained back during adsorption. Liu et al. [156] developed a seasonal storage system and evaluated that the storage capacity increases with the evaporator temperature and decreases with desorption temperature.

As shown in Figure 3b an open system is less complex in its design. It can be directly connected to the ambient air where the moisture for sorption process is obtained; there are no evaporator or condenser. During the charging mode hot air flows into the sorption reactor releasing water vapor into the air itself. Output is saturated warm air. When heat is needed, cold wet air from the environment is blown into the sorption reactor. Open systems are usually equipped with one or more fans to ensure the ambient air flow into the sorption reactor [129].

The key component of the above described systems is the thermochemical reactor. The reactor can be integrated [293] or separated [294]. In an integrated reactor, the material is stored in the tank where it reacts, while the chamber where the reaction takes place is separated from the thermochemical material storage tank. In a separate reactor the dissociation between the thermal power and the installation storage capacity increases the storage density of the process since there is no need for vapor diffusers and heat exchangers are integrated into the reactor. Moreover, this kind of reactor can also work in steady-state conditions, providing a constant thermal power output [295].

Energy and exergy methods to assess the performances of closed and open systems have been carried by Abedin and Rosen [294]. The authors compared open and closed systems based on use of zeolites 13X. 50% and 9% are the values obtained for energy and exergy efficiency, respectively, in closed systems, 69% and 23% in open ones. Since the exergy efficiencies of both systems are lower than the energy efficiencies it means that there is a margin for loss reduction and efficiency for TCTESs [119]. From a numerical comparison between the two designs, Michel et al. [290] concluded that heat transfer is the main limitation in closed systems while it is mass transfer (vapor transfer to the adsorbent during discharging) in open ones.

Many prototypes of both type of systems have been developed. One of the first open prototypes, in operation since 1996, is the zeolite 13X storage system built in a school in Munich by ZAE Bayern [295]. The system was designed for peak shaving of the heating load in order to be operated jointly with district heating in winter to supply it during the off-peak in summer. The charging temperature is about 130 °C while the storage capacity is 1300–1400 kWh. Heat released during the discharging mode is used to produce water vapor. A more recent prototype of ZAE Bayern was developed in 2015 [129]. It is an open system based on zeolite 13X for transportable sorption heat storage purposes. Waste heat from an incineration plant at 130 °C is used as thermal source during discharging mode. The charging temperature was 60 °C and a storage capacity of 0.6 MJ/kg was measured.

Among closed prototypes, one of the first was developed within the HYDES (High Energy Density Sorption Heat Storage) project [296]. The prototype in function from 1998 to 2001 was a solar thermal energy storage system for space heating purposes based on silica gel/$H_2O$. Solar thermal collectors were used as low temperature heat source for the evaporator. The charging temperature was about 82 °C, the sorption one 32 °C, a power output of about 2.87 kW and 1.7 kW were measured during discharging and charging phase.

A prototype of closed system is currently being developed at GEPASUD laboratory (French Polynesia) [173]. It is a conventional mechanical vapor compression (MVC) driven by grid and PV electricity integrated with a thermochemical reactor based on the use of $BaCl_2/NH_3$ as working fluids pair. The prototype has the aim to demonstrate that a thermochemical reactor coupled with a PV-driven mechanical compressor is an effective innovative solution offering energy storage capabilities for cooling purposes. The prototype uses ammonia not only as thermochemical material but also as refrigerant liquid. Among thermochemical storage materials, ammonia is expected to be established in the market for small and medium refrigeration [297–299].

The existing prototypes show a mature development of the TCTESs in heat-to-heat and heat-to-power applications. Collectors and concentrating solar plants (CSP) are mainly used as a heat source for the evaporator of the thermochemical devices. In particular, coupling storage into CSP systems enables dispatchable generation, whereby utilities produce power to match demand overcoming intermittency challenges faced by renewable energy production. Another field of wide application of TCTESs is the recovery of industrial waste heat [300–303]. Kuwata et al. [302] investigated the potential of the ammonium chloride $SrCl_2$ in applications based on utilization of industrial waste heat. Thermochemical energy storage could be a key technology able to bridge the gap between the wasted heat as the source and provided to customers at the time and place they need it [267,268]. A more detailed review on this field was developed in [304]. A list of some prototypes is given in Table 2 and in Table 3 for open and closed thermochemical systems respectively.

**Table 2.** Example of prototypes of open systems for thermochemical storage.

| Project Name/Institution | Description | Storage System |
|---|---|---|
| MONOSORP [305] (2006) | • Storage system for space heating<br>• Charging temperature $T_c$ = 20 °C<br>• Discharging temperature $T_d$ = 180 °C | Zeolite 4A |
| Institute for Solar Technology SPF [241] (2006) | ○ Storage system for space heating.<br>○ $T_c$ = 20 °C<br>○ $T_d$ = 180 °C | Zeolite 13X |
| ECN [1] [227] (2010) | • Lab scale packed bed reactor for seasonal storage of solar heat<br>• Discharge time about 25 h<br>• Storage energy density measured 0.14 MJ/kg | $MgCl_2 \cdot 6H_2O$ |
| CWS [2] [306] (2011) | ○ System integrated with a water tank (STES) for heating purposes<br>○ $T_c$ = 35 °C<br>○ $T_d$ = 180 °C | LiCl with Zeolite 13X used as additive |
| ECN [211] (2013) | • Lab scale packed bed reactor for heating purposes (Heat Power 150 W)<br>• $T_c$ = 10 °C<br>• $T_d$ = 50 °C | $MgCl_2 \cdot H_2O$ |
| Energy hub-ECN [178,179] (2013–2014) | ○ Lab scale two packed bed modules for heating purposes<br>○ $T_c$ = 70 °C<br>○ $T_d$ = 185 °C<br>○ Heat Power 400 W | Zeolite 13X |
| ASIC [3] [176] (2014) | • Storage system for space heating and domestic hot water<br>• $T_c$ = 25 °C<br>• $T_d$ = 180 (230) °C | Zeolite 4A (Zeolite 13X) |
| STAID [4] [180] (2015) | ○ Storage system integrated in a domestic ventilation system for space heating during peak hours<br>○ $T_c$ = 57 °C<br>○ $T_d$ = 120–180 °C<br>○ Storage energy density 0.41 GJ/m$^3$ | Zeolite 13X |
| ESSI [5] [276] (2016) | • Packed bed reactor for house heating<br>• $T_c$ = 25 °C<br>• $T_d$ = 80 °C<br>• Thermal power measured during sorption mode 0.3–0.8 kW<br>• Thermal power measured during desorption mode 0.4–1.6 kW | $SrBr_2 \cdot 6H_2O$ |
| STAID [181] (2016) | ○ Storage system for space heating<br>○ $T_c$ = 20 °C<br>○ $T_d$ = 120–180 °C | Zeolite 13X |
| NSFC [6] [159] (2017–2018) | • Lab-scale prototype experimentally investigated to store low-temperature heat for space heating<br>• $T_c$ = 20 °C<br>• $T_d$ = 30 °C<br>• Thermal power (56.7–136) W | Activated alumina/LiCl |

[1] Energy Research Center of The Netherlands. [2] Chemische WarmeSpeicherung. [3] Austrian Solar Innovation Center. [4] Stockage Inter Saisonnier de l'Energie Thermique dans les Batiments. [5] European. Support to Social Innovation. [6] Natural National Science Foundation of China.

**Table 3.** Example of prototypes of closed systems for thermochemical storage.

| Project Name/Institution | Description | Storage System |
|---|---|---|
| SWEAT [1]/ECN [229] (2004) | • Solid sorption storage for cooling purposes.<br>• $T_c$ = 15–25 °C<br>• $T_d$ = 77–86 °C<br>• Thermal power measured in discharging mode 0.5–0.7 kW<br>• Thermal power measured in charging mode 1.2 kW. | $Na_2S/H_2O$ |
| MCES [2] [242] (2004) | ○ Solid sorption storage for cooling and heating purposes.<br>○ $T_c$ = 65 °C<br>○ $T_d$ = 80–95 °C<br>○ Storage energy density 8 MJ/kg. | $Na_2S{\cdot}9H_2O$ and graphite used as additive |
| MODESTORE [141,307] (2006) | • Storage system for heating purposes<br>• $T_c$ = 25 °C<br>• $T_d$ = 88 °C<br>• Thermal power measured during discharging mode 0.5 kW<br>• Thermal power measured during charging mode 1 kW. | Silica gel |
| SOLAR-STORE [308] (2006) | ○ Solid sorption storage for heating and cooling purposes.<br>○ $T_c$ = 35 °C<br>○ $T_d$ = 80 °C<br>○ Heating density power 47–49 kWh/m$^3$<br>○ Cooling density power 27–36 kWh/m$^3$ | $SrBr_2$ with expanded natural graphite |
| SOLAR-STORE [278] (2008) | • Solid sorption storage for heating and cooling purposes.<br>• $T_c$ = 35 °C<br>• $T_d$ = 80 °C<br>• Heating power 60 kW<br>• Cooling power 40 kW | $SrBr_2$ |
| Fraunhofher [136] (2012) | ○ Solid sorption storage for waste heat industrial recovery<br>○ $T_c$ = 30 °C<br>○ $T_d$ = 9–200 °C<br>○ Heat storage capacity 0.54–0.79 MJ/kg | Zeolite/$CaCl_2$ |
| E-hub/Project [190] (2012) | • Storage system for dwellings<br>• $T_c$ = 85–88 °C<br>• Heat density power 164 W/kg. | Zeolite |
| E-hub/Project [189] (2014) | ○ Lab-scale prototype for space heating<br>○ $T_c$ = 20–30 °C<br>○ $T_d$ = 80–120 °C<br>○ Storage energy density 0.045 GJ/m$^3$ | Zeolite 5A |
| COMTES [3] [309] (2015) | • Solid sorption system for space heating and domestic heat water.<br>• $T_d$ = 75 °C<br>• Storage energy density 0.4 GJ/m$^3$ | Zeolite 13XBF |
| COMTES [163] (2015) | ○ Liquid sorption system for diurnal storage<br>○ $T_d$ > 50 °C<br>○ Power output approximately 1 kW | NaOH/$H_2O$ |

**Table 3.** *Cont.*

| Project Name/Institution | Description | Storage System |
|---|---|---|
| SJTU [4] [160] (2016) | • Solid sorption system for space heating and domestic heat water.<br>• $T_c$ = 40 °C<br>• $T_d$ = 85 °C<br>• Storage energy density 0.873 kWh/kg. | LiCl with expanded graphite |
| HSR-SPF [5] [164] (2018) | ○ Liquid seasonal thermal storage system<br>○ $T_c$ = 22 °C<br>○ $T_d$ = 50 °C | $NaOH/H_2O$ |
| Heat STRESS [170] (2019) | • Solid sorption system for seasonal thermal storage for domestic application<br>• $T_c$ = 40 °C<br>• $T_d$ = 70 °C | $CaCl_2/NH_3$ |
| University of Newcastle [245] (2019) | ○ Hybrid energy storage system to store energy from wind, solar and/or off-peak electricity simultaneously.<br>○ Reaction take places a T > 800 °C | $Co_3O_4/CoO$ |
| RESTRUCTURE [247] (2019) | • Pilot prototype integrated with Concentrated Solar Power (CSP) for power production<br>• Reaction take places in the temperature interval (800–1000) °C | $Co_3O_4/CoO$ |

[1] Salt Water Energy Accumulation and Transformation. [2] Modular Chemical Energy Storage. [3] Combined Development of Compact Thermal Energy Storage Technologies. [4] Institute of Refrigeration and Cryogenics (China) [5] Institute fur Solartechnik.

## 4. Thermochemical Storage in Power-to-Heat Applications

### *4.1. Thermochemical Storage Energy Systems in Power-to-Heat Applications: Case Studies*

PtH technologies show a mature development with latent and sensible storage while only a limited number of applications with thermochemical storage is available in literature [310–317]. Existing applications focus on different aspects, hence a net comparison was not possible. Based on the usage of the heat stored, in this work the applications were divided into power-to-heat and power-to-heat-to-power as shown in Figure 4. In the first case, heat stored is used in the form of thermal energy for heating and cooling purposes. In the second case, heat, released during the discharging phase, is used to generate electricity when it is needed.

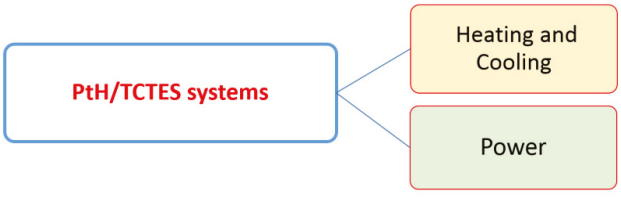


**Figure 4.** Thermochemical storage and power-to-heat uses.

Cammarata et al. [139] developed a hybrid thermochemical storage device to store the excess of power generation. The system was developed for household applications for low to medium temperature range (50–100 °C). The scheme of this case study is shown in Figure 5.

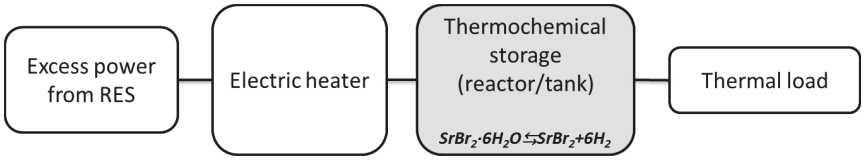


**Figure 5.** PtH/TCTES system developed by Cammarata et al. [139].

The system is based on the reversible hydration/dehydration of $SrBr_2 \cdot 6H_2O$ and graphite as additive material. The power converted into heat by a heat pump driven by solar and wind energy is carried out to the tank storage where the endothermic dehydration reaction takes place at temperature < 100 °C. From the reaction $SrBr_2$ (sorbent) and $H_2O$ (sorbate) are formed ($SrBr_2 \cdot 6H_2O \leftrightarrows SrBr_2 + 6H_2O$), the sorbate is condensed for use in the discharging process in the case of closed system or released in the environment in the case of open system. Heat stored is use both heating demand and supply of electricity during the discharging phase. Their results showed that an energy storage density of 500 kJ/kg can be achieved at a temperature of 80 °C, a value of 600 kJ/kg by increasing the temperature to 150 °C. This study shows for the first time how the composite formulation of $SbBr_2$ affects the energy density, heat and mass transfer and reaction kinetics.

Ferrucci et al. [173] developed a hybrid system for household applications. This integrates a thermochemical system with an air conditioning system driven by grid and photovoltaic electricity. The cooling system is a conventional Mechanical Vapor Compression (MVC) while the storage device is a packed-bed reactor with eight compartments based on the use of $BaCl_2/NH_3$ as working pair. The scheme of this case study is shown in Figure 6.

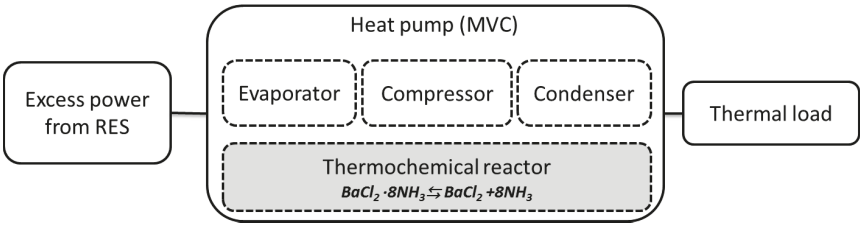


**Figure 6.** PtH/TCTES system developed by Ferrucci et al. [173] and by Fitò et al. [315].

When there is a surplus of electricity generation and no cooling needs, the extra power is used to run the compressor in order to store energy for later use. By means of a smart controller, during the storage process, the evaporator is disconnected from the circuit and the reactor is connected to the compressor. The desorption heat is provided by a low grade waste heat source at 50 °C or by an electric heater in direct contact with the thermochemical reactor. $BaCl_2$ reacts with ammonia ($NH_3$) to form $BaCl_2 \cdot 8NH_3$ with an energy density estimated in an approximate value of 200 kJ per kg of reactor. The coefficient of performance, exergy efficiency and cooling capacity were used as indicators to compare a traditional MVC cycle without thermochemical storage and the hybrid system proposed. As example, the authors showed that the COP of the hybrid system, for a given source temperature, is higher than the one of a conventional one. The hybrid system was compared with alternative energy storage processes. In particular Pb and Li-ion batteries (electrochemical storage), ice and chilled water thermal storage was chosen as alternative devices to thermochemical reactor. Their results showed that the hybrid system proposed has a cooling capacity (60 Wh/L) six times larger than chilled water system but comparable to that one of ice storage systems. MVC systems with electrochemical batteries have the highest cooling capacity, 190 Wh/L for MVC and Pb battery and 420 Wh/L for MVC and Li battery respectively, but much shorter life span than MVC with thermochemical storage. The COP of the hybrid system (4.8) is comparable to Pb batteries (4.2), Li-ion batteries (4.2) and chiller (4.2) systems.

The hybrid system is an example of compressor-driven method for energy storage and deferred cooling. This application for space cooling is not yet widely explored in literature.

Fitò et al. [315] analyzed an ammonia-based refrigeration system consisting in the hybridization of compression refrigeration with thermochemical storage. The proposed hybrid system has the typical architecture of a MVC cycle (evaporator, compressor, condenser, reservoir and throttling valve), a grid-connected photovoltaic installation and a thermochemical storage reactor. The scheme of this case study is shown in Figure 6.

MVC cycle and thermochemical storage system have the same condenser, evaporator and refrigerant fluid ($NH_3$). The storage device is a packed-bed reactor based on the use of $BaCl_2/NH_3$ as working pair. Both the PV installation and the grid are used to meet the electricity requirements for cold production. When there is a surplus of power generation from RES and no cooling demand, the power in excess is used to store energy in the form of heat driving the desorption phase of the reactor. Thermochemical process enables the storage of energy in the form of chemical potential for a deferred cold production without running the compressor. The heat of desorption is provided by waste heat or solar collectors at about 50 °C. The authors demonstrated an overall thermochemical cycle has a COP (1–1.4) higher than a conventional MVC operating without thermochemical storage.

Finck et al. [175] developed a hybrid compression thermochemical refrigeration system (HCTSR) to show the potential power flexibility of thermal storage and power-to-heat.

Power flexibility is in this specific case defined as the thermal response of TES tanks and related electricity consumption of the heat pump during charging, discharging and store mode. The scheme of this case study is shown in Figure 7.

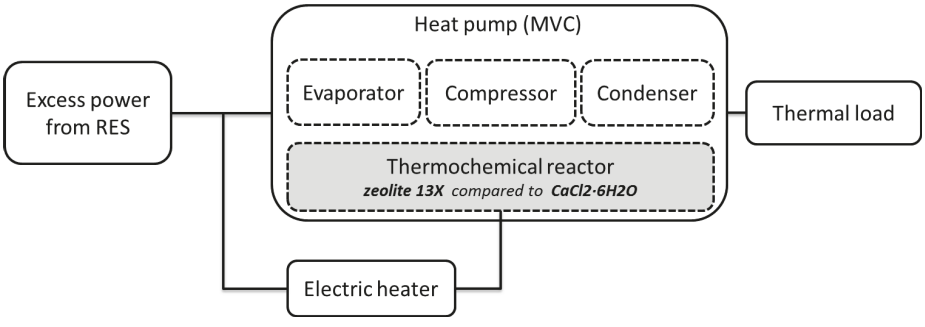


**Figure 7.** PtH/TCTES system developed by Finck et al. [175].

HCTRS, consists of an MVC cycle and a thermochemical reactor. The heat pump and an electric heater serve as power-to-heat conversion while the storage tank as the source of flexibility. The thermochemical storage device is a packed bed reactor based on zeolite 13X and water as working pair. During desorption, the electric heater serves as a dehydration source. During adsorption, the heat stored is used for space heating or domestic hot water. The system with thermochemical storage was compared with the one obtained coupling the same MVC to a sensible and latent storage tank. Water and $CaCl_2{\cdot}6H_2O$ were used as sensible and latent material respectively. Results show that assuming the same dimensions for the storage tank (a cylindrical vessel of 0.5 $m^3$) and a volume flow of heat transfer medium of 1 $m^3/h$, the thermochemical system has an energy capacity (0.05 GJ) lower than the other storage systems (0.15 GJ). The available storage capacity (COC) and storage efficiency ($\eta_{OC}$) were used to compare the energy flexibility of the three different thermal storage systems. COC is defined as the amount of energy that is shifted during the optimal control to minimize the electricity consumption costs for operating the heat pump and the electric heater. $\eta_{OC}$ indicates the effective use of the heat stored to compensate power-to-heat devices during optimal control. Results show that the thermochemical storage has the lower values for both COC (5.6 kWh) and $\eta_{OC}$ (0.96).

The following studies are examples of power-to-heat-to-power applications in which the heat stored is converted into electricity by a power plant when it is needed.

Wu et al. [245] proposed a hybrid energy system to store excess energy from renewable sources. The system consists of a compressed air energy storage (CAES) integrated with a thermochemical reactor based on the use of the metal oxide redox pair $Co_3O_4$/CoO as sorption working material. In contrast to a conventional Compressed Air Energy Storage (CAES) [317] in which compressed air is superheated by means the combustion of fossil fuel, in the proposed hybrid system this function is replaced by the sorption reactor. The scheme of this case study is shown in Figure 8.

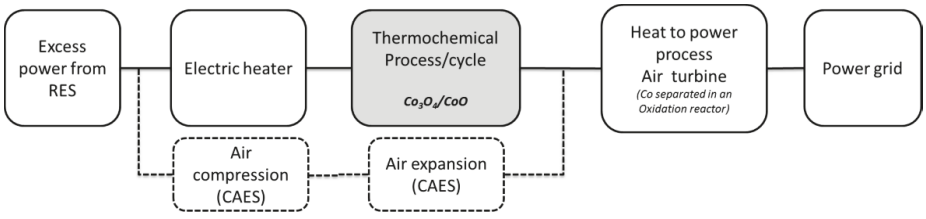


**Figure 8.** PtH/TCTES system developed by Wu et al. [245].

The proposed system consists of five compressors powered by electricity to compress air and an electric heater as heat source for the charging phase of the thermochemical storage process. The thermal charging phase takes place, in parallel with the CAES compression phase, with the reduction of $Co_3O_4$ into CO and $CO_2$ ($2Co_3O_4 \leftrightarrows 6CoO + O_2$) carried out at 870 °C and 0.1 bar. The discharging phase takes place and the energy stored in the compressed air and metal oxide CoO (heat released by the exothermic reaction is transferred to air) is converted back into electricity throw air turbines. A value of 3.9 kWh/m$^3$ was evaluated for the energy storage density, defined in this case as the total power output per unit volume of the stored air (the same as the volume of the storage cavern). Moreover, it was estimated that 65% of the energy storage density relies on thermochemical part of the system while the remaining 35% is achieved via the CAES. The authors demonstrated that, in terms of storage energy density, the hybrid system has a value comparable to a conventional CAES (3–6 kWh/m$^3$) operating at the same conditions. Based on a thermodynamic analysis it was estimated an efficiency of 56.4%. In comparison to conventional CAES plants, authors showed that this value is higher than the efficiency of the commercialized Huntfort (42%) and McIntosh (54%) CAES plants.

Fernandez et al. [235] developed a power-to-heat-to-power system based on the calcination/carbonation of calcium carbonate as sorption process and a closed $CO_2$ Brayton regenerative cycle. The scheme of this case study is shown in Figure 9.

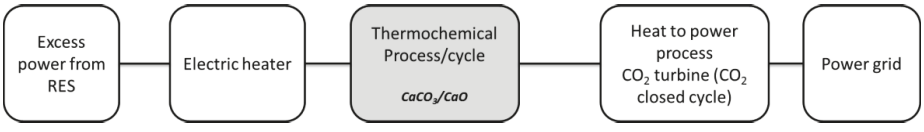


**Figure 9.** PtH/TCTES system developed by Fernandez et al. [235].

During the charging phase, the electric power is converted into thermal power by Joule effect to heat up the calciner (Fluidized bed thermochemical reactor). In the reactor the calcination endothermic reaction takes place under atmospheric pressure at 950 °C, CaO and $CO_2$ are formed ($CaCO_3 \leftrightarrows CaO + CO_2$). During the discharging phase, that takes place at 75 bar and 25 °C, power is generated in a $CO_2$ turbine connected to an asynchronous generator that converts mechanical power into electricity. CaO and $CO_2$ are carried out in the carbonator reactor where the exothermic carbonation reaction occurs. The presence of a calciner and a carbonator is indicative that in the system charging and discharging

cycles are well differentiated and independent. The system is connected to the grid to export electrical power generated during the discharging phase. The proposed system was simulated under different charging and discharging operations modes to assess its potential as large-scale electric energy storage system estimating a maximum reachable efficiency of 39%.

Wu et al. [316] developed a phase change redox (PCR) system to convert electricity surplus into heat and to store it using a $CuO/Cu_2O$ cycle. The scheme of this case study is shown in Figure 10.

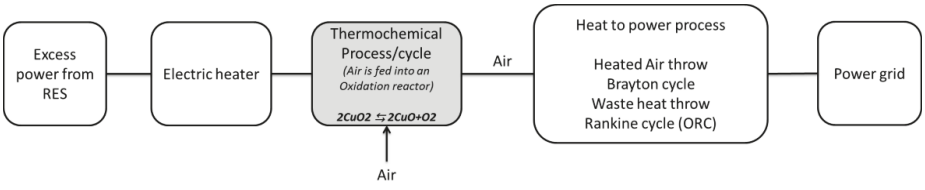


**Figure 10.** PtH/TCTES system developed by Wu et al. [316].

When there is a surplus of electricity from grid or solar/wind plants heat provided by Joule heating is used for the charging phase of the sorption process. During this phase, $CuO_2$ is reduced into CuO and $O_2$ ($2CuO_2 \leftrightarrows 2CuO + O_2$). The molten $CuO/CuO_2$ requires a high temperature of about 1200 °C during the charging phase. When electricity demand in the grid occurs the discharging phase starts. During this phase, the exothermic reaction takes place and the stored molten $CuO/CuO_2$ is oxidized and cooled into an oxidation reactor using air. Heated air is used into a Brayton cycle coupled with a bottoming organic Rankine cycle (ORC). Energy storage density and round trip efficiency were the indicators used to assess the energy storage performances. Energy storage density is here defined as the heat stored per mass unit of the raw material CuO while the round trip efficiency is the amount of electricity that can be recovered for a given energy input. The PCR system coupled to the Brayton and Rankine power generation cycles is able to achieve a round trip efficiency of about 50%. Advantages of the proposed PCR system are high-energy storage density, high round trip efficiency, enhancement of $CuO/Cu_2O$ reversibility, abundant and low-cost raw material and oxygen as a valuable by-product. The main disadvantages and potential limits can be summarized as systems complexity, high-temperature heat source, high operating temperature and high equipment, operation and maintenance costs.

Rodriguez et al. [318] proposed an innovative hybrid absorption system based on the thermochemical technology to store electrical energy at large scale. The system consists of two storage tanks to accumulate a liquid solution at two different levels of pressure, a compressor powered by the excess renewable energy, a thermochemical storage tank (using of $NH_3/LiNO_3$, where $NH_3$ is the solute while $LiNO_3$ is the sorbent) and an independent vapor expander/turbine (T) located between the high and low pressure tanks that drives an electrical generator. The scheme of this case study is shown in Figure 11.

When there is an excess of renewable electricity generation, the charging phase takes place increasing the pressure difference between the two reservoirs. The authors highlighted that the amount of energy required to pressurize the gas in the proposed hybrid cycle is lower than pressurizing a gas with no phase change. During the discharging phase, the turbine transforms the stored energy into mechanical energy driving a generator and returning the electricity into the grid. Numerical simulations were carried out in order to evaluate the performance of the storage system. For a nominal renewable power of 18 kW and an energy output of 8 kW, 44.3% and 0.36 MWh were the values found for the efficiency and energy storage respectively. The viability of using of an absorption thermochemical energy stored system inherently combined with a gas compression cycle was demonstrated only theoretically.

The features of the cases described in this section are summarized in Table 4.

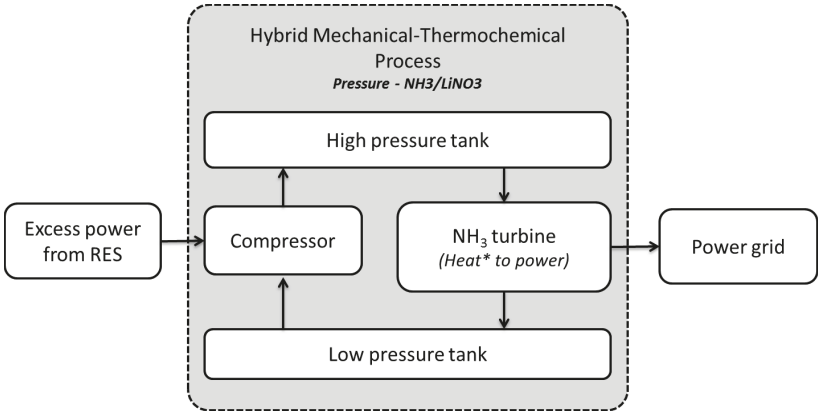


**Figure 11.** PtH/TCTES system developed by Rodriguez et al. [318]. * Heat is exchanged between the two tanks in order to compensate the ammonia expansion/compression cycle.

**Table 4.** Thermochemical storage in PtH and PtH/HtP applications.

| References | Application | Storage Material | Performance Indicators |
|---|---|---|---|
| Cammarata et al. [139] | Power-to-heat (household application) | $SrBr_2/H_2O$ | Energy density: 500 kJ/kg |
| Ferrucci et al. [173] | Power-to-heat (integrated into electric driven cooling system) | $BaCl_2/NH_3$ | Energy density: 200 kJ/kg<br>COP = 4.8 |
| Finck et al. [175] | Power-to-heat (integrated into electric driven cooling system) | Zeolite 13X/$H_2O$ | Capacity: 5.6 kWh<br>Efficiency: 0.96 |
| Wu et al. [245] | Power-to-heat (to power) | $Co_3O_4/CoO$ | Energy density: 3.9 kWh/m$^3$<br>Efficiency: 56.4% |
| Fernandez et al. [235] | Power-to-heat (to power) | $CaCO_3/CaO$ | Overall plant Efficiency: 39% |
| Wu et al. [316] | Power-to-heat (to power) | $CuO/Cu_2O$ | Energy density: 1600 kJ/kg<br>Efficiency: 50% |
| Rodriguez et al. [318] | Power-to-heat (to power) | $NH_3/LiNO_3$ | Capacity: 0.36 MWh<br>Efficiency: 44.3% |

### *4.2. Discussion and Outlook*

The articles reviewed show emerging power-to-heat/thermochemical applications as flexible coupling systems to address both integration of renewable energies and additional grid flexibility. High efficiency in balancing the excess of renewable generation is the key aspect that could led these applications towards an increasing development in the next future.

Investigating the demand flexibility of power-to-heat conversion with thermochemical systems was a common aim of all authors. All three dimensions of flexibility were investigated: size (energy), time (power) and costs. A number of indicators were proposed to quantify the energy flexibility in terms of available storage capacity and/or efficiency. The usage of a non-common quantification method to estimate the energy flexibility makes difficult a straightforward comparison among the reviewed studies. Despite this limit, important considerations can be argued as follows.

According to the thermodynamic and numerical analyses, the overall efficiency of the coupled system range from 39% to 56%. The highest value is obtained in power-to-heat/thermochemical applications coupled to power cycle [317], overcoming typical efficiencies of conventional power cycles. The reason lies in the use of raw thermochemical materials requiring higher operating temperatures, which increase the upper limit of the achievable thermodynamic efficiency according to Carnot

principles. This suggests that more efforts should be paid to the design and test of thermochemical materials and related physical–chemical reactions, in order to boost further the process efficiency in view of the development of optimized systems.

The studies reported in [246,317] suggest that the high efficiency and flexibility of these innovative applications could be able to facilitate the integration in the power system not only of the photovoltaic but also of the wind power. A development in the wind energy integration could be crucial in energy systems characterized by a large share of wind power.

High storage density, low heat loss, long storage period, highly compact energy storage are the main advantages common to all the power-to-heat/thermochemical technologies. Despite this, a series of limits, such as the high costs of the materials and the complexity of the equipment, makes these applications still not mature for large scale/market adoption as shown by the few prototypes developed and tested so far. Costs abatement and process simplification in optimized systems require further efforts for the development of techno-economically competitive applications. Moreover, the deployment at large-scale of these potential low-carbon technologies will require significant investments and the revision of the present infrastructures.

## 5. Conclusions

In this work, to provide a comprehensive review on the state of art of thermochemical storage systems and their applications in power-to-heat technologies, theoretical, experimental and numerical studies and their recent advancements and potential perspectives were discussed.

This paper reviews the current literature that refers to the development and exploitation of thermochemical storage systems connected to power-to-heat technologies to power grid support. The operation principles both of thermochemical and of power-to-heat are presented, thermochemical materials and processes are compared. Power-to-heat conversion is likely the most mature and favorable technology enabling power flexibility. It is particularly suitable in energy systems with high shares of renewable generation. In order to increase the flexibility of the energy system, power-to-heat technologies coupled to thermal storage devices are among the most promising alternatives. Thermal storage is able to provide several benefits such as load management, power quality and continuous power supply. When there is an excess of generation, electricity is converted into heat and stored for subsequent use on demand. In this way, additional power in the situations of increased load is provided, thus contributing to peak shaving, load shifting and energy conservation. The conversion of power into heat is generally performed by electrical resistances or via heat pumps. Despite converting electric power into heat is not convenient from a thermodynamic perspective, power-to-heat applications are gaining an increasing attention due to the low prices of renewable electricity and the increasing surplus of produced electricity that cannot be used. Several advantages, e.g., high efficiency for balancing excess renewable generation and high potential on reduction of $CO_2$ emissions and fossil fuels, could be the key elements for a larger development in the future trends of these technologies.

There are several examples of sensible and latent thermal storage in power-to-heat applications, while only a limited number of applications of thermochemical storage in the power-to-heat field are available. High energy storage density, no heat loss during the storage, no self-discharge and long charge/discharge, broad availability and suitable temperature ranges are some important advantages of thermochemical storage systems.

However, the high complexity and costs of these technologies limit the real applications, while only few prototype-scale systems have been studied. To improve their implementation, comprehensive analyses and investigations are further required. In contrast, thermochemical storage is widely used into heat-to-power sector. Heat-to-power and power-to-heat sectors are among the most relevant options available to balance fluctuating renewable energy sources and hence power grid. This particular interaction between electricity and heat sectors will play an important role towards the cost effective transition to a low carbon energy system with a high penetration of renewable generation.

**Author Contributions:** All authors conceived the research idea and the framework of this review. All authors have read and approved the final manuscript.

**Funding:** This research received no external funding.

**Conflicts of Interest:** All authors declare no conflicts of interest.

## Nomenclature

| | |
|---|---|
| AB | Storage material |
| A,B | Reaction products |
| ALPOs | Aluminophosphates |
| CAES | Compressed air energy storage |
| Cp | Heat capacity (J/(kg K)) |
| CHP | Combined heat and power |
| COP | Coefficient of Performance |
| CSP | Collectors and Concentrating Solar Plant |
| DHS | District heating systems |
| DSM | Demand-side management |
| Δh | Phase change enthalpy (°C) |
| ΔH | Standard reaction enthalpy (J/mol) |
| ΔS | Standard reaction entropy (J/(°C mol)) |
| ΔT | Temperature difference (°C) |
| GHG | Greenhouse gases |
| HCTSR | Hybrid compression thermochemical refrigeration system |
| HPs | Heat pumps |
| HtP | Heat to power |
| LTES | Latent thermal energy storage |
| m | Mass (kg) |
| MVC | Mechanical vapor compression |
| ORC | Organic Rankine cycle |
| PCM | Phase change materials |
| PCR | Phase change redox |
| PtH | Power-to-heat |
| PV | Photovoltaic |
| PV-CaL | Photovoltaic Calcium looping |
| $Q_l$ | Latent energy stored (J) |
| $Q_s$ | Sensible energy stored (J) |
| RES | Renewable energy sources |
| SAPOs | Silico-aluminophosphates |
| STES | Sensible heat storage |
| T | Turbine |
| $T_c$ | Charging temperature (°C) |
| $T_d$ | Discharging temperature (°C) |
| TCTES | Thermochemical thermal energy storage |
| TES | Thermal energy storage |
| TESs | Thermal energy storage systems |
| VRE | Variable renewable electricity |

## References

1. Intergovernmental Panel on Climate Change Climate Change 2014: Mitigation of Climate Change: Working Group III Contribution to the IPCC Fifth Assessment Report. Available online: https://www.ipcc.ch/site/assets/uploads/2018/02/ipcc_wg3_ar5_frontmatter.pdf (accessed on 23 April 2020).
2. Climate Change 2014: Mitigation of Climate Change. Fifth Assessment Report of the Intergovernmental Panel on Climate Change. Available online: https://www.buildup.eu/en/practices/publications/ipcc-2014-climate-change-2014-mitigation-climate-change-contribution-working (accessed on 23 April 2020).

3. Dagoumas, A.S.; Koltsaklis, N.E. Review of models for integrating renewable energy in the generation expansion planning. *Appl. Energy* **2019**, *242*, 1573–1587. [CrossRef]
4. Iovine, A.; Rigaut, T.; Damm, G.; De Santis, E.; Di Benedetto, M.D. Power management for a DC MicroGrid integrating renewables and storages. *Control Eng. Pract.* **2019**, *85*, 59–79. [CrossRef]
5. Matamala, C.; Moreno, R.; Sauma, E. The value of network investment coordination to reduce environmental externalities when integrating renewables: Case on the Chilean transmission network. *Energy Policy* **2019**, *126*, 251–263. [CrossRef]
6. Arteconi, A.; Hewitt, N.J.; Polonara, F. Domestic demand-side management (DSM): Role of heat pumps and thermal energy storage (TES) systems. *Appl. Therm. Eng.* **2013**, *51*, 155–165. [CrossRef]
7. Fang, J.; Liu, Q.; Guo, S.; Lei, J.; Jin, H. Spanning solar spectrum: A combined photochemical and thermochemical process for solar energy storage. *Appl. Energy* **2019**, *247*, 116–126. [CrossRef]
8. Hsieh, E.; Anderson, R. Grid flexibility: The quiet revolution. *Electr. J.* **2017**, *30*, 1–8. [CrossRef]
9. Huber, M.; Dimkova, D.; Hamacher, T. Integration of wind and solar power in Europe: Assessment of flexibility requirements. *Energy* **2014**, *69*, 236–246. [CrossRef]
10. Denholm, P.; Margolis, R.M. Evaluating the limits of solar photovoltaics (PV) in traditional electric power systems. *Energy Policy* **2007**, *35*, 2852–2861. [CrossRef]
11. DeCesaro, J.; Porter, K.; Milligan, M. Wind Energy and Power System Operations: A Review of Wind Integration Studies to Date. *Electr. J.* **2009**, *22*, 34–43.
12. Lund, P.D.; Lindgren, J.; Mikkola, J.; Salpakari, J. Review of energy system flexibility measures to enable high levels of variable renewable electricity. *Renew. Sustain. Energy Rev.* **2015**, *45*, 785–807. [CrossRef]
13. Salpakari, J.; Mikkola, J.; Lund, P.D. Improved flexibility with large-scale variable renewable power in cities through optimal demand side management and power-to-heat conversion. *Energy Convers. Manag.* **2016**, *126*, 649–661. [CrossRef]
14. Bertsch, J.; Growitsch, C.; Lorenczik, S.; Nagl, S. Flexibility in Europe's power sector—An additional requirement or an automatic complement. *Energy Econ.* **2016**, *53*, 118–131. [CrossRef]
15. Denholm, P.; Hand, M. Grid flexibility and storage required to achieve very high penetration of variable renewable electricity. *Energy Policy* **2011**, *39*, 1817–1830. [CrossRef]
16. Reynders, G.; Amaral Lopes, R.; Marszal-Pomianowska, A.; Aelenei, D.; Martins, J.; Saelens, D. Energy flexible buildings: An evaluation of definitions and quantification methodologies applied to thermal storage. *Energy Build.* **2018**, *166*, 372–390. [CrossRef]
17. Vigna, I.; Pernetti, R.; Pasut, W.; Lollini, R. New domain for promoting energy efficiency: Energy Flexible Building Cluster. *Sustain. Cities Soc.* **2018**, *38*, 526–533. [CrossRef]
18. Petersen, M.K.; Edlund, K.; Hansen, L.H.; Bendtsen, J.; Stoustrup, J. A taxonomy for modeling flexibility and a computationally efficient algorithm for dispatch in Smart Grids. In Proceedings of the American Control Conference, Washington, DC, USA, 17–19 June 2013.
19. Graditi, G.; Di Silvestre, M.L.; Gallea, R.; Sanseverino, E.R. Heuristic-based shiftable loads optimal management in smart micro-grids. *IEEE Trans. Ind. Inform.* **2015**, *11*, 271–280. [CrossRef]
20. Ferruzzi, G.; Cervone, G.; Delle Monache, L.; Graditi, G.; Jacobone, F. Optimal bidding in a Day-Ahead energy market for Micro Grid under uncertainty in renewable energy production. *Energy* **2016**, *106*, 194–202. [CrossRef]
21. Enescu, D.; Chicco, G.; Porumb, R.; Seritan, G. Thermal energy storage for grid applications: Current status and emerging trends. *Energies* **2020**, *13*. [CrossRef]
22. van der Roest, E.; Snip, L.; Fens, T.; van Wijk, A. Introducing Power-to-H3: Combining renewable electricity with heat, water and hydrogen production and storage in a neighbourhood. *Appl. Energy* **2020**, *257*, 114024. [CrossRef]
23. Kohlhepp, P.; Harb, H.; Wolisz, H.; Waczowicz, S.; Müller, D.; Hagenmeyer, V. Large-scale grid integration of residential thermal energy storages as demand-side flexibility resource: A review of international field studies. *Renew. Sustain. Energy Rev.* **2019**, *101*, 527–547. [CrossRef]
24. Kiviluoma, J.; Meibom, P. Influence of wind power, plug-in electric vehicles, and heat storages on power system investments. *Energy* **2010**, *35*, 1244–1255. [CrossRef]
25. Stadler, I. Power grid balancing of energy systems with high renewable energy penetration by demand response. *Util. Policy* **2008**, *16*, 90–98. [CrossRef]

26. Bloess, A.; Schill, W.; Zerrahn, A. Power-to-heat for renewable energy integration: A review of technologies, modeling approaches, and fl exibility potentials. *Appl. Energy* **2018**, *212*, 1611–1626. [CrossRef]
27. Hasan, K.N.; Preece, R.; Milanović, J.V. Existing approaches and trends in uncertainty modelling and probabilistic stability analysis of power systems with renewable generation. *Renew. Sustain. Energy Rev.* **2019**, *101*, 168–180. [CrossRef]
28. Steffen, B.; Weber, C. Efficient storage capacity in power systems with thermal and renewable generation. *Energy Econ.* **2013**, *36*, 556–567. [CrossRef]
29. Beccali, M.; Cellura, M.; Mistretta, M. Environmental effects of energy policy in sicily: The role of renewable energy. *Renew. Sustain. Energy Rev.* **2007**, *11*, 282–298. [CrossRef]
30. Navarro, L.; de Gracia, A.; Colclough, S.; Browne, M.; McCormack, S.J.; Griffiths, P.; Cabeza, L.F. Thermal energy storage in building integrated thermal systems: A review. Part 1. active storage systems. *Renew. Energy* **2016**, *88*, 526–547. [CrossRef]
31. De Gracia, A.; Cabeza, L.F. Phase change materials and thermal energy storage for buildings. *Energy Build.* **2015**, *103*, 414–419. [CrossRef]
32. Palizban, O.; Kauhaniemi, K. Energy storage systems in modern grids—Matrix of technologies and applications. *J. Energy Storage* **2016**, *6*, 248–259. [CrossRef]
33. Palomba, V.; Ferraro, M.; Frazzica, A.; Vasta, S.; Sergi, F.; Antonucci, V. Experimental and numerical analysis of a SOFC-CHP system with adsorption and hybrid chillers for telecommunication applications. *Appl. Energy* **2018**, *216*, 620–633. [CrossRef]
34. Vasta, S.; Brancato, V.; La Rosa, D.; Palomba, V.; Restuccia, G.; Sapienza, A.; Frazzica, A. Adsorption heat storage: State-of-the-art and future perspectives. *Nanomaterials* **2018**, *8*. [CrossRef] [PubMed]
35. Scapino, L.; Zondag, H.A.; Van Bael, J.; Diriken, J.; Rindt, C.C.M. Energy density and storage capacity cost comparison of conceptual solid and liquid sorption seasonal heat storage systems for low-temperature space heating. *Renew. Sustain. Energy Rev.* **2017**, *76*, 1314–1331. [CrossRef]
36. Scapino, L.; Zondag, H.A.; Van Bael, J.; Diriken, J.; Rindt, C.C.M. Sorption heat storage for long-term low-temperature applications: A review on the advancements at material and prototype scale. *Appl. Energy* **2017**, *190*, 920–948. [CrossRef]
37. Feng, D.; Feng, Y.; Qiu, L.; Li, P.; Zang, Y.; Zou, H.; Yu, Z.; Zhang, X. Review on nanoporous composite phase change materials: Fabrication, characterization, enhancement and molecular simulation. *Renew. Sustain. Energy Rev.* **2019**, *109*, 578–605. [CrossRef]
38. Badenhorst, H. A review of the application of carbon materials in solar thermal energy storage. *Sol. Energy* **2019**, *192*, 35–68. [CrossRef]
39. Bott, C.; Dressel, I.; Bayer, P. State-of-technology review of water-based closed seasonal thermal energy storage systems. *Renew. Sustain. Energy Rev.* **2019**, *113*, 109241. [CrossRef]
40. Palacios, A.; Cong, L.; Navarro, M.E.; Ding, Y.; Barreneche, C. Thermal conductivity measurement techniques for characterizing thermal energy storage materials—A review. *Renew. Sustain. Energy Rev.* **2019**, *108*, 32–52. [CrossRef]
41. Wu, S.; Yan, T.; Kuai, Z.; Pan, W. Thermal conductivity enhancement on phase change materials for thermal energy storage: A review. *Energy Storage Mater.* **2020**, *25*, 251–295. [CrossRef]
42. Ümitcan, H.; Keles, D.; Chiodi, A.; Hartel, R.; Mikuli, M. Analysis of the power-to-heat potential in the European energy system. *Energy Strategy Rev.* **2018**, *20*, 6–19.
43. Tarroja, B.; Mueller, F.; Eichman, J.D.; Samuelsen, S. Metrics for evaluating the impacts of intermittent renewable generation on utility load-balancing. *Energy* **2012**, *42*, 546–562. [CrossRef]
44. Geyer, P.; Buchholz, M.; Buchholz, R.; Provost, M. Hybrid thermo-chemical district networks—Principles and technology. *Appl. Energy* **2017**, *186*, 480–491. [CrossRef]
45. Federal Energy Regulatory Commission. FERC Benefits of Demand Response in Electricity Markets and Recommendations for Achieving Them. Available online: https://eetd.lbl.gov/sites/all/files/publications/report-lbnl-1252d.pdf (accessed on 23 April 2020).
46. Khudhair, A.M.; Farid, M. A review on energy conservation in building applications with thermal storage by latent heat using phase change materials. *Energy Convers Manag.* **2004**, *45*, 263–275. [CrossRef]
47. Tyagi, V.V.; Buddhi, D. PCM thermal storage in buildings: A state of art. *Renew. Sustain. Energy Rev.* **2007**, *11*, 1146–1166. [CrossRef]

48. Hauer, A.; Fischer, S.; Heinemann, U.; Schreiner, M.S.W. Thermochemical energy storage and heat transformation of district heat for balancing of power in a district heat network (TCS II) Final report. In Proceedings of the Final Report, Bayerisches Zentrum Fuer Angewandte Energieforschung e.V., Wuerzburg, Germany, 1 February 1999.
49. Hauer, A.; Avemann, E.L. Open Absorption Systems for Air Conditioning and Thermal Energy Storage. In *Thermal Energy Storage for Sustainable Energy Consumption*; Springer: Dordrecht, The Netherlands, 2007; pp. 429–444.
50. Wang, W.; Hu, Y.; Yan, J.; Nyström, J.; Dahlquist, E. Combined heat and power plant integrated with mobilized thermal energy storage (M-TES) system. *Front. Energy Power Eng. China* **2010**, *4*, 469–474. [CrossRef]
51. De Coninck, R.; Helsen, L. Quantification of flexibility in buildings by cost curves—Methodology and application. *Appl. Energy* **2016**, *162*, 653–665. [CrossRef]
52. Hachem-Vermette, C.; Guarino, F.; La Rocca, V.; Cellura, M. Towards achieving net-zero energy communities: Investigation of design strategies and seasonal solar collection and storage net-zero. *Sol. Energy* **2019**, *192*, 169–185. [CrossRef]
53. Shkatulov, A.; Ryu, J.; Kato, Y.; Aristov, Y. Composite material "$Mg(OH)_2$/vermiculite": A promising new candidate for storage of middle temperature heat. *Energy* **2012**, *44*, 1028–1034. [CrossRef]
54. Aristov, Y.I. Challenging offers of material science for adsorption heat transformation: A review. *Appl. Therm. Eng.* **2013**, *50*, 1610–1618. [CrossRef]
55. Christidis, A.; Koch, C.; Pottel, L.; Tsatsaronis, G. The contribution of heat storage to the profitable operation of combined heat and power plants in liberalized electricity markets. *Energy* **2012**, *41*, 75–82. [CrossRef]
56. Aghaei, J.; Alizadeh, M.I. Multi-objective self-scheduling of CHP (combined heat and power)-based microgrids considering demand response programs and ESSs (energy storage systems). *Energy* **2013**, *55*, 1044–1054. [CrossRef]
57. Meroueh, L.; Chen, G. Thermal energy storage radiatively coupled to a supercritical Rankine cycle for electric grid support. *Renew. Energy* **2020**, *145*, 604–621. [CrossRef]
58. Fischer, D.; Bernhardt, J.; Madani, H.; Wittwer, C. Comparison of control approaches for variable speed air source heat pumps considering time variable electricity prices and PV. *Appl. Energy* **2017**, *204*, 93–105. [CrossRef]
59. Fischer, D.; Toral, T.R.; Lindberg, K.B.; Wille-Haussmann, B.; Madani, H. Investigation of Thermal Storage Operation Strategies with Heat Pumps in German Multi Family Houses. *Energy Procedia* **2014**, *58*, 137–144. [CrossRef]
60. Battaglia, M.; Haberl, R.; Bamberger, E.; Haller, M. Increased self-consumption and grid flexibility of PV and heat pump systems with thermal and electrical storage. *Energy Procedia* **2017**, *135*, 358–366. [CrossRef]
61. Oudalov, A.; Cherkaoui, R.; Beguin, A. Sizing and optimal operation of battery energy storage system for peak shaving application. In Proceedings of the 2007 IEEE Lausanne POWERTECH, Lausanne, Switzerland, 1–5 July 2007; pp. 621–625.
62. Levron, Y.; Shmilovitz, D. Power systems' optimal peak-shaving applying secondary storage. *Electr. Power Syst. Res.* **2012**, *89*, 80–84. [CrossRef]
63. Péan, T.Q.; Salom, J.; Costa-Castelló, R. Review of control strategies for improving the energy flexibility provided by heat pump systems in buildings. *J. Process Control* **2019**, *74*, 35–49. [CrossRef]
64. Pilpola, S.; Lund, P.D. Different flexibility options for better system integration of wind power. *Energy Strateg. Rev.* **2019**, *26*, 100368. [CrossRef]
65. Stinner, S.; Huchtemann, K.; Müller, D. Quantifying the operational flexibility of building energy systems with thermal energy storages. *Appl. Energy* **2016**, *181*, 140–154. [CrossRef]
66. Le, K.X.; Huang, M.J.; Wilson, C.; Shah, N.N.; Hewitt, N.J. Tariff-based load shifting for domestic cascade heat pump with enhanced system energy efficiency and reduced wind power curtailment. *Appl. Energy* **2020**, *257*, 113976. [CrossRef]
67. Angenendt, G.; Zurmühlen, S.; Rücker, F.; Axelsen, H.; Sauer, D.U. Optimization and operation of integrated homes with photovoltaic battery energy storage systems and power-to-heat coupling. *Energy Convers. Manag. X* **2019**, *1*, 100005. [CrossRef]
68. Lamaison, N.; Collette, S.; Vallée, M.; Bavière, R. Storage influence in a combined biomass and power-to-heat district heating production plant. *Energy* **2019**, *186*, 115714. [CrossRef]

69. Olsthoorn, D.; Haghighat, F.; Mirzaei, P.A. Integration of storage and renewable energy into district heating systems: A review of modelling and optimization. *Sol. Energy* **2016**, *136*, 49–64. [CrossRef]
70. Lund, H.; Werner, S.; Wiltshire, R.; Svendsen, S.; Thorsen, J.E.; Hvelplund, F.; Mathiesen, B.V. 4th Generation District Heating (4GDH). Integrating smart thermal grids into future sustainable energy systems. *Energy* **2014**, *68*, 1–11. [CrossRef]
71. Münster, M.; Morthorst, P.E.; Larsen, H.V.; Bregnbæk, L.; Werling, J.; Lindboe, H.H.; Ravn, H. The role of district heating in the future Danish energy system. *Energy* **2012**, *48*, 47–55. [CrossRef]
72. Mikkola, J.; Lund, P.D. Modeling flexibility and optimal use of existing power plants with large-scale variable renewable power schemes. *Energy* **2016**, *112*, 364–375. [CrossRef]
73. Li, Z.; Wu, W.; Shahidehpour, M.; Wang, J.; Zhang, B. Combined heat and power dispatch considering pipeline energy storage of district heating network. *IEEE Trans. Sustain. Energy* **2016**, *7*, 12–22. [CrossRef]
74. Cellura, M.; Campanella, L.; Ciulla, G.; Guarino, F.; Lo Brano, V.; Cesarini, D.N.; Orioli, A. The redesign of an Italian building to reach net zero energy performances: A case study of the SHC Task 40—ECBCS Annex 52. *ASHRAE Trans.* **2011**, *117*, 331–339.
75. Cellura, M.; Ciulla, G.; Guarino, F.; Longo, S. The redesign of a Rural Building in a Heritage Site in Italy: Towards the Net Zero Energy Target. *Buildings* **2017**, *7*, 68. [CrossRef]
76. Werner, S. International review of district heating and cooling. *Energy* **2017**, *137*, 617–631. [CrossRef]
77. Schmidt, D. Low Temperature District Heating for Future Energy Systems. *Energy Procedia* **2018**, *149*, 595–604. [CrossRef]
78. del Hoyo Arce, I.; Herrero López, S.; López Perez, S.; Rämä, M.; Klobut, K.; Febres, J.A. Models for fast modelling of district heating and cooling networks. *Renew. Sustain. Energy Rev.* **2018**, *82*, 1863–1873. [CrossRef]
79. Andersen, A.N.; Østergaard, P.A. Support schemes adapting district energy combined heat and power for the role as a flexibility provider in renewable energy systems. *Energy* **2020**, *192*, 116639. [CrossRef]
80. Ortiz, J.; Guarino, F.; Salom, J.; Corchero, C.; Cellura, M. Stochastic model for electrical loads in Mediterranean residential buildings: Validation and applications. *Energy Build.* **2014**, *80*, 23–36. [CrossRef]
81. Guarino, F.; Cassarà, P.; Longo, S.; Cellura, M.; Ferro, E. Load match optimisation of a residential building case study: A cross-entropy based electricity storage sizing algorithm. *Appl. Energy* **2015**, *154*, 380–391. [CrossRef]
82. Guney, M.S.; Tepe, Y. Classification and assessment of energy storage systems. *Renew. Sustain. Energy Rev.* **2017**, *75*, 1187–1197. [CrossRef]
83. Tronchin, L.; Manfren, M.; Nastasi, B. Energy efficiency, demand side management and energy storage technologies—A critical analysis of possible paths of integration in the built environment. *Renew. Sustain. Energy Rev.* **2018**, *95*, 341–353. [CrossRef]
84. Singh Gaur, A.; Fitiwi, D.Z.; Curtis, J. Heat Pumps and Their Role in Decarbonising Heating Sector: A Comprehensive Review. Available online: http://aei.pitt.edu/102238/ (accessed on 23 April 2020).
85. Vanhoudt, D.; Geysen, D.; Claessens, B.; Leemans, F.; Jespers, L.; Van Bael, J. An actively controlled residential heat pump: Potential on peak shaving and maximization of self-consumption of renewable energy. *Renew. Energy* **2014**, *63*, 531–543. [CrossRef]
86. Sweetnam, T.; Fell, M.; Oikonomou, E.; Oreszczyn, T. Domestic demand-side response with heat pumps: Controls and tariffs. *Build. Res. Inf.* **2019**, *47*, 344–361. [CrossRef]
87. Patteeuw, D.; Henze, G.P.; Helsen, L. Comparison of load shifting incentives for low-energy buildings with heat pumps to attain grid flexibility benefits. *Appl. Energy* **2016**, *167*, 80–92. [CrossRef]
88. Hedegaard, K.; Mathiesen, B.V.; Lund, H.; Heiselberg, P. Wind power integration using individual heat pumps—Analysis of different heat storage options. *Energy* **2012**, *47*, 284–293. [CrossRef]
89. Fischer, D.; Madani, H. On heat pumps in smart grids: A review. *Renew. Sustain. Energy Rev.* **2017**, *70*, 342–357. [CrossRef]
90. Bach, B.; Werling, J.; Ommen, T.; Münster, M.; Morales, J.M.; Elmegaard, B. Integration of large-scale heat pumps in the district heating systems of Greater Copenhagen. *Energy* **2016**, *107*, 321–334. [CrossRef]
91. Lund, R.; Persson, U. Mapping potential heat sources for heat pumps in district heating in Denmark. *Energy* **2016**, *110*, 129–138. [CrossRef]
92. Arat, H.; Arslan, O. Optimization of district heating system aided by geothermal heat pump: A novel multistage with multilevel ANN modelling. *Appl. Therm. Eng.* **2017**, *111*, 608–623. [CrossRef]

93. Chua, K.J.; Chou, S.K.; Yang, W.M. Advances in heat pump systems: A review. *Appl. Energy* **2010**, *87*, 3611–3624. [CrossRef]
94. Wang, R.; Zhai, X. *Handbook of Energy Systems in Green Buildings*; Springer: Berlin/Heidelberg, Germany, 2018; ISBN 9783662491201.
95. Chwieduk, D. Analysis of Utilisation of Renewable Energies As Heat Sources for Heat. *Renew. Energy* **1996**, *9*, 720–723. [CrossRef]
96. Chwieduk, B.; Chwieduk, D. Performance analysis of a PV driven heat pump system during a heating season in high latitude countries. In Proceedings of the 12 th IEA Heat Pump Conference, Warsaw, Poland, 29 May 2017; pp. 1–10.
97. Kim, J.H.; Shcherbakova, A. Common failures of demand response. *Energy* **2011**, *36*, 873–880. [CrossRef]
98. Hu, J.; Chen, W.; Yang, D.; Zhao, B.; Song, H.; Ge, B. Energy performance of ETFE cushion roof integrated photovoltaic/thermal system on hot and cold days. *Appl. Energy* **2016**, *173*, 40–51. [CrossRef]
99. Bogdan, Ž.; Kopjar, D. Improvement of the cogeneration plant economy by using heat accumulator. *Energy* **2006**, *31*, 2285–2292. [CrossRef]
100. Beck, T.; Kondziella, H.; Huard, G.; Bruckner, T. Optimal operation, configuration and sizing of generation and storage technologies for residential heat pump systems in the spotlight of self-consumption of photovoltaic electricity. *Appl. Energy* **2017**, *188*, 604–619. [CrossRef]
101. Franco, A.; Fantozzi, F. Experimental analysis of a self consumption strategy for residential building: The integration of PV system and geothermal heat pump. *Renew. Energy* **2016**, *86*, 1075–1085. [CrossRef]
102. Jarre, M.; Noussan, M.; Simonetti, M. Primary energy consumption of heat pumps in high renewable share electricity mixes. *Energy Convers. Manag.* **2018**, *171*, 1339–1351. [CrossRef]
103. Zhao, X.; Fu, L.; Wang, X.; Sun, T.; Wang, J.; Zhang, S. Flue gas recovery system for natural gas combined heat and power plant with distributed peak-shaving heat pumps. *Appl. Therm. Eng.* **2017**, *111*, 599–607. [CrossRef]
104. Tjaden, T.; Schnorr, F.; Weniger, J.; Bergner, J.; Quaschning, V. Einsatz von PV-Systemen mit Wärmepumpen und Batteriespeichern zur Erhöhung des Autarkiegrades in Einfamilienhaushalten. In Proceedings of the 30. Symp. Photovoltaische Solarenergi, Berlin, Germany, 4–6 March 2015; p. 20.
105. Fischer, D.; Rautenberg, F.; Wirtz, T.; Wille-Haussmann, B.; Madani, H. Smart Meter Enabled Control for Variable Speed Heat Pumps to Increase PV Self-Consumption. In Proceedings of the 24th IIR International Congress of Refrigeration, Yokohama, Japan, 16–22 August 2015; pp. 4049–4056.
106. Binder, J.; Williams, C.O.O.; Kelm, T. Increasing pv self-consumption, domestic energy autonomy and grid compatibility of pv systems using heat pumps, thermal storage and battery storage. *27 Eur. Photovolt. Sol. Energy Conf. Exhib.* **2012**, 4030–4034. [CrossRef]
107. David, A.; Mathiesen, B.V.; Averfalk, H.; Werner, S.; Lund, H. Heat Roadmap Europe: Large-scale electric heat pumps in district heating systems. *Energies* **2017**, *10*, 578. [CrossRef]
108. Hong, J.; Kelly, N.J.; Richardson, I.; Thomson, M. Assessing heat pumps as flexible load. *Proc. Inst. Mech. Eng. Part A J. Power Energy* **2013**, *227*, 30–42. [CrossRef]
109. Klaassen, E.A.M.; Asare-Bediako, B.; De Koning, C.P.; Frunt, J.; Slootweg, J.G. Assessment of an algorithm to utilize heat pump flexibility-theory and practice. In Proceedings of the 2015 IEEE Eindhoven PowerTech, Eindhoven, The Netherlands, 29 June–2 July 2015.
110. Arteconi, A.; Polonara, F. Assessing the demand side management potential and the energy flexibility of heat pumps in buildings. *Energies* **2018**, *11*, 1846. [CrossRef]
111. Lizana, J.; Chacartegui, R.; Barrios-Padura, A.; Valverde, J.M. Advances in thermal energy storage materials and their applications towards zero energy buildings: A critical review. *Appl. Energy* **2017**, *203*, 219–239. [CrossRef]
112. Tatsidjodoung, P.; Le Pierrès, N.; Luo, L. A review of potential materials for thermal energy storage in building applications. *Renew. Sustain. Energy Rev.* **2013**, *18*, 327–349. [CrossRef]
113. Ciulla, G.; Lo Brano, V.; Cellura, M.; Franzitta, V.; Milone, D. A finite difference model of a PV-PCM system. *Energy Procedia* **2012**, *30*, 198–206. [CrossRef]
114. Bastien, D.; Athienitis, A.K. Passive thermal energy storage, part 2: Design methodology for solaria and greenhouses. *Renew. Energy* **2017**, *103*, 537–560. [CrossRef]

115. Carrillo, A.J.; González-Aguilar, J.; Romero, M.; Coronado, J.M. Solar Energy on Demand: A Review on High Temperature Thermochemical Heat Storage Systems and Materials. *Chem. Rev.* **2019**, *119*, 4777–4816. [CrossRef] [PubMed]
116. Del Pero, C.; Aste, N.; Paksoy, H.; Haghighat, F.; Grillo, S.; Leonforte, F. Energy storage key performance indicators for building application. *Sustain. Cities Soc.* **2018**, *40*, 54–65. [CrossRef]
117. Sarbu, I.; Sebarchievici, C. A comprehensive review of thermal energy storage. *Sustainability* **2018**, *10*, 191. [CrossRef]
118. Cabeza, L.F.; Solé, A.; Barreneche, C. Review on sorption materials and technologies for heat pumps and thermal energy storage. *Renew. Energy* **2017**, *110*, 3–39. [CrossRef]
119. Abedin, A.H. A Critical Review of Thermochemical Energy Storage Systems. *Open Renew. Energy J.* **2011**, *4*, 42–46. [CrossRef]
120. A Review on High Temperature Thermochemical Heat Energy Storage. *Renew. Sustain. Energy Rev.* Available online: https://oatao.univ-toulouse.fr/15979/ (accessed on 23 April 2020).
121. Aydin, D.; Casey, S.P.; Riffat, S. The latest advancements on thermochemical heat storage systems. *Renew. Sustain. Energy Rev.* **2015**, *41*, 356–367. [CrossRef]
122. Alva, G.; Liu, L.; Huang, X.; Fang, G. Thermal energy storage materials and systems for solar energy applications. *Renew. Sustain. Energy Rev.* **2017**, *68*, 693–706. [CrossRef]
123. Thermochemical Energy Storage Systems: Modelling, Analysis and Design. Available online: https://ir.library.dc-uoit.ca/handle/10155/119 (accessed on 23 April 2020).
124. Kuznik, F.; Johannes, K. Thermodynamic efficiency of water vapor/solid chemical sorption heat storage for buildings: Theoretical limits and integration considerations. *Appl. Sci.* **2020**, *10*, 489. [CrossRef]
125. Ding, Y.; Riffat, S.B. Thermochemical energy storage technologies for building applications: A state-of-the-art review. *Int. J. Low-Carbon Technol.* **2013**, *8*, 106–116. [CrossRef]
126. Yu, N.; Wang, R.Z.; Wang, L.W. Sorption thermal storage for solar energy. *Prog. Energy Combust. Sci.* **2013**, *39*, 489–514. [CrossRef]
127. Chen, X.; Wang, F.; Han, Y.; Yu, R.; Cheng, Z. Thermochemical storage analysis of the dry reforming of methane in foam solar reactor. *Energy Convers. Manag.* **2018**, *158*, 489–498. [CrossRef]
128. Sorption Thermal Energy Storage. Available online: https://link.springer.com/chapter/10.1007/978-3-319-96640-3_4 (accessed on 23 April 2020).
129. Krönauer, A.; Lävemann, E.; Brückner, S.; Hauer, A. Mobile Sorption Heat Storage in Industrial Waste Heat Recovery. *Energy Procedia* **2015**, *73*, 272–280. [CrossRef]
130. Reiser, A.; Bogdanović, B.; Schlichte, K. The application of Mg-based metal-hydrides as heat energy storage systems. *Int. J. Hydrogen Energy* **2000**, *25*, 425–430. [CrossRef]
131. Stengler, J.; Linder, M. Thermal energy storage combined with a temperature boost: An underestimated feature of thermochemical systems. *Appl. Energy* **2020**, *262*, 114530. [CrossRef]
132. Tesio, U.; Guelpa, E.; Verda, V. Integration of thermochemical energy storage in concentrated solar power. Part 2: Comprehensive optimization of supercritical $CO_2$ power block. *Energy Convers. Manag. X* **2020**, *6*, 100038. [CrossRef]
133. Koohi-Fayegh, S.; Rosen, M.A. A review of energy storage types, applications and recent developments. *J. Energy Storage* **2020**, *27*, 101047. [CrossRef]
134. Wu, S.; Zhou, C.; Doroodchi, E.; Moghtaderi, B. Techno-economic analysis of an integrated liquid air and thermochemical energy storage system. *Energy Convers. Manag.* **2020**, *205*, 112341. [CrossRef]
135. Lizana, J.; Bordin, C.; Rajabloo, T. Integration of solar latent heat storage towards optimal small-scale combined heat and power generation by Organic Rankine Cycle. *J. Energy Storage* **2020**, *29*, 101367. [CrossRef]
136. Lass-Seyoum, A.; Blicker, M.; Borozdenko, D.; Friedrich, T.; Langhof, T. Transfer of laboratory results on closed sorption thermo- chemical energy storage to a large-scale technical system. *Energy Procedia* **2012**, *30*, 310–320. [CrossRef]
137. van Helden, W.; Thür, A.; Weber, R.; Furbo, S.; Gantenbein, P.; Heinz, A.; Salg, F.; Kerskes, H.; Williamson, T.; Sörensen, H.; et al. Parallel development of three com- pact systems for seasonal solar thermal storage: Introduction. In Proceedings of the Innostock 2012, 12th International Conference on Energy Storage, Llleida, Spain, 16–18 May 2012.

138. van Essen, V.M.; Zondag, H.A.; Schuitema, R.; van Helden, W.G.J.; Rindt, C.C.M.; Van Essen, V.M.; Zondag, H.A.; Schuitema, R.; Van Helden, W.G.J.; Rindt, C.C.M. Materials for thermochemical storage: Characterization of magnesium sulfate. In Proceedings of the Proceedings Eurosun, Lisbon, Portugal, 7–10 October 2008; pp. 4–9.
139. Cammarata, A.; Verda, V.; Sciacovelli, A.; Ding, Y. Hybrid strontium bromide-natural graphite composites for low to medium temperature thermochemical energy storage: Formulation, fabrication and performance investigation. *Energy Convers. Manag.* **2018**, *166*, 233–240. [CrossRef]
140. Poppi, S.; Sommerfeldt, N.; Bales, C.; Madani, H.; Lundqvist, P. Techno-economic review of solar heat pump systems for residential heating applications. *Renew. Sustain. Energy Rev.* **2018**, *81*, 22–32. [CrossRef]
141. IUPAC Compendium of Chemical Terminology. Available online: http://publications.iupac.org/compendium/index.html (accessed on 24 March 2020).
142. Kuravi, S.; Trahan, J.; Goswami, D.Y.; Rahman, M.M.; Stefanakos, E.K. Thermal energy storage technologies and systems for concentrating solar power plants. *Prog. Energy Combust. Sci.* **2013**, *39*, 285–319. [CrossRef]
143. Sobri, S.; Koohi-Kamali, S.; Rahim, N.A. Solar photovoltaic generation forecasting methods: A review. *Energy Convers. Manag.* **2018**, *156*, 459–497. [CrossRef]
144. Stutz, B.; Le Pierres, N.; Kuznik, F.; Johannes, K.; Palomo Del Barrio, E.; Bédécarrats, J.P.; Gibout, S.; Marty, P.; Zalewski, L.; Soto, J.; et al. Stockage thermique de l'énergie solaire. *Comptes Rendus Phys.* **2017**, *18*, 401–414. [CrossRef]
145. Le Pierrès, N.; Huaylla, F.; Stutz, B.; Perraud, J. Long-term solar heat storage process by absorption with the KCOOH/$H_2O$ couple: Experimental investigation. *Energy* **2017**, *141*, 1313–1323. [CrossRef]
146. Bush, H.E.; Loutzenhiser, P.G. Solar electricity via an Air Brayton cycle with an integrated two-step thermochemical cycle for heat storage based on $Fe_2O_3/Fe_3O_4$ redox reactions: Thermodynamic and kinetic analyses. *Sol. Energy* **2018**, *174*, 617–627. [CrossRef]
147. Hutchings, K.N.; Wilson, M.; Larsen, P.A.; Cutler, R.A. Kinetic and thermodynamic considerations for oxygen absorption/desorption using cobalt oxide. *Solid State Ionics* **2006**, *177*, 45–51. [CrossRef]
148. Singh, A.; Tescari, S.; Lantin, G.; Agrafiotis, C.; Roeb, M.; Sattler, C. Solar thermochemical heat storage via the $Co_3O_4$/CoO looping cycle: Storage reactor modelling and experimental validation. *Sol. Energy* **2017**, *144*, 453–465. [CrossRef]
149. Balasubramanian, G.; Ghommem, M.; Hajj, M.R.; Wong, W.P.; Tomlin, J.A.; Puri, I.K. Modeling of thermochemical energy storage by salt hydrates. *Int. J. Heat Mass Transf.* **2010**, *53*, 5700–5706. [CrossRef]
150. Visscher, K.; Veldhuis, J.B.J. Comparison of candidate materials for seasonal storage of solar heat through dynamic simulation of building and renewable energy system. In Proceedings of the Ninth International IBPSA Conference, Montreal, QC, Canada, 15–18 August 2005; pp. 1285–1292.
151. Lucio, B.; Romero, M.; González-Aguilar, J. Analysis of solid-state reaction in the performance of doped calcium manganites for thermal storage. *Solid State Ionics* **2019**, *338*, 47–57. [CrossRef]
152. Imponenti, L.; Albrecht, K.J.; Wands, J.W.; Sanders, M.D.; Jackson, G.S. Thermochemical energy storage in strontium-doped calcium manganites for concentrating solar power applications. *Sol. Energy* **2017**, *151*, 1–13. [CrossRef]
153. Henninger, S.K.; Habib, H.A.; Janiak, C. MOFs as Adsorbents for Low Temperature Heating and Cooling Applications. *J. Am. Chem. Soc.* **2009**, *131*, 2776–2777. [CrossRef] [PubMed]
154. N'Tsoukpoe, K.E.; Perier-Muzet, M.; Le Pierrès, N.; Luo, L.; Mangin, D. Thermodynamic study of a LiBr–$H_2O$ absorption process for solar heat storage with crystallisation of the solution. *Sol. Energy* **2014**, *104*, 2–15. [CrossRef]
155. Leonzio, G. Solar systems integrated with absorption heat pumps and thermal energy storages: State of art. *Renew. Sustain. Energy Rev.* **2017**, *70*, 492–505. [CrossRef]
156. Hui, L.; N'Tsoukpoe, K.E.; Lingai, L. Evaluation of a seasonal storage system of solar energy for house heating using different absorption couples. *Energy Convers Manag.* **2011**, *52*, 2427–2436. [CrossRef]
157. Li, G.; Hwang, Y.; Radermacher, R. Radermacher Review of cold storage materials for air condition application. *Int. J. Refrig* **2012**, *35*, 2053–2077. [CrossRef]
158. Yu, N.; Wang, R.Z.; Wang, L.W. Theoretical and experimental investigation of a closed sorption thermal storage prototype using LiCl/water. *Energy* **2015**, *93*, 1523–1534. [CrossRef]
159. Zhang, Y.N.; Wang, R.Z.; Li, T.X. Experimental investigation on an open sorption thermal storage system for space heating. *Energy* **2017**, *141*, 2421–2433. [CrossRef]

160. Zhao, Y.J.; Wang, R.Z.; Li, T.X.; Nomura, Y. Investigation of a 10 kWh sorption heat storage device for effective utilization of low-grade thermal energy. *Energy* **2016**, *113*, 739–747. [CrossRef]
161. Advanced Storage Concepts for Solar and Low Energy Buildings of the Solar Heating and Cooling Programme of the International Energy Agency. 23 Pages Final Report of Subtask B—Chemical and Sorption Storage. Available online: https://www.iea-shc.org/publications-category?CategoryID=63 (accessed on 23 April 2020).
162. Rammelberg, H.U.; Schmidt, T.; Ruck, W. Hydration and dehydration of salt hydrates and hydroxides for thermal energy storage—kinetics and energy release. *Energy Procedia* **2012**, *30*, 362–369. [CrossRef]
163. Fumey, B.; Weber, R.; Gantenbein, P.; Daguenet-Frick, X.; Stoller, S.; Fricker, R.; Dorer, V. Operation Results of a Closed Sorption Heat Storage Prototype. *Energy Procedia* **2015**, *73*, 324–330. [CrossRef]
164. Daguenet-Frick, X.; Dudita, M.; Omlin, L.; Paul, G. Seasonal Thermal Energy Storage with Aqueous Sodium Hydroxide—Development and Measurements on the Heat and Mass Exchangers. *Energy Procedia* **2018**, *155*, 286–294. [CrossRef]
165. Lepinasse, E.; Spinner, B. Production de froid par couplage de re´acteurs solide-gaz II: Performance d'un pilote de 1 à 2 kW. *Rev. Int. Froid.* **1994**, *17*, 323–328. [CrossRef]
166. Bao, H.S.; Oliveira, R.Z.; Wang, R.Z.; Wang, L.W. Choice of low temperature salt for a resorption refrigerator. *Ind. Eng. Chem. Res.* **2010**, *49*, 4897–4903. [CrossRef]
167. Bao, H.S.; Wang, R.Z.; Wang, L.W. A resorption refrigerator driven by low grade thermal energy. *Energy Convers. Manag.* **2011**, *52*, 2339–2344. [CrossRef]
168. Oliveira, R.G.; Wang, R.Z.; Kiplagat, J.K.; Wang, C.Y. Novel composite sorbent for resorption systems and for chemisorption air conditioners driven by low generation temperature. *Renew. Energy* **2009**, *34*, 2757–2764. [CrossRef]
169. Wang, C.; Zhang, P.; Wang, R.Z. Performance of solid–gas reaction heat transformer system with gas valve control. *Chem. Eng. Sci.* **2010**, *65*, 2910–2920. [CrossRef]
170. Ma, Z.; Bao, H.; Roskilly, A.P. Seasonal solar thermal energy storage using thermochemical sorption in domestic dwellings in the UK. *Energy* **2019**, *166*, 213–222. [CrossRef]
171. Wu, S.; Li, T.X.; Yan, T.; Wang, R.Z. Advanced thermochemical resorption heat transformer for high-efficiency energy storage and heat transformation. *Energy* **2019**, *175*, 1222–1233. [CrossRef]
172. Nevau, P.; Mazet, N.; Michel, B. Experimental investigation of an innovative thermochemical process operating with a hydrate salt and moist air for thermal storage of solar energy. *Appl. Energy* **2014**, *129*, 177–186.
173. Ferrucci, F.; Stitou, D.; Ortega, P.; Lucas, F. Mechanical compressor-driven thermochemical storage for cooling applications in tropical insular regions. Concept and efficiency analysis. *Appl. Energy* **2018**, *219*, 240–255. [CrossRef]
174. Lehmann, C.; Beckert, S.; Gläser, R.; Kolditz, O.; Nagel, T. Assessment of adsorbate density models for numerical simulations of zeolite-based heat storage applications. *Appl. Energy* **2017**, *185*, 1965–1970. [CrossRef]
175. Finck, C.; Li, R.; Kramer, R.; Zeiler, W. Quantifying demand flexibility of power-to-heat and thermal energy storage in the control of building heating systems. *Appl. Energy* **2018**, *209*, 409–425. [CrossRef]
176. Zettl, B.; Englmair, G.; Steinmaurer, G. Development of a revolving drum reactor for open-sorption heat storage processes. *Appl. Therm. Eng.* **2014**, *70*, 42–49. [CrossRef]
177. Kerskes, H.; Mette, B.; Bertsch, F.; Asenbeck, S.; Drück, H. Development of a thermo-chemical energy storage for solar thermal applications. In Proceedings of the ISES, Solar World Congress, Kassel, Germany, 28 August–2 September 2011.
178. Energy-Hub for Residential and Commercial Districts and Transport.D3.2 Report on a Combination of Thermal Storage Techniques and Components. Available online: https://www.e-hub.org/pdf/D3.2_Thermal_storage_techniques_components.pdf (accessed on 23 April 2020).
179. de Boer, R.; Smeding, S.; Zondag, H.A.; Krol, G. Development of a prototype system for seasonal solar heat storage using an open sorption process. In Proceedings of the Eurotherm Semin, #99—Adv Therm Energy Storage, Lleida, Spain, 28–30 May 2014; pp. 1–9.
180. Johannes, K.; Kuznik, F.; Hubert, J.-L.; Durier, F.; Obrecht, C. Design and characterisation of a high powered energy dense zeolite thermal energy storage system for buildings. *Appl. Energy* **2015**, *159*, 80–86. [CrossRef]

181. Tatsidjodoung, P.; Le Pierrès, N.; Heintz, J.; Lagre, D.; Luo, L.; Durier, F. Experimental and numerical investigations of a zeolite 13X/water reactor for solar heat storage in buildings. *Energy Convers. Manag.* **2016**, *108*, 488–500. [CrossRef]
182. Mehlhorn, D.; Valiullin, R.; Kärger, J.; Schumann, K.; Brandt, A.; Unger, B. Transport enhancement in binderless zeolite X- and A-type molecular sieves revealed by PFG NMR diffusometry. *Elesvier* **2014**, *188*, 126–132. [CrossRef]
183. Chan, K.C.; Chao, C.Y.H.; Sze-To, G.N.; Hui, K.S. Performance predictions for a new zeolite 13X/$CaCl_2$ composite adsorbent for adsorption cooling systems. *Int. J. Heat Mass Transf.* **2012**, *55*, 3214–3224. [CrossRef]
184. Hongois, S.; Kuznik, F.; Stevens, P.; Roux, J.J. Development and characterisation of a new MgSO4-zeolite composite for long-term thermal energy storage. *Sol. Energy Mater. Sol. Cells* **2011**, *95*, 1831–1837. [CrossRef]
185. Whiting, G.T.; Grondin, D.; Stosic, D.; Bennici, S.; Auroux, A. Zeolite-$MgCl_2$ composites as potential long-term heat storage materials: Influence of zeolite properties on heats of water sorption. *Sol. Energy Mater. Sol. Cells* **2014**, *128*, 289–295. [CrossRef]
186. Dawoud, B.; Aristov, Y. Experimental study on the kinetics of water vapour sorption on selective water sorbents, silica gel and alumina under typical operating conditions of sorption heat pumps. *Int. J. Heat Mass Transf.* **2003**, *46*, 273–281. [CrossRef]
187. Jänchen, J.; Schumann, K.; Thrun, E.; Brandt, A.; Unger, B.; Hellwig, U. Preparation, hydrothermal stability and thermal adsorption storage properties of binderless zeolite beads. *Int. J. Low-Carbon Technol.* **2012**, *7*, 275–279. [CrossRef]
188. Englmair, G.; Zettl, B.; Lager, D. Characterisation of a Rotating Adsorber Designed for Thermochemical Heat Storage Processes. In Proceedings of the EUROSUN2014, International Conference on Solar Energy and Buildings, EuroSun Aix-les-Bains, France, 16–19 September 2015; pp. 1–8.
189. Finck, C.; Henquet, E.; van Soest, C.; Oversloot, H.; de Jong, A.-J.; Cuypers, R.; van't Spijker, H. Experimental Results of a 3 kWh Thermochemical Heat Storage Module for Space Heating Application. *Energy Procedia* **2014**, *48*, 320–326. [CrossRef]
190. Cuypers, R.; Maraz, N.; Eversdijk, J.; Finck, C.; Henquet, E.; Oversloot, H.; van't Spijker, H.; de Geus, A. Development of a Seasonal Thermochemical Storage System. *Energy Procedia* **2012**, *30*, 207–214. [CrossRef]
191. Jänchen, J.; Ackermann, D.; Weiler, E.; Stach, H.; Brösicke, W. Calorimetric investigation on zeolites, AlPO4's and $CaCl_2$ impregnated attapulgite for thermochemical storage of heat. *Thermochim. Acta* **2005**, *434*, 37–41. [CrossRef]
192. Engel, G. Sorption thermal energy storage: Hybrid coating/granules adsorber design and hybrid TCM/PCM operation. *Energy Convers. Manag.* **2019**, *184*, 466–474. [CrossRef]
193. Calabrese, L.; Brancato, V.; Palomba, V.; Frazzica, A.; Cabeza, L.F. Magnesium sulphate-silicone foam composites for thermochemical energy storage: Assessment of dehydration behaviour and mechanical stability. *Sol. Energy Mater. Sol. Cells* **2019**, *200*, 109992. [CrossRef]
194. Fasano, M.; Falciani, G.; Brancato, V.; Palomba, V.; Asinari, P.; Chiavazzo, E.; Frazzica, A. Atomistic modelling of water transport and adsorption mechanisms in silicoaluminophosphate for thermal energy storage. *Appl. Therm. Eng.* **2019**, *160*, 114075. [CrossRef]
195. Oliveira, R.G.; Wang, R. A consolidated calcium chloride-expanded graphite compound for use in sorption refrigeration systems. *Carbon N. Y.* **2007**, *45*, 390–396. [CrossRef]
196. Oliveira, R.G.; Wang, R.Z.; Wang, C. Evaluation of the cooling performance of a consolidated expanded graphite-calcium chloride reactive bed for chemi- sorption icemaker. *Int. J. Refrig.* **2007**, *30*, 103–112. [CrossRef]
197. Van Pal, M.D.; Smeding, S. Thermally driven ammonia-salt type ii heat pump: Development and test of a prototype licl. *Energy* **2007**, 2–7. [CrossRef]
198. Aidoun, Z.; Ternan, M. Salt impregnated carbon fibres as the reactive medium in a chemical heat pump: The $NH_3$–$CoCl_2$ system. *Appl. Therm. Eng.* **2002**, *22*, 1163–1174. [CrossRef]
199. Ristic´, A.; Logar, N.Z.; Henninger, S.K. The performance of small-pore- microporous aluminophosphates in low-temperature solar energy storage: The structure-property relationship. *Adv. Funct. Mater.* **2012**, *22*, 1952–1957. [CrossRef]
200. Kuznik, F.; Johannes, K.; Obrecht, C.; David, D. A review on recent developments in physisorption thermal energy storage for building applications. *Renew. Sustain. Energy Rev.* **2018**, *94*, 576–586. [CrossRef]

201. Jänchen, J.; Ackermann, D.; Stach, H.; Brösicke, W. Studies of the water adsorption on Zeolites and modified mesoporous materials for seasonal storage of solar heat. *Sol. Energy* **2004**, *76*, 339–344. [CrossRef]
202. Developed Materials for Thermal Energy Storage: Synthesis and Characterization. Available online: https://www.sciencedirect.com/science/article/pii/S1876610214027453 (accessed on 23 April 2020).
203. Ponomarenko, I.V.; Glaznev, I.S.; Gubar, A.V.; Aristov, Y.I.; Kirik, S.D. Synthesis and water sorption properties of a new composite "$CaCl_2$ confined into SBA-15 pores". *Microporous Mesoporous Mater.* **2010**, *129*, 243–250. [CrossRef]
204. Tanashev, Y.Y.; Krainov, A.V.; Aristov, Y. Thermal conductivity of composite sorbents "salt in porous matrix" for heat storage and transformation. *Appl. Therm. Eng.* **2014**, *61*, 96–99. [CrossRef]
205. Mahon, D.; Henshall, P.; Claudio, G.; Eames, P.C. Feasibility study of $MgSO_4$ $^+$ zeolite based composite thermochemical energy stores charged by vacuum flat plate solar thermal collectors for seasonal thermal energy storage. *Renew. Energy* **2020**, *145*, 1799–1807. [CrossRef]
206. Wang, Q.; Xie, Y.; Ding, B.; Yu, G.; Ye, F.; Xu, C. Structure and hydration state characterizations of $MgSO_4$-zeolite 13x composite materials for long-term thermochemical heat storage. *Sol. Energy Mater. Sol. Cells* **2019**, *200*, 110047. [CrossRef]
207. Posern, K.; Kaps, C. Calorimetric studies of thermochemical heat storage materials based on mixtures of $MgSO_4$ and $MgCl_2$. *Thermochim. Acta* **2010**, *129*, 243–250. [CrossRef]
208. Casey, S.P.; Elvins, J.; Riffat, S.; Robinson, A. Salt impregnated desiccant matrices for "open" thermochemical energy storage—Selection, synthesis and characterisation of candidate materials. *Energy Build.* **2014**, *84*, 412–425. [CrossRef]
209. Chen, C.; Lovegrove, K.M.; Sepulveda, A.; Lavine, A.S. Design and optimization of an ammonia synthesis system for ammonia-based solar thermochemical energy storage. *Sol. Energy* **2018**, *159*, 992–1002. [CrossRef]
210. Liu, T.; Bai, Z.; Zheng, Z.; Liu, Q.; Lei, J.; Sui, J.; Jin, H. 100 kWe power generation pilot plant with a solar thermochemical process: Design, modeling, construction, and testing. *Appl. Energy* **2019**, *251*, 113217. [CrossRef]
211. Zondag, H.; Kikkert, B.; Smeding, S.; de Boer, R.; Bakker, M. Prototype thermo- chemical heat storage with open reactor system. *Appl. Energy* **2013**, *109*, 360–365. [CrossRef]
212. Study on Medium-Temperature Chemical Heat Storage Using Mixed Hydroxides. Available online: https://www.sciencedirect.com/science/article/abs/pii/S0140700709000449 (accessed on 23 April 2020).
213. Bayon, A.; Bader, R.; Jafarian, M.; Fedunik-Hofman, L.; Sun, Y.; Hinkley, J.; Miller, S.; Lipiński, W. Techno-economic assessment of solid–gas thermochemical energy storage systems for solar thermal power applications. *Energy* **2018**, *149*, 473–484. [CrossRef]
214. Mastronardo, E.; Bonaccorsi, L.; Kato, Y.; Piperopoulos, E.; Milone, C. Efficiency improvement of heat storage materials for $MgO/H_2O/Mg(OH)_2$ chemical heat pumps. *Appl. Energy* **2016**, *162*, 31–39. [CrossRef]
215. Shkatulov, A.; Krieger, T.; Zaikovskii, V.; Chesalov, Y.; Aristov, Y. Doping magnesium hydroxide with sodium nitrate: A new approach to tune the dehydration reactivity of heat-storage materials. *ACS Appl. Mater. Interfaces* **2014**, *6*, 19966–19977. [CrossRef]
216. Sunku Prasad, J.; Muthukumar, P.; Desai, F.; Basu, D.N.; Rahman, M.M. A critical review of high-temperature reversible thermochemical energy storage systems. *Appl. Energy* **2019**, *254*, 113733. [CrossRef]
217. Huang, C.; Xu, M.; Huai, X. Experimental investigation on thermodynamic and kinetic of calcium hydroxide dehydration with hexagonal boron nitride doping for thermochemical energy storage. *Chem. Eng. Sci.* **2019**, *206*, 518–526. [CrossRef]
218. Sheppard, D.A.; Humphries, T.D.; Buckley, C.E. Sodium-based hydrides for thermal energy applications. *Appl. Phys. A Mater. Sci. Process.* **2016**, *122*, 406. [CrossRef]
219. Shen, D.; Zhao, C.Y. Thermal analysis of exothermic process in a magnesium hydride reactor with porous metals. *Chem. Eng. Sci.* **2013**, *98*, 273–281. [CrossRef]
220. Rönnebro, E.C.E.; Whyatt, G.; Powell, M.; Westman, M.; Zheng, F.; Fang, Z.Z. Metal hydrides for high-temperature power generation. *Energies* **2015**, *8*, 8406–8430. [CrossRef]
221. Pan, Z.; Zhao, C.Y. Dehydration/hydration of $MgO/H_2O$ chemical thermal storage system. *Energy* **2015**, *82*, 611–618. [CrossRef]
222. Shkatulov, A.I.; Kim, S.T.; Miura, H.; Kato, Y.; Aristov, Y.I. Adapting the $MgO\text{-}CO_2$ working pair for thermochemical energy storage by doping with salts. *Energy Convers. Manag.* **2019**, *185*, 473–481. [CrossRef]

223. Gigantino, M.; Kiwic, D.; Steinfeld, A. Thermochemical energy storage via isothermal carbonation-calcination cycles of MgO-stabilized SrO in the range of 1000–1100 °C. *Sol. Energy* **2019**, *188*, 720–729. [CrossRef]
224. Donkers, P.A.J.; Pel, L.; Adana, O.C.G. Experimental studies for the cyclability of salt hydrates for thermochemical heat storage. *J. Energy Storage* **2016**, *5*, 25–32. [CrossRef]
225. Solé, A.; Martorell, I.; Cabeza, L.F. State of the art on gas-solid thermochemical energy storage systems and reactors for building applications. *Renew. Sustain. Energy Rev.* **2015**, *47*, 386–398. [CrossRef]
226. Gil, A.; Medrano, M.; Martorell, I.; Lázaro, A.; Dolado, P.; Zalba, B.; Cabeza, L.F. State of the art on high temperature thermal energy storage for power generation. Part 1—Concepts, materials and modellization. *Renew. Sustain. Energy Rev.* **2010**, *14*, 31–55. [CrossRef]
227. Zondag, H.A.; van Essen, V.M.; Bleijendaal, L.P.J.; Kikkert, B.; Bakker, M. Application of $MgCl_2$ $6H_2O$ for thermochemical seasonal solar heat storage. In Proceedings of the 5th Int Renew Energy Storage Conference IRES 2010, Berlin, Germany, 22–24 November 2010.
228. Mehrabadi, A.; Farid, M. New salt hydrate composite for low-grade thermal energy storage. *Energy* **2018**, *164*, 194–203. [CrossRef]
229. De Boer, R.; Haije, W.G.; Veldhuis, J.B.J.; Smeding, S.F. Solid-sorption cooling with integrated thermal storage the SWEAT prototype. In Proceedings of the International Conference Heat Powered Cycles, Larnaca, Cyprus, 10–13 October 2004.
230. Sakamoto, Y.; Yamamoto, H. Performance of Thermal Energy Storage Unit Using Solid Ammoniated Salt ($CaCl_2$-$NH_3$ System). *Nat. Resour.* **2014**, *5*, 337–342.
231. Review on Advanced of Solar Assisted Chemical Heat Pump Dryer for Agriculture Produce. Available online: https://www.sciencedirect.com/science/article/abs/pii/S1364032110003473 (accessed on 23 April 2020).
232. Stitou, D.; Mazet, N.; Mauran, S. Experimental investigation of a solid/gas thermochemical storage process for solar air conditioning. *Energy* **2012**, *41*, 261–270. [CrossRef]
233. Chen, X.; Zhang, D.; Wang, Y.; Ling, X.; Jin, X. The role of sensible heat in a concentrated solar power plant with thermochemical energy storage. *Energy Convers. Manag.* **2019**, *190*, 42–53. [CrossRef]
234. Khosa, A.A.; Zhao, C.Y. Heat storage and release performance analysis of $CaCO_3$/CaO thermal energy storage system after doping nano silica. *Sol. Energy* **2019**, *188*, 619–630. [CrossRef]
235. Fernández, R.; Ortiz, C.; Chacartegui, R.; Valverde, J.M.; Becerra, J.A. Dispatchability of solar photovoltaics from thermochemical energy storage. *Energy Convers. Manag.* **2019**, *191*, 237–246. [CrossRef]
236. Ortiz, C.; Valverde, J.M.; Chacartegui, R.; Perez-Maqueda, L.A. Carbonation of Limestone Derived CaO for Thermochemical Energy Storage: From Kinetics to Process Integration in Concentrating Solar Plants. *ACS Sustain. Chem. Eng.* **2018**, *6*, 6404–6417. [CrossRef]
237. Meroueh, L.; Yenduru, K.; Dasgupta, A.; Jiang, D.; AuYeung, N. Energy storage based on $SrCO_3$ and Sorbents—A probabilistic analysis towards realizing solar thermochemical power plants. *Renew. Energy* **2019**, *133*, 770–786. [CrossRef]
238. Takasu, H.; Hoshino, H.; Tamura, Y.; Kato, Y. Performance evaluation of thermochemical energy storage system based on lithium orthosilicate and zeolite. *Appl. Energy* **2019**, *240*, 1–5. [CrossRef]
239. Kerskes, H.; Mette, B.; Bertsch, F.; Asenbeck, S.; Drück, H. Chemical energy storage using reversible solid/gas-reactions (CWS)—Results of the research project. *Energy Procedia* **2012**, *30*, 294–304. [CrossRef]
240. Pebernet, L.; Ferrieres, X.; Pernet, S.; Michielsen, B.L.; Rogier, F.; Degond, P. Discontinuous Galerkin method applied to electromagnetic compatibility problems: Introduction of thin wire and thin resistive material models. *IET Sci. Meas. Technol.* **2008**, *2*, 395–401. [CrossRef]
241. Bales, C.; Gantenbein, P.; Jaenig, D.; Kerskes, H.; Summer, K.; Van Essen, M.; Weber, R. Laboratory Tests of Chemical Reactions and Prototype Sorption Storage Units, A Report of IEA Solar Heating and Cooling programme—Task 32. *Sol. Heat. Cool. Program. IET Sci. Meas. Technol.* **2008**, *2*, 395–401.
242. Iammak, K.; Wongsuwan, W.; Kiatsiriroj, T. Investigation of modular chemical energy storage performance. In Proceedings of the Proc jt int conf energy environ, Hua Hin, Thailand, 1–3 December 2004.
243. Koepf, E.; Villasmil, W.; Meiera, A. Pilot-scale solar reactor operation and characterization for fuel production via the Zn/ZnO thermochemical cycle. *J. Appl. Energy* **2015**, *165*, 1004–1023. [CrossRef]
244. Agrafiotis, C.; Thomey, D.; de Oliveira, L.; Happich, C.; Roeb, M.; Sattler, C.; Tsongidis, N.I.; Sakellariou, K.G.; Pagkoura, C.; Karagiannakis, G.; et al. Oxide particles as combined heat storage medium and sulphur trioxide decomposition catalysts for solar hydrogen production through sulphur cycles. *Int. J. Hydrogen Energy* **2019**, *44*, 9830–9840. [CrossRef]

245. Wu, S.; Zhou, C.; Doroodchi, E.; Moghtaderi, B. Thermodynamic analysis of a novel hybrid thermochemical-compressed air energy storage system powered by wind, solar and/or off-peak electricity. *Energy Convers. Manag.* **2019**, *180*, 1268–1280. [CrossRef]
246. Tescari, S.; Singh, A.; Agrafiotis, C.; de Oliveira, L.; Breuer, S.; Schlögl-Knothe, B.; Roeb, M.; Sattler, C. Experimental evaluation of a pilot-scale thermochemical storage system for a concentrated solar power plant. *Appl. Energy* **2017**, *189*, 66–75. [CrossRef]
247. Zhou, X.; Mahmood, M.; Chen, J.; Yang, T.; Xiao, G.; Ferrari, M.L. Validated model of thermochemical energy storage based on cobalt oxides. *Appl. Therm. Eng.* **2019**, *159*, 113965. [CrossRef]
248. Yilmaz, D.; Darwish, E.; Leion, H. Investigation of the combined Mn-Si oxide system for thermochemical energy storage applications. *J. Energy Storage* **2020**, *28*, 101180. [CrossRef]
249. Smithson, G.L.; Bakhshi, N.N. The kinetics and mechanism of the hydation of magnesium oxide in a batch reactor. *Can. J. Chem. Eng.* **1969**, *47*, 508–513. [CrossRef]
250. Feitknecht, W.; Braun, H. Der Mechanismus der Hydratation von Magnesiumoxid mit Wasserdampf. *Helv. Chim. Acta* **1967**, *50*, 2040–2053. [CrossRef]
251. Dai, L.; Long, X.F.; Lou, B.; Wu, J. Thermal cycling stability of thermochemical energy storage system $Ca(OH)_2$/CaO. *Appl. Therm. Eng.* **2018**, *133*, 261–268. [CrossRef]
252. Schaube, F.; Kohzer, A.; Schutz, J.; Worner, A.; Müller-Steinhagen, H. De- and rehy- dration of $Ca(OH)_2$ in a reactor with direct heat transfer for thermochemical heat storage. Part A: Experimental results. *Chem. Eng. Res. Des.* **2013**, *91*, 856–864. [CrossRef]
253. Fujii, I.; Tsuchiya, K.; Higano, M.; Yamada, J. Studies of an energy storage system by use of the reversible chemical reaction: $CaO + H_2O \rightleftharpoons Ca(OH)_2$. *Sol. Energy* **1985**, *34*, 367–377. [CrossRef]
254. Yan, J.; Zhao, C.Y. Experimental study of $CaO/Ca(OH)_2$ in a fixed-bed reactor for thermochemical heat storage. *Appl. Energy* **2016**, *175*, 277–284. [CrossRef]
255. Cosquillo Mejia, A.; Afflerbach, S.; Linder, M.; Schmidt, M. Experimental analysis of encapsulated $CaO/Ca(OH)_2$ granules as thermochemical storage in a novel moving bed reactor. *Appl. Therm. Eng.* **2020**, *169*, 114961. [CrossRef]
256. Long, X.F.; Dai, L.; Lou, B.; Wu, J. The kinetics research of thermochemical energy storage system Ca(OH)(2)/CaO. *Int. J. Energy Res.* **2017**, *41*, 1004–1013. [CrossRef]
257. Andre, L.; Abanades, S.; Flamant, G. Screening of thermochemical systems based on solid-gas reversible reactions for high temperature solar thermal energy storage. *Renew. Sustain. Energy Rev.* **2016**, *64*, 707–715. [CrossRef]
258. Yuan, Y.; Li, Y.; Zhao, J. Development on thermochemical energy storage based on CaO-based materials: A review. *Sustainability* **2018**, *10*, 2660. [CrossRef]
259. Composite Material for High-Temperature Thermochemical Energy Storage Using Calcium Hydroxide and Ceramic Foam. Available online: https://onlinelibrary.wiley.com/doi/full/10.1002/est2.53 (accessed on 29 March 2020).
260. Ogura, H.; Yamamoto, T.; Kage, H. Efficiencies of $CaO/H_2O/Ca(OH)_2$ Chemical Heat Pump for Heat Storing and Heating/Cooling. *Energy* **2003**, *28*, 1479–1493. [CrossRef]
261. Arjmand, M.; Liu, L.; Neretnieks, I. Exergetic Efficiency of High-Temperature-Lift Chemical Heat Pump (CHP) Based on $CaO/CO_2$ and $CaO/H_2O$ Working Pairs. *Int. J. Energy Res.* **2013**, *37*, 1122–1131. [CrossRef]
262. Mette, B.; Kerskes, H.; Drück, H.; Müller-Steinhagen, H. New highly efficient regeneration process for thermochemical energy storage. *Appl. Energy* **2013**, *109*, 352–359. [CrossRef]
263. Shelyapina, M.G. Metal hydrides for energy storage. *Handb. Ecomater.* **2019**, *2*, 775–810.
264. Humphries, T.D.; Sheppard, D.A.; Li, G.; Rowles, M.R.; Paskevicius, M.; Matsuo, M.; Aguey-Zinsou, K.F.; Sofianos, M.V.; Orimo, S.I.; Buckley, C.E. Complex hydrides as thermal energy storage materials: Characterisation and thermal decomposition of $Na_2Mg_2NiH_6$. *J. Mater. Chem. A* **2018**, *6*, 9099–9108. [CrossRef]
265. Ward, P.A.; Corgnale, C.; Teprovich, J.A.; Motyka, T.; Hardy, B.; Sheppard, D.; Buckley, C.; Zidan, R. Technical challenges and future direction for high-efficiency metal hydride thermal energy storage systems. *Appl. Phys. A Mater. Sci. Process.* **2016**, *122*, 426. [CrossRef]
266. Liu, Y.; He, J.; Teprovich, J.A.; Zidan, R.; Ward, P.A. High temperature thermal energy storage in the CaAl2 system. *J. Alloys Compd.* **2017**, *735*, 2611–2615.

267. Javadian, P.; Gharibdoust, S.H.P.; Li, H.W.; Sheppard, D.A.; Buckley, C.E.; Jensen, T.R. Reversibility of LiBH4 Facilitated by the LiBH4-Ca(BH4)2 Eutectic. *J. Phys. Chem. C* **2017**, *121*, 18439–18449. [CrossRef]
268. Nguyen, T.T.; Sheppard, D.A.; Buckley, C.E. Lithium imide systems for high temperature heat storage in concentrated solar thermal systems. *J. Alloys Compd.* **2017**, *716*, 291–298. [CrossRef]
269. Ouyang, L.; Liu, F.; Wang, H.; Liu, J.; Yang, X.-S.; Sun, L.; Zhu, M. Magnesium-based hydrogen storage compounds: A review. *J. Alloys Compd.* **2020**, *832*, 154865. [CrossRef]
270. Sheppard, D.A.; Buckley, C.E. The potential of metal hydrides paired with compressed hydrogen as thermal energy storage for concentrating solar power plants. *Int. J. Hydrogen Energy* **2019**, *44*, 9143–9163. [CrossRef]
271. Manickam, K.; Mistry, P.; Walker, G.; Grant, D.; Buckley, C.E.; Humphries, T.D.; Paskevicius, M.; Jensen, T.; Albert, R.; Peinecke, K.; et al. Future perspectives of thermal energy storage with metal hydrides. *Int. J. Hydrogen Energy* **2019**, *44*, 7738–7745. [CrossRef]
272. Experimental Study of Salt Hydrates for Thermochemical Seasonal Heat Storage. Available online: https://research.tue.nl/en/publications/experimental-study-of-salt-hydrates-for-thermochemical-seasonal-h (accessed on 23 April 2020).
273. Mukherjee, A.; Majumdar, R.; Saha, S.K.; Kumar, L.; Subramaniam, C. Assessment of open thermochemical energy storage system performance for low temperature heating applications. *Appl. Therm. Eng.* **2019**, *156*, 453–470. [CrossRef]
274. N'Tsoukpoe, K.E.; Schmidt, T.; Rammelberg, H.U.; Watts, B.A.; Ruck, W.K.L. A systematic multi-step screening of numerous salt hydrates for low temperature ther- mochemical energy storage. *Appl. Energy* **2014**, *124*, 1–16. [CrossRef]
275. Seasonal Storage Coupled to a Solar Combisystem: Dynamic Simulations for Process Dimensioning. Available online: http://proceedings.ises.org/paper/eurosun2010/eurosun2010-0262-Tanguy.pdf (accessed on 29 March 2020).
276. Fopah-lele, A.; Gaston, J. Solar Energy Materials & Solar Cells A review on the use of $SrBr_2 \cdot 6H_2O$ as a potential material for low temperature energy storage systems and building applications. *Sol. Energy Mater. Sol. Cells* **2017**, *164*, 175–187.
277. Lahmidi, H.; Mauran, S.; Goetz, V. Definition, test and simulation of a thermochemical storage process adapted to solar thermal systems. *Sol. Energy* **2006**, *80*, 883–893. [CrossRef]
278. Mauran, S.; Lahmidi, H.; Goetz, V. Solar heating and cooling by a thermochemical process. First experiments of a prototype storing 60 kW h by a solid/gas reaction. *Sol. Energy* **2008**, *82*, 623–636. [CrossRef]
279. Clark, R.J.; Mehrabadi, A.; Farid, M. State of the art on salt hydrate thermochemical energy storage systems for use in building applications. *J. Energy Storage* **2020**, *27*, 101145. [CrossRef]
280. Humphries, T.D.; Møller, K.T.; Rickard, W.D.A.; Sofianos, M.V.; Liu, S.; Buckley, C.E.; Paskevicius, M. Dolomite: A low cost thermochemical energy storage material. *J. Mater. Chem. A* **2019**, *7*, 1206–1215. [CrossRef]
281. Serrano, D.; Horvat, A.; Sobrino, C.; Sánchez-Delgado, S. Thermochemical conversion of C. cardunculus L. in nitrate molten salts. *Appl. Therm. Eng.* **2019**, *148*, 136–146. [CrossRef]
282. Benitez-Guerrero, M.; Sarrion, B.; Perejon, A.; Sanchez-Jimenez, P.E.; Perez-Maqueda, L.A.; Manuel Valverde, J. Large-scale high-temperature solar energy storage using natural minerals. *Sol. Energy Mater. Sol. Cells* **2017**, *168*, 14–21. [CrossRef]
283. Barker, R. The Reversibility of the Reaction $CaCO_3(s) \rightleftharpoons CaO(s) + CO_2$ (g). *J. Appl. Chem. Biotechnol.* **1973**, *23*, 733–742. [CrossRef]
284. Wu, H.; Salles, F.; Zajac, J. A Critical Review of Solid Materials for Low-Temperature Thermochemical Storage of Solar Energy Based on Solid-Vapour Adsorption in View of Space Heating Uses. *Molecules* **2019**, *24*, 945. [CrossRef] [PubMed]
285. Belz, K.; Kuznik, F.; Werner, K.F.; Schmidt, T.; Ruck, W.K.L. Thermal energy storage systems for heating and hot water in residential buildings. *Elsevier Inc.* **2015**, 441–465. [CrossRef]
286. Requirements to Consider when Choosing a Thermochemical Material for Solar Energy Storage. Available online: https://www.sciencedirect.com/science/article/abs/pii/S0038092X13003484 (accessed on 23 April 2020).
287. Criado, Y.A.; Alonso, M.; Abanades, J.C. Enhancement of a $CaO/Ca(OH)_2$ based material for thermochemical energy storage. *Sol. Energy* **2016**. Available online: https://www.sciencedirect.com/topics/engineering/thermochemical-energy-storage (accessed on 23 April 2020).

288. Schmidt, M.; Linder, M. Power generation based on the $Ca(OH)_2$/CaO thermochemical storage system–Experimental investigation of discharge operation modes in lab scale and corresponding conceptual process design. *Appl. Energy* **2017**, *203*, 594–607. [CrossRef]
289. Fopah-Lele, A.; Rohde, C.; Neumann, K.; Tietjen, T.; Rönnebeck, T.; N'Tsoukpoe, K.E.; Osterland, T.; Opel, O.; Ruck, W.K.L. Lab-scale experiment of a closed thermo- chemical heat storage system including honeycomb heat exchanger. *Energy* **2016**, *114*, 225–238. [CrossRef]
290. Michel, B.; Neveu, P.; Mazet, N. Comparison of closed and open thermochemical processes, for long-term thermal energy storage applications. *Energy* **2014**, *72*, 702–716. [CrossRef]
291. Eigenberger, G.; Ruppel, W. Catalytic fixed-bed reactors. In *Ullmann's Encyclopedia of Industrial Chemistry*; Wiley–VCH Verlag GmbH & Co. KGaA: Weinheim, Germany, 2015; Volume 122, pp. 197–205.
292. Zondag, H.A.; Schuitema, R.; Bleijendaal, L.P.J.; Gores, J.C.; van Essen, M.; van Helden, W.B. R&D of thermochemical reactor concepts to enable heat storage of solar energy in residential houses. In Proceedings of the 3rd International Conference on Energy Sustainability, San Francisco, CA, USA, 19–23 July 2009.
293. Farcot, L.; Le Pierrès, N.; Michel, B.; Fourmigué, J.-F.; Papillon, P. Numerical investigations of a continuous thermochemical heat storage reactor. *J. Energy Storage* **2018**, *20*, 109–119. [CrossRef]
294. Abedin, A.H.; Rosen, M.A. Assessment of a closed thermochemical energy storage using energy and exergy methods. *Appl. Energy* **2012**, *93*, 18–23. [CrossRef]
295. Romanchenko, D.; Kensby, J.; Odenberger, M.; Johnsson, F. Thermal energy storage in district heating: Centralised storage vs. storage in thermal inertia of buildings. *Energy Convers. Manag.* **2018**, *162*, 26–38. [CrossRef]
296. High Energy Density Sorption Heat Storage for Solar Space Heating (Hydes Heat Storage), Final Report of EU Project in the JOULE III Program. Available online: https://op.europa.eu/en/publication-detail/-/publication/91c4b9d0-5775-4bc4-9c2c-184804739041 (accessed on 23 April 2020).
297. Nwulu, N.I.; Xia, X. Optimal dispatch for a microgrid incorporating renewables and demand response. *Renew. Energy* **2017**, *101*, 16–28. [CrossRef]
298. Li, T.X.; Wang, R.Z.; Yan, T.; Ishugah, T.F. Integrated energy storage and energy upgrade, combined cooling and heating supply, and waste heat recovery with solid-gas thermochemical sorption heat transformer. *Int. J. Heat Mass Transf.* **2014**, *76*, 237–246. [CrossRef]
299. Yan, T.; Wang, C.Y.; Li, D. Performance analysis of a solid-gas thermochemical composite sorption system for thermal energy storage and energy upgrade. *Appl. Therm. Eng.* **2019**, *150*, 512–521. [CrossRef]
300. Yang, S.; Deng, C.; Liu, Z. Optimal design and analysis of a cascade $LiBr/H_2O$ absorption refrigeration/transcritical $CO_2$ process for low-grade waste heat recovery. *Energy Convers. Manag.* **2019**, *192*, 232–242. [CrossRef]
301. Nasri, M.; Burger, I.; Michael, S.; Friedrich, H.E. Waste heat recovery for fuel cell electric vehicle with thermochemical energy storage. In Proceedings of the 1th International Conference on Ecological Vehicles and Renewable Energies, Monte Carlo, Monaco, 6–8 April 2016; pp. 1–6.
302. Kuwata, K.; Masuda, S.; Kobayashi, N.; Fuse, T.; Okamura, T. Thermochemical Heat Storage Performance in the Gas/Liquid-Solid Reactions of $SrCl_2$ with $NH_3$. *Nat. Resour.* **2016**, *7*, 655–665.
303. Jarimi, H.; Aydin, D.; Yanan, Z.; Ozankaya, G.; Chen, X.; Riffat, S. Review on the recent progress of thermochemical materials and processes for solar thermal energy storage and industrial waste heat recovery. *Int. J. Low-Carbon Technol.* **2019**, *14*, 44–69. [CrossRef]
304. Kerkes, H.; Sommr, K.; Muller, H. Monosorp—ein Integrales Konzept zur Solarthermischen Gebaudeheizung mit Sorptionwarmespeicher. Available online: https://elib.dlr.de/54282/ (accessed on 29 March 2020).
305. Development of a Thermo-Chemical Energy Storage for Solar Thermal Applications. Available online: http://www.t.task20.iea-shc.org/data/sites/1/publications/Task42-Development_of_a_Thermo-Chemical_Energy_Storage_for_Solar_Thermal_Applications.pdf (accessed on 29 March 2020).
306. Particle Reactors for Solar Thermochemical Processes. Available online: https://www.sciencedirect.com/science/article/abs/pii/S0038092X17304917 (accessed on 23 March 2020).
307. Modularer Energiespeicher nach dem Sorptionsprinzip mit hoher Energiedichte (MODESTORE). Available online: https://www.aee-intec.at/modularer-energiespeicher-nach-dem-sorptionsprinzip-mit-hoher-energiedichte-modestore-p45 (accessed on 29 March 2020).
308. Mustafa Omer, A. Ground-source heat pumps systems and applications. *Renew. Sustain. Energy Rev.* **2008**, *12*, 344–371. [CrossRef]

309. Zalba, B.; Marín, J.M.; Cabeza, L.F.; Mehling, H. Review on thermal energy storage with phase change: Materials, heat transfer analysis and applications. *Appl. Therm. Eng.* **2003**, *23*, 251–283. [CrossRef]
310. Liu, M.; Steven Tay, N.H.; Bell, S.; Belusko, M.; Jacob, R.; Will, G.; Saman, W.; Bruno, F. Review on concentrating solar power plants and new developments in high temperature thermal energy storage technologies. *Renew. Sustain. Energy Rev.* **2016**, *53*, 1411–1432. [CrossRef]
311. Hewitt, N.J. Heat pumps and energy storage—The challenges of implementation. *Appl. Energy* **2012**, *89*, 37–44. [CrossRef]
312. Ground Source Heat Pumps. Available online: https://www.sciencedirect.com/topics/engineering/ground-source-heat-pump (accessed on 23 March 2020).
313. Molten Silicon Storage of Concentrated Solar Power with Integrated Thermophotovoltaic Energy Conversion. Available online: https://aip.scitation.org/doi/10.1063/1.5067099 (accessed on 24 March 2020).
314. Datas, A.; Ramos, A.; Martí, A.; del Cañizo, C.; Luque, A. Ultra high temperature latent heat energy storage and thermophotovoltaic energy conversion. *Energy* **2016**, *107*, 542–549. [CrossRef]
315. Fitó, J.; Coronas, A.; Mauran, S.; Mazet, N.; Perier-Muzet, M.; Stitou, D. Hybrid system combining mechanical compression and thermochemical storage of ammonia vapor for cold production. *Energy Convers. Manag.* **2019**, *180*, 709–723. [CrossRef]
316. Wu, S.; Zhou, C.; Doroodchi, E.; Moghtaderi, B. A unique phase change redox cycle using CuO/$Cu_2O$ for utility-scale energy storage. *Energy Convers. Manag.* **2019**, *188*, 366–380. [CrossRef]
317. Zhou, Q.; Du, D.; Lu, C.; He, Q.; Liu, W. A review of thermal energy storage in compressed air energy storage system. *Energy* **2019**, *188*, 115993. [CrossRef]
318. Rodriguez-Hidalgo, M.C.; Rodriguez-Aumente, P.A.; Lecuona-Neumann, A.; Legrand, M. Thermo-chemical storage for renewable energies based on absorption: Getting a uniform injection into the grid. *Appl. Therm. Eng.* **2019**, *146*, 338–345. [CrossRef]


applied sciences

MDPI

*Article*

# Adsorption Cold Storage for Mobile Applications

**Salvatore Vasta, Valeria Palomba, Davide La Rosa and Antonino Bonanno ***

Istituto per le Tecnologie Avanzate per l'Energia (ITAE-CNR), Via S. Lucia sopra Contesse n°5, 98126 S. Lucia, Messina, Italy; salvatore.vasta@itae.cnr.it (S.V.); valeria.palomba@itae.cnr.it (V.P.); davide.larosa@itae.cnr.it (D.L.R.)

* Correspondence: antonino.bonanno@itae.cnr.it; Tel.: +39-090-624-427

Received: 4 February 2020; Accepted: 11 March 2020; Published: 18 March 2020

**Featured Application: The present article describes the realization and testing of two different types of cold storage for a mobile refrigeration application, based on two innovative adsorbent reactors. The proposed solution uses the heat produced by the ICE to drive an adsorption cold storage system. It could be used as a back-up refrigeration system during a vehicle-stopping period (e.g., the operator's lunch break), reducing vehicle $CO_2$ emissions.**

**Abstract:** In recent years, hot and cold storage systems demonstrated themselves to be key components, especially in systems for waste heat exploitation. Moreover, mobile A/C and refrigeration set new efficiency challenges in the field of goods and passengers transport. In such a context, adsorption cold storage devices enable new possibilities and show promising features: high energy density and the possibility of being operated both for heat and cold release to the user. However, only a few studies on small and compact systems for mobile applications have been carried out so far, especially for cold storage exploiting low-temperature sources (<100 °C). The present paper describes the realization and testing of two different types of cold storage based on two innovative adsorbent reactors: a pelletized adsorber filled with commercial FAM Z02 zeolite, and a composite adsorber based on an aluminum porous structure and a SAPO-34 coating. An already developed testing procedure was employed to characterize the prototypes under cold storage mode for mobile refrigeration purposes. The test clearly showed that prototypes can store up to 580 Wh, with an average power during the discharging phase that ranges from 200 W to 820 W and an energy efficiency of 0.3 $Wh_{discharged}/Wh_{charged}$ for the operations in the selected conditions, thus revealing promising opportunities for future further developments.

**Keywords:** adsorption; cold storage; mobile refrigeration; FAM Z02; SAPO-34; zeolite

## 1. Introduction

The use of renewable energy sources and waste energy is an important task in order to fulfill the newest energy demands [1], especially for heating/cooling and refrigeration purposes, not only for stationary applications (residential and industrial buildings) but also for mobile uses.

Nowadays, mobile A/C and refrigeration are solely based on vapor compression systems, wherein the compressor is mechanically driven by the vehicle engine. Although it is subjected to a phase-out, the most used refrigerant is still HFC-134a, with a global warming potential (GWP) of 1300: if services and end-of-life are considered, it results in equivalent $CO_2$ emissions in the range 15–37 g/km for a vehicle traveling 12,000 km/y [2,3]. Such an environmental impact, neglected by manufacturers and regulations, is equivalent to 16%–39% of the limits set by European emission standards for new passenger cars in 2020.

Refrigerated freight transport is mainly achieved through vapour compression as well, often run by low-efficiency, high-emission auxiliary units (diesel or electric), and presents several criticalities,

including a low COP (Coefficient of Performance) ≈ 0.5–1.75, the employment of R404a, and a GWP of 3922 [4]. Alternative systems based on eutectic solutions (cold storage in phase change materials) or cryogenic cooling (with liquid nitrogen) are have been spreading recently. These scale down the issue of refrigerant losses, but do not avoid the energy consumption by refrigeration.

Contrarily, the heat generated by internal combustion engines (ICE) can supply thermally-driven technologies, in order to provide refrigeration for transport. Thermoelectric systems can combine the Seebeck and Peltier effects to generate electric power by heat and produce cooling power by electricity, but their low efficiency prevents practical use. Alternatives could be thermoacoustic refrigeration and the ejector refrigeration cycle. Despite the prospective low cost and durability, which resulted in interest from automotive manufacturers such as Mazda and Peugeot, thermoacoustic refrigeration for mobile applications is still at a basic research level, due to its low efficiency, just like the ejector refrigeration cycle.

Instead, great effort has been applied in the field of adsorption storage for refrigeration for road transport applications, which represent a mature technology: several working pairs have been studied for mobile applications (water/ammonia, silica gel/water, zeolite/water) and commercial products have been available for stationary applications since decades ago. On the other hand, they are generally affected by high specific volume and weight, entailing the need for further development to be successfully applied to transport A/C and refrigeration. This has been a specific subject of the TOPMACS European project, whose aims included the development of a sorption A/C system for heavy trucks supplied by the heat from the engine coolant loop rather than by the flue gases [5]. This TOPMACS prototype was designed and realized by ITAE-CNR [6].

Food and medicine transportation are two further sectors wherein cooling demand requires significant energy consumption. Most of the studies aimed at the reduction of such consumption focused on the use of high-temperature waste heat from the flue gases of the I.C. engine, needed to run a sorption appliance intended for ice-making or sub-zero refrigeration.

To that end, cold storage is a viable technology: the use of sensible heat is the most commonly used technology, even if latent heat, sorption heat, and thermochemical heat storage technology are always more often used nowadays [7]. Thanks to the great advancements in the last few years, adsorption technology has become even more frequently used for cooling/heating production, thanks also to the different units available on the market [8,9]. Cooling (from the evaporator) or heating (from the adsorber) effects could be achieved as a function of working conditions. Thanks to its environmental advantages, water is the most used working fluid, even though other substances could be used, especially when a low evaporation temperature (below 0 °C) would be achieved.

However, few studies on small and compact systems for mobile applications have been carried out so far [10].

In [11] the authors theoretically and experimentally investigated the performance of a 1 kW lab-scale prototype based on LiCl-Water pair. Even though the system was designed for heat storage, experiments showed it was possible to generate cold during the discharging process. However, the authors only provide heating mode performance and efficiency: with an input of 2708 kJ, the recovered heat was 2517 kJ, resulting in a heat storage efficiency of 93% with a heat storage density of 874 kJ/kg consolidated sorbent or 2622 kJ per kg of pure LiCl. Jiang et al. [12] studied an innovative modular sorption cell for cold and heat cogeneration. Results showed good performance in terms of energy density and power density: the stored energy density ranges from 580 kJ/kg to 1368 kJ/kg, whereas cold density ranges from 400 kJ/kg to 1134 kJ/kg; heat and cold power density range from 322 W/kg to 1502 W/kg and from 222 W/kg to 946 W/kg.

The present paper describes the experimental testing of two different types of cold storage for mobile refrigeration applications based on two innovative adsorbent reactors: a pelletized adsorber filled with commercial FAM Z02 zeolite, and a composite adsorber based on an aluminum, porous structure and a SAPO-34 coating.

## 2. Materials and Methods

### *2.1. Concept Description*

The main idea behind the study we conducted is the possibility of using waste heat from the I.C.E. of a small vehicle for the transport of perishable goods (e.g., food or medicine) to refrigerate the load compartment during the parking phases for a limited time (1–2 h). While the vehicle is running, the heat taken from the engine-cooling loop is used to "recharge" the cold storage system located near the refrigerated compartment. During a stop, when the internal combustion engine is no longer able to supply mechanical or thermal energy, the system is "discharged" to generate the cold necessary to maintain the temperature in the load compartment Figure 1. The "recharge" phase considered in this study hypothesizes that the ICE is at the normal working temperature (85–90 °C) which is maintained almost constant by the engine cooling system already installed in the vehicle. The ICE warm-up cycle was not considered due to the lower engine efficiency.

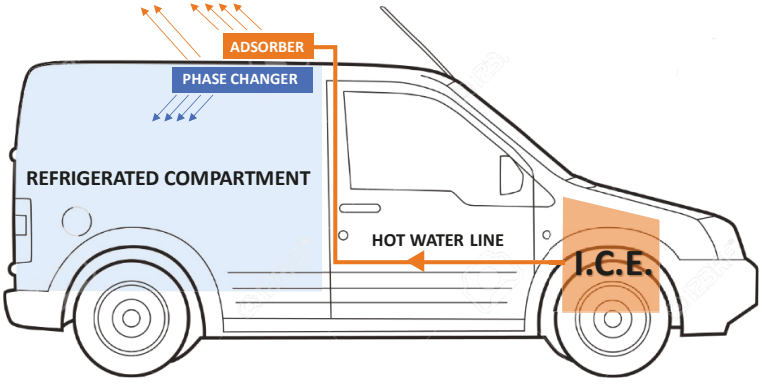


**Figure 1.** General scheme of a possible integration on the vehicle of the cold storage system studied.

### *2.2. Design of the Adsorber*

The first task carried out within the research was the sizing and design of the small cold sorption storage system. The system realized consists of an adsorber and a phase-changer, and it operates according to the working principle already described in [13].

In order to size the adsorber (amount of zeolite necessary) data, the constraints provided by an industrial company—which works in the field of small refrigeration systems for vans—have been taken into account. The thermal losses through the shell of the condenser/evaporator have been roughly considered as well. In Table 1 the main data and constraints are shown. However, the constraints refer to the full-scale system to be realized after lab tests. Indeed, for evaluation purposes, a prototype with 25% of the final capacity was designed, as reported in the bottom lines of Table 1.

The reactor realized mainly consists of an aluminum heat exchanger and a zeolitic adsorbent material: the pelletized adsorber is made of a finned heat exchanger (of automotive origin) having flat aluminum tubes, filled with FAM Z02 pellets with a grain size of 0.5–0.8 mm; the composite adsorber is instead based on an aluminum heat exchanger with flat-type tubes and a porous aluminum structure coated with SAPO-34 zeolitic coating.

**Table 1.** Data and constraints used for the full-size system and for the demonstrator.

| | **Parameter** | **Value** | |
|---|---|---|---|
| Full Scale | Storage Capacity | 2 kWh | |
| | Discharge Time | 2 h | |
| | Avg. Power | 1 kW | |
| | Water needed | 2.9 l | |
| | Design temperatures | Adsorber | Phase Changer |
| | Charge | 95 °C | 35 °C |
| | Discharge | 35 °C | 10 °C |
| | Useful ΔX | 15% | |
| | Amount of Zeolite | 19.4 kg | |
| | Spec. Zeolite density | 800 g/l foam | |
| | Foam Volume | 24.2 l | |
| | Volume of tubes | 2.4 l | |
| | Total volume | 26.6 l | |
| | Required storage time | > 1 h | |
| | Specific Capacity | 75 Wh/l | |
| | Specific Power | 28 W/l | |
| | **Parameter** | **Value** | |
| Prototype (lab-scale) | Portion of product | 25% | |
| | Storage Capacity | 500 Wh | |
| | Avg. Power | 250 W | |
| | Volume of foam | 6.1 l | |
| | Total volume | 6.7 l | |

A further step has been considered for a more accurate design of the system, by considering the thermal losses of the shell as well. Table 2 shows the obtained results: the columns "theoretical" and "real" refer to the ideal sizing (no thermal losses considered) and to a more accurate calculation respectively. The latter results, therefore, take into account an 80 W heat dissipation through the shell of the condenser/evaporator and a safety factor of 1.1 as well.

**Table 2.** Main results of the preliminary sizing process.

| **Adsorber Design** | | | |
|---|---|---|---|
| | | **Theoretical** | **Real** |
| Total Capacity | Wh | 500 | 636.40 |
| Total Capacity | kJ | 1800 | 2291.04 |
| Water latent heat | kJ/kg | 2272 | 2272 |
| Water to be evaporated | kg | 0.792 | 1.008 |
| Expected adsorption capacity | kg/kg | 0.15 | 0.15 |
| Minimum zeolite mass | kg | 5.28 | 6.72 |
| Foam density | kg/l | 0.8 | 0.8 |
| Minimum adsorber volume | l | 6.60 | 8.40 |

### *2.3. The Phase Changer*

For the phase changer, an existing condenser/evaporator, already developed at ITAE for mobile applications, was used. It is made up of two highly efficient commercial heat exchangers, represented in Figure 2. They have copper fins and stainless steel tubes, to avoid corrosion issues when in direct contact with liquid water. Each heat exchanger has a surface area on the fin side of 0.988 $m^2$; the tube side has a 0.078 $m^2$ thermal contact area; and the fin density is 16 FPI (fins per inch). The exchangers were connected in parallel by means of a hydraulic circuit made with steel pipes and compression fittings on the outside of the vacuum chamber. The vacuum chamber, in which the heat exchanger

has been placed, is made of AISI 316 stainless steel and is equipped with vacuum flanges for the connections of all the relevant equipment.

(**a**) (**b**)

**Figure 2.** The phase exchanger: (**a**) the exchangers used; (**b**) the phase changer, already assembled, used in the prototype.

*2.4. The Hydraulic Circuit*

The schematic layout of the realized testing bench is shown in Figure 3, wherein both the hydraulic circuit and the electronic connections to the acquisition system are depicted. Figure 4 shows the experimental setup installed at CENTROPROVE of the ITAE-CNR Institute in Messina.

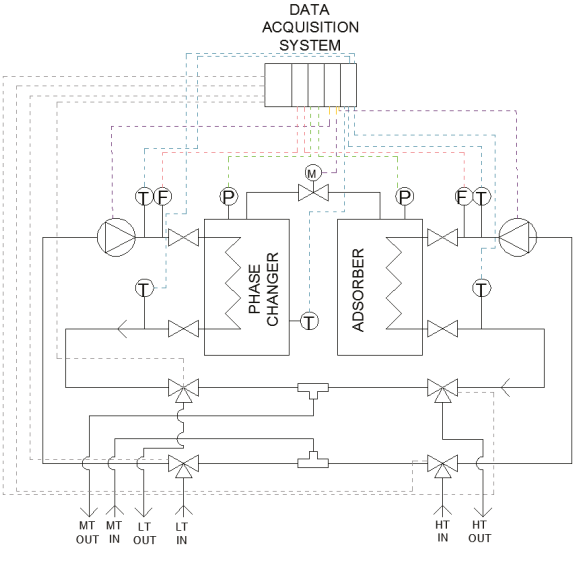


**Figure 3.** Layout of hydraulic circuit and data acquisition system.

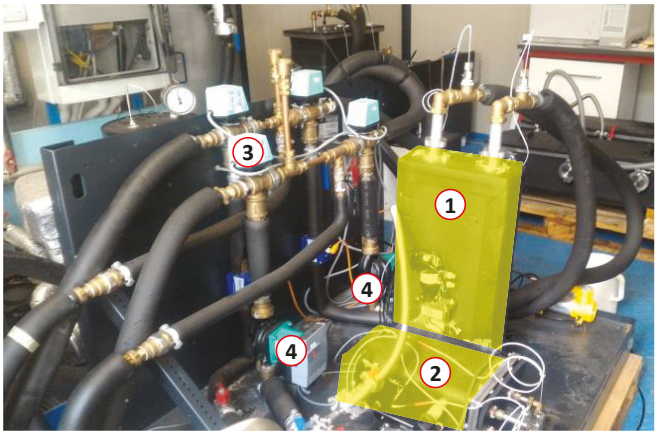


**Figure 4.** The cold storage prototype (highlighted) connected to the testing bench. (1) composite adsorber based on an aluminum, porous structure and a SAPO-34 coating; (2) phase-changer; (3) switching valves; (4) pumps.

A data acquisition and control system was realized by a specific software implemented in LabVIEW; it allows the fully automatic operation of the system and records all the measured parameters. The control system uses Compact FieldPoint® acquisition boards for the connection and management of the transducers and the valves. The parameters monitored by the system are shown in Table 3. Moreover, the commands for the deviating valves and to control the speed of the two pumps on the bench have been implemented.

**Table 3.** Parameters monitored during the tests.

| Monitored Parameter | |
|---|---|
| T in/out Adsorber;<br>T in/out Phase Changer (CON/EVAP);<br>Phase changer HTF flow rate;<br>Phase changer Pressure;<br>T ambient. | T liquid phase into Phase Changer;<br>Adsorber HTF (Heat Transfer Fluid) flow rate;<br>Adsorber pressure;<br>T shell; |

### *2.5. Testing Procedure*

To guarantee the repeatability of the tests and to provide reliable data to be used, for example, as input for calculation methods or the development of numerical models, a specific testing procedure has been developed during the preliminary phase of the activity.

The test is performed as follows: after all the set levels of temperature have been defined, the adsorption cycles are started and oscillation in temperatures is monitored. Once a steady-state condition has been reached, a record is started and all the energy flows are measured for 1 h or 6 cycles (for the longest cycle times), by evaluating the thermal power exchanged across each adsorption machine component. The last three cycles are then analyzed for performance evaluation.

Three main figures of merit have been considered for the assessment of the performance of the small storage:

- The average discharge power during each cycle, calculated as the mean power during the discharge phase.

$$\dot{Q}_{ave} = \frac{\int_0^{t_{\text{discharge}}} \dot{m}_{ev} c_p (T_{in,ev} - T_{out,ev}) dt}{t_{\text{discharge}}} \quad (1)$$

- The stored energy for mass unit of the adsorbent, calculated as the ratio of the total energy stored during each test and the total mass of adsorbent:

$$E_{ev} = \frac{\int_0^{t_{\text{discharge}}} \dot{m}_{ev} c_p (T_{in,ev} - T_{out,ev}) dt}{m_{adsorbent}} \quad (2)$$

- The thermal COP of the system; in this case, corresponds to the storage efficiency of the system, since it is the ratio between the cooling energy recovered and the energy used as input.

$$COP = \frac{\int_0^{t_{\text{discharge}}} \dot{m} c_p (T_{in,ev} - T_{out,ev}) \cdot dt}{\int_0^{t_{\text{charge}}} \dot{m} c_p \left(T_{in,ads} - T_{out,ads}\right) \cdot dt} \quad (3)$$

#### 2.5.1. Testing Procedure for a Pelletized Adsorber

The storage testing conditions are summarized in Table 4. As is visible, the inlet temperature for the heat source has been kept constant to 90 °C, while different condensation temperatures and evaporation temperatures have been considered: from 25 °C to 40 °C for the former and from 10 °C to 22 °C for the latter. Such a choice has been realized in order to cover a wide range of different possible applications for the system, corresponding to different climates and different user requirements.

**Table 4.** Testing condition, pelletized adsorber.

| Parameter | Value |
|---|---|
| Charge/discharge time (s) | 2700, 3600, 4500 |
| High temperature inlet (°C) | 90 |
| Medium temperature inlet (°C) | 25, 28, 30, 33, 35, 38, 40 |
| Low temperature inlet (°C) | 10, 15, 18, 20, 22 |
| Adsorber Flow rate (kg/min) | 12 |
| Phase changer flow rate (kg/min) | 10 |

#### 2.5.2. Testing Procedure with the Composite Adsorber Based on an Aluminum, Porous Structure and a SAPO-34 Coating

Compared to the adsorber realized with zeolite pellets, more focus has been put on the composite adsorber based on an aluminum, porous structure and a SAPO-34 coating, to have as wide a characterization as possible. To that end, different testing conditions were considered, which can be divided into three main categories:

- Initial "mapping" tests, aimed at defining the achievable energy capacity under different boundary conditions.
- "Charge effect" tests, aimed at defining the possible benefits arising from realizing the charge of the system with a low condensation temperature. Such tests were realized in various boundary conditions as well, in order to obtain information useful for different applications.
- Four temperature tests, during which the charging of the system with a low condensation temperature, the release of adsorption heat, and the removal of heat at different temperatures have been analyzed.

During the tests of the composite adsorber based on an aluminum, porous structure and a SAPO-34 coating, attention was paid in order to have some experimental points be under conditions comparable with those already tested with the pellet adsorber, so as to realize a direct comparison of the two technologies. However, since a wide range of applications could be imagined for the small cold storage system tested, different condensation and evaporation temperatures were considered as well. Moreover, the effect of the flow rate at the phase changer and the adsorber has been evaluated.

It is worth remarking that, for all the tests reported in the present section, the operation of the system was realized at three different temperature levels:

- Heat of desorption is provided at the temperature of the heat source—HT (high temperature);
- Heat of condensation and heat of adsorption are released at the same temperature—MT (medium temperature);
- Heat of evaporation is provided at a temperature level suitable for the user—LT (low temperature).

The testing conditions are summarized in Table 5.

**Table 5.** Testing conditions for the first characterization tests of the composite adsorber based on an aluminum, porous structure and a SAPO-34 coating.

| Parameter | Value |
|---|---|
| Charge/discharge time (s) | 600, 750, 900, 1200 |
| High temperature inlet (°C) | 85, 90 |
| Medium temperature inlet (°C) | 28, 30, 33, 35, 38 |
| Low temperature inlet (°C) | 5, 10, 12, 15, 18, 20 |
| Adsorber Flow rate (kg/min) | 8, 12, 15 |
| Phase changer flow rate (kg/min) | 5, 10, 15, 18 |

## 3. Results

### *3.1. Trend of a Typical Test*

In this section, a typical test will be briefly discussed. In Figure 5a, the typical trends of the temperatures in the components are reported for a 90/38/20 (HT/MT/LT) test. They are consistent with the operation of typical sorption storage: during the first half of the cycle, the adsorber is heated, while the condenser is cooled down. Both the temperatures are constant, indicating a good capacity of the testing bench in terms of maintaining the set conditions. During the second part of the cycle, the useful effect is visualized by the reduction in the temperature at the evaporator (the blue line in the figure), while the adsorber is cooled. During the tests, the same temperature was used both for condensation and for adsorption (three temperature levels).

Instead, in Figure 5b, the power and energy measured at the phase changer are reported. In particular, the power in the negative part of the chart is the condensation power, while the one in the positive part is the evaporation one. Energy (which is represented on the secondary axis on the right) has been instead calculated only for the evaporation, representing the useful effect on the cycle in the present configuration. The curve, in particular, represents the cumulative energy recovered, which, for the examined cycle, amounts to 580 Wh.

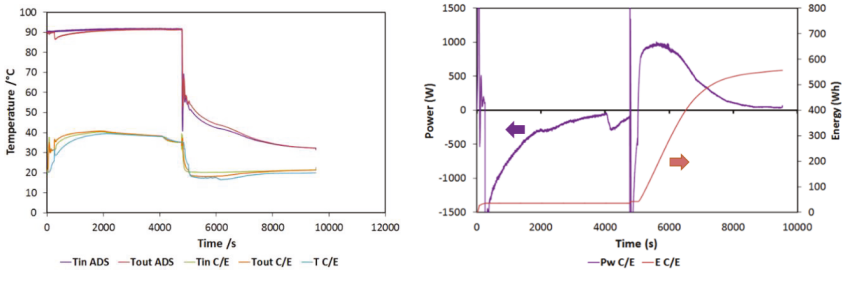


(**a**) (**b**)

**Figure 5.** (**a**) Typical temperature trends for a reference test; (**b**) power and energy for a reference test. HT (high temperature) = 90 °C; MT (medium temperature) = 38 °C; LT (low temperature) = 20 °C.

### *3.2. Testing Results for a Pelletized Adsorber*

In this section, the results obtained during the tests will be discussed. It is worth noticing that most of them were mainly used afterward for future comparison with the other adsorber, and therefore, new aggregation tables or charts can be found in the following parts of this paper.

In Figure 6a, the effect of charge/discharge time is shown. This was the first parameter investigated, in order to find out the optimum value to be used in the evaluation of other operating conditions. Two different boundary conditions were investigated—90/35/15 and 90/30/17 cycles, corresponding to more severe and less severe operating conditions. The cold energy recovered and discharge power are shown in the picture. The trends obtained are: increasing energy recovered for higher charge/discharge times and decreasing power for higher charge/discharge times. The trends are more marked for the less severe condition (90/30/17), where a higher amount of working fluid can be processed. Moreover, the decreasing in the output power is not very high, going from 2700 s to 4500 s, probably because of the saturation of the material: after 2700 s, the uptake exchanged, though still present (as testified by the increasing energy stored) is lower than in the first part of the cycle. In Figure 6b, the effect of evaporation temperature over the discharge power and the energy capacity is shown. As expected, the higher the evaporation temperature, the higher the energy recovered. Moreover, with a 2nd grade polynomial equation, it is possible to describe the obtained trend, as often happens for such kind of sorption devices. Two curves, parameterized according to condensation temperature, are reported. The highest discharge power is 400 W, obtained for the lower condensation temperature (30 °C) and an evaporation temperature of 22 °C. Instead, for a 35 °C condensation temperature, the obtained discharge powers are very low. The energy recovered arrives at 400 Wh for the higher evaporation temperatures.

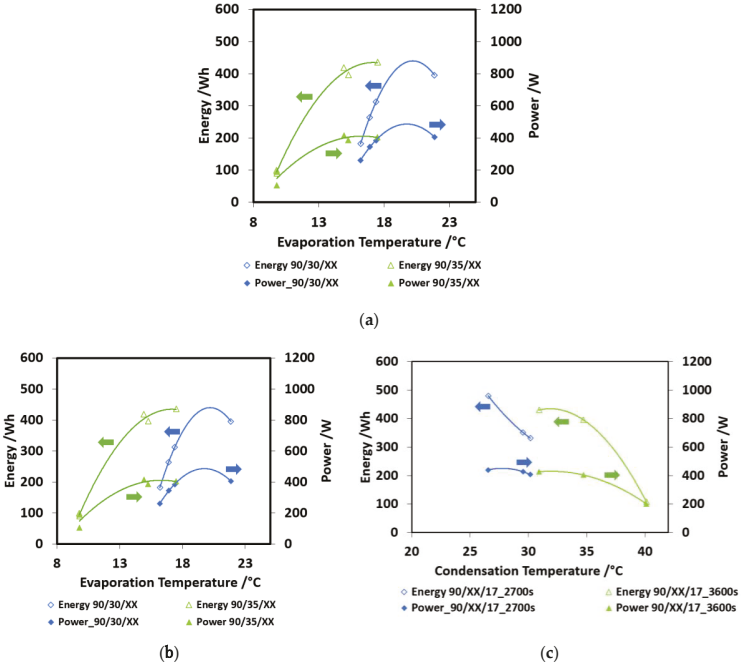


**Figure 6.** (**a**) The effect of charge/discharge time, pelletized adsorber; (**b**) the effect of evaporation temperature; (**c**) the effect of condensation temperature. In all these figures, the following nomenclature has been used: HT/MT/LT. When the term XX appears, this means that the specific value (e.g., LT) is variable and must be read on the specific figure (e.g., Figure 6b).

Finally, in Figure 6c, the effect of condensation temperature is shown. The curves are parameterized as a function of discharge times. The results are similar to those of the previous graphs: higher condensation temperatures lead to low powers, around 200 W, and low energy capacity (200 Wh for 40 °C condensation and 2700 s discharge time), whereas more power is available at a lower condensation temperature (300 Wh for 30 °C condensation and 3600 s discharge time).

### *3.3. Testing Results with a Composite Adsorber Based on an Aluminum, Porous Structure and a SAPO-34 Coating*

In this section, the results of the characterization tests are reported, by using the same evaluation parameters previously explained. A direct comparison with the pelletized adsorber will be specifically addressed in a dedicated section.

In Figure 7a, tests with two different evaporation temperatures (12 °C and 15 °C) and different cycle times are presented. In particular, for the tests here shown, the durations of charge and discharge are the same. The results are presented both in terms of energy (e.g., 85/30/12_E) and power (e.g., 85/30/12_P): as expected, power decreases with increasing cycle time. However, energy, once 900 s of charge/discharge time is reached, has a plateau, indicating that this is the optimal choice.

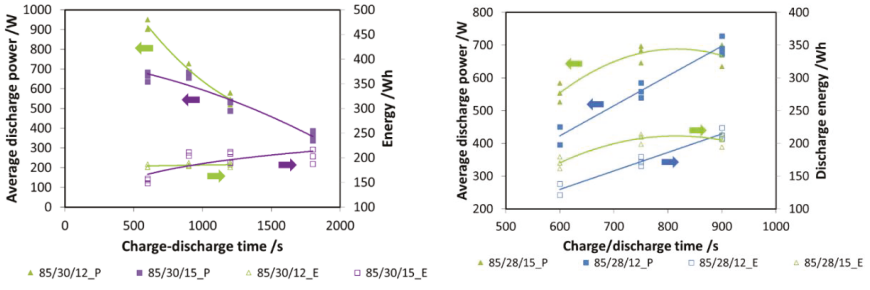


(**a**) (**b**)

**Figure 7.** (**a**) The effect of charge/discharge time, composite adsorber; (**b**) the effect of charge time, composite adsorber.

Subsequently, the effect of charging time was evaluated: it is well known that the desorption process is faster than adsorption [14]. For a discharging time fixed at 900 s, charging times of 600 s and 750 s were evaluated, again considering two different evaporation temperatures. The results are presented in Figure 7b: for an evaporation temperature of 15 °C, the optimal charging time is 750 s, since no evident benefit from increasing the duration of charge is measured. Instead, for a 12 °C evaporation, a cycle with the same durations of charge and discharge is the best option. Such results were used for the realization of the other tests.

In Figure 8a,b, the effects of evaporation temperature and driving temperature are shown for discharge power and recovered cold energy, respectively. All the tests have been performed for a charge and discharge duration of 900 s with a condensation/adsorption temperature of 30 °C. This part of the experimental test was carried out with the aim of evaluating the effects of two possible ICE operative temperatures (85 °C and 90 °C) and the effect of the cabin's inside temperature, assuming it at different constant levels (from 10 °C to 20 °C). It is visible that higher driving temperatures are beneficial, especially to discharge power, since an increment of about 15% can be obtained. The average discharge power measured, especially with 90 °C driving temperature, is as high as 850 W. By moving from an evaporation temperature of 10 °C to 15 °C, a great increase is observed; after such a temperature, a plateau is reached. For a lower driving temperature, discharge power in the range 500–730 W has been measured. The effect on recovered energy, though smaller, is still recognizable: for 85 °C tests,

energy recovered lied in the range of 170–220 Wh, while for the higher temperature, the maximum energy recovered was about 220 Wh.

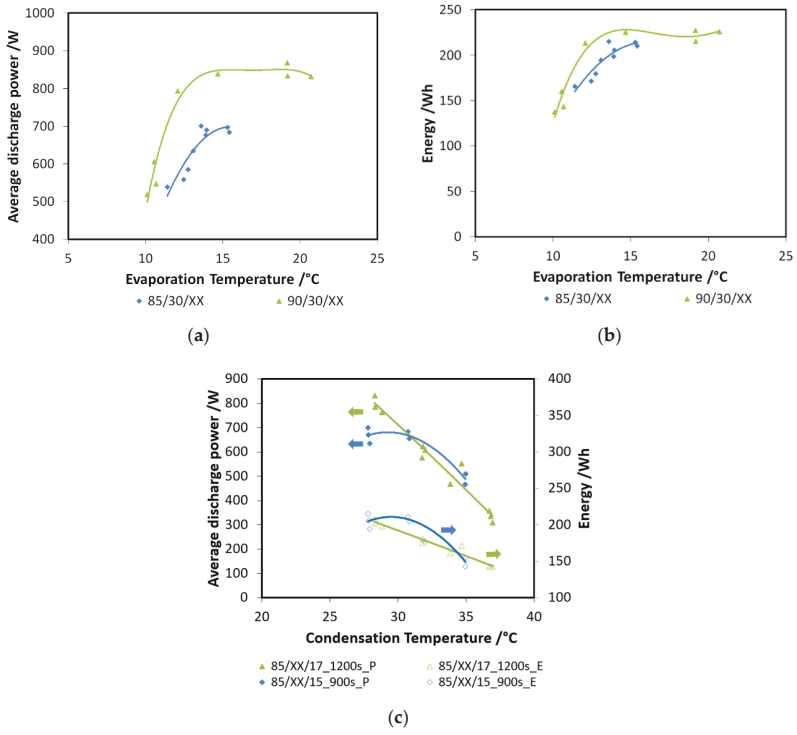


**Figure 8.** (**a**) The effects of evaporation temperature (XX—must be read on the figure) and driving temperature (85 °C or 90 °C) on discharge power for the composite adsorber; (**b**) the effects of evaporation temperature (XX—must be read on the figure) and driving temperature (85 °C or 90 °C) on recovered cold energy for the composite adsorber; (**c**) the effect of condensation (XX—must be read on the figure) temperature for the composite adsorber.

The effect of condensation temperature is summarized in Figure 8c: both the recovered energy (e.g., 85/XX/17_1200s_E) and discharged power (e.g., 85/XX/17_1200s_P) decrease for higher condensation temperatures. The effect is more marked for the lower evaporation temperatures, corresponding to a higher pressure lift between the evaporator and the condenser.

Subsequently, the effect of the flow rate in the two components has been evaluated, since it represents a key design parameter. In Figure 9a, the effect of the flow rate in the adsorber has been evaluated, considering both the discharge power and energy. The trend obtained is clear: there is an optimum value of flow rate allowing the maximizing of the performance of the system, which is 12 kg/min. Indeed, lower flow rates probably worsen the heat transfer inside the heat exchanger of the adsorber, while higher flow rates are as detrimental. Moreover, they lead to very a small temperature difference that might negatively affect the practical application. Therefore, the value of 12 kg/min has been considered for all the other tests.

The same analysis has been done for the phase changer, by varying its flow rate in the range of 8–18 kg/min. In this case, the effect is smaller, with a slightly increasing trend for higher flow rates, as shown in Figure 9b. Such a result further highlights that the key parameter is the heat transfer inside the adsorber, since it affects the adsorption efficiency and dynamics.

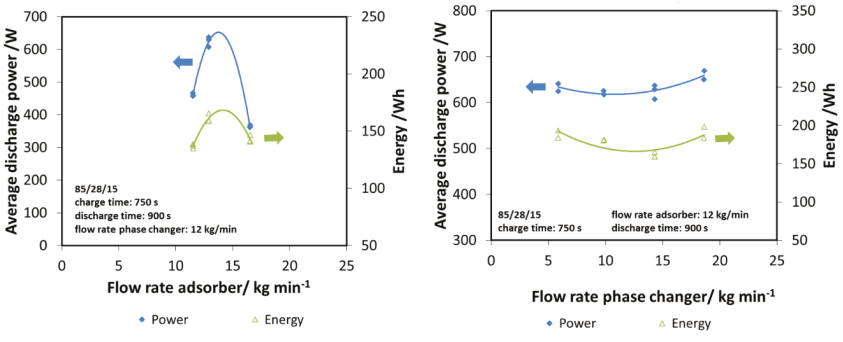


**Figure 9.** (**a**) The effect of adsorber flow rate, composite adsorber; (**b**) the effect of the flow rate of the phase changer, composite adsorber.

### 3.3.1. "Deep Charge" Tests

After the first characterization of the small storage prototype, another series of tests were realized, with the aim of finding out whether the charge of the system at a lower temperature could hold some benefit on the performance and the amount of energy stored. In this case, the operation of the system is still realized at the following three temperature levels:

- Heat of desorption is provided at the temperature of the heat source, HT;
- Heat of condensation is released at a low temperature, LT;
- Heat of adsorption is released at the temperature of adsorption, MT;
- Heat of evaporation is provided at a temperature level suitable for the user, LT.

The condensation and evaporation temperatures of the tests then are equal. This allows simulating, for example, the case of short-term storage realized with condensation taking place at a very low external temperature.

The results of the analysis are shown in Figure 10a,b for discharge power and stored energy, respectively. The performance indicators are represented as a function of adsorption temperature. In particular, three different evaporation/condensation temperatures have been tested (7, 10, and 15 °C), and for each of them, three different adsorption temperatures (30, 35, and 40 °C). The tendency reported in the graphs is clear: there is a benefit in realizing the charge of the system at a lower temperature with respect to adsorption temperature.

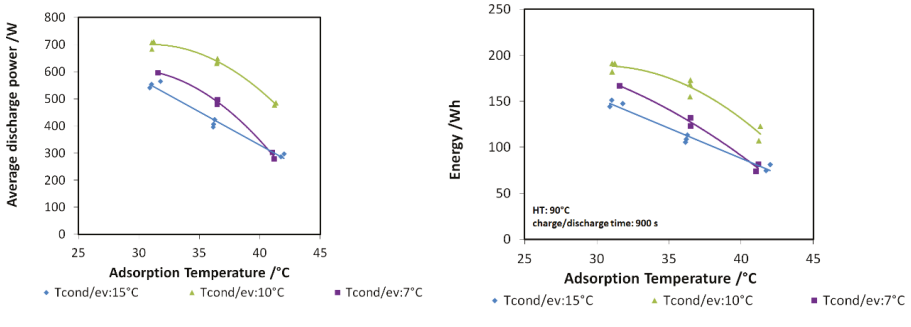


**Figure 10.** (**a**) The effect of "deep charging" on discharge power, composite adsorber; (**b**) the effect of "deep charging" on stored energy, composite adsorber.

Indeed, the lower the difference between adsorption and condensation temperature, the higher the discharge power and energy recovered, especially when the useful effect has to be provided at 7 or 10 °C. The findings described here are further highlighted in Figure 11, where the case of a 10 °C evaporation temperature has been considered. The green points represent the tests with "deep charge," while the purple line represents the tests in which the condensation and adsorption temperatures are equal ("normal charge"). It is possible to see that, for the three adsorption temperatures tested (3T), an increase of about 20%–25% in the stored energy is achieved by means of deep charge.

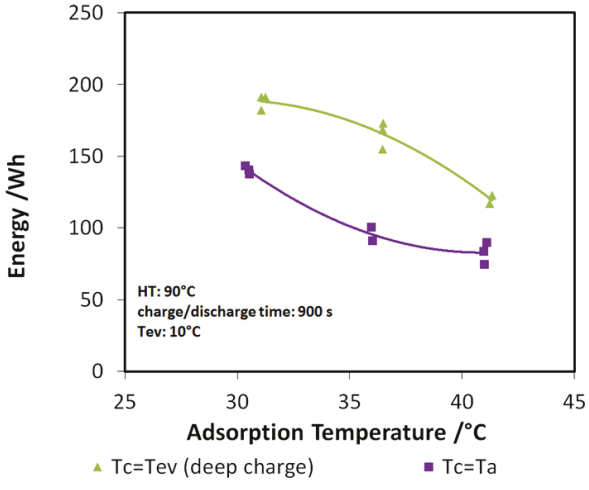


**Figure 11.** Effect of "deep charge" on the stored energy for evaporation temperature of 10 °C.

Such results have led to the realization of another run of tests, at four temperature levels (4T), as described in the next section.

3.3.2. Four Temperatures Tests

Once the beneficial effect of "deep charge" on the system had been assessed, further tests were realized by considering the operation of the system at four temperature levels (4T) instead of three (3T). In this case, the operation of the system is realized at the following different temperature levels:

- Heat of desorption is provided at the temperature of the heat source, HT;
- Heat of condensation is released at 10 °C;
- Heat of adsorption is released at the temperature of adsorption, Ta;
- Heat of evaporation is provided at a temperature level suitable for the user, LT.

The characteristic of such tests is that the condensation temperature is lower than adsorption temperature, simulating, for example, the charging of the system through a "booster" or at low ambient temperatures typical of northern countries.

The results of the evaluation are summarized in Figures 12 and 13 for the discharge power and stored energy for different evaporation temperatures and a driving temperature of 95 °C. As suggested by the results on "deep charge" tests, by making the cold storage work at four different temperature levels, there is a benefit; that is, higher evaporation temperatures. In this case, indeed, the difference in the uptake exchanged during charge in three temperature and four temperature tests is higher because the difference between the condensation temperatures in the two types of tests is higher.

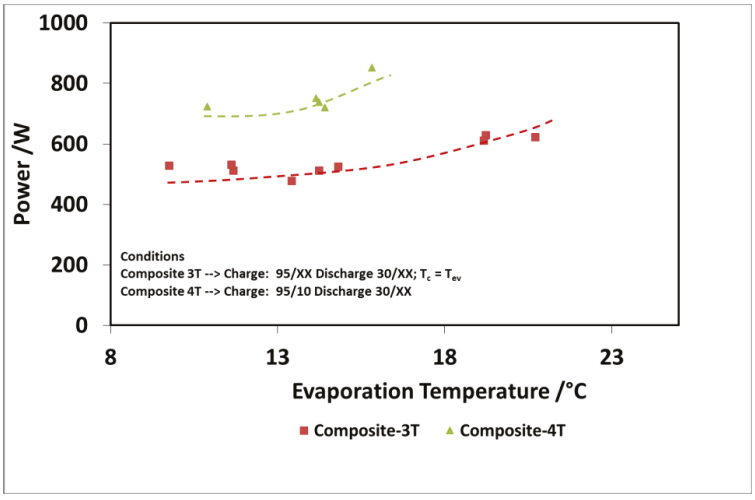


**Figure 12.** Comparison of 3T and 4T operation on discharge power—composite adsorber.

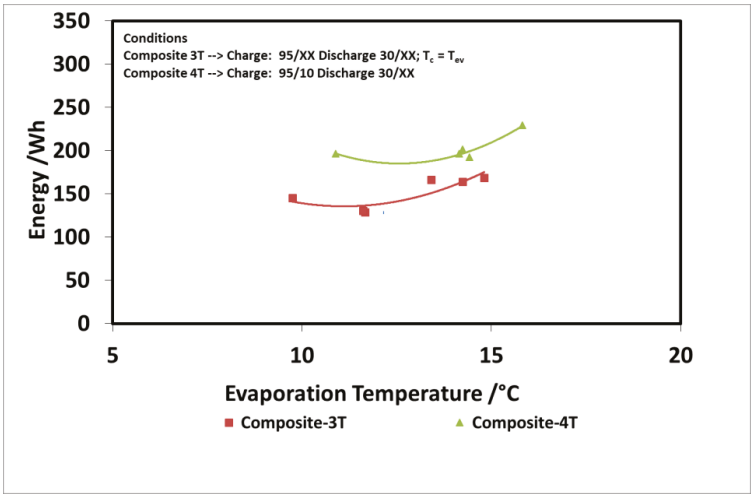


**Figure 13.** Comparison of 3T and 4T operation on stored energy—composite adsorber.

### *3.4. Comparison between the Adsorbers*

A comparison between the adsorbers has been realized to highlight the benefits arising from the use of a composite technology based on an aluminum, porous structure and a SAPO-34 coating. In Figure 14, the power trend after the beginning of adsorption process is shown for the two types of adsorbers. This is a qualitative measure of the adsorption dynamics in the two different cases. As expected, the peak power of the composite adsorber based on an aluminum, porous structure and a SAPO-34 coating is double with respect to the pellet one, and the whole duration of adsorption is significantly lower (900 s against 4500 s); meanwhile, the pellet adsorber is able to accomplish a more constant discharge.

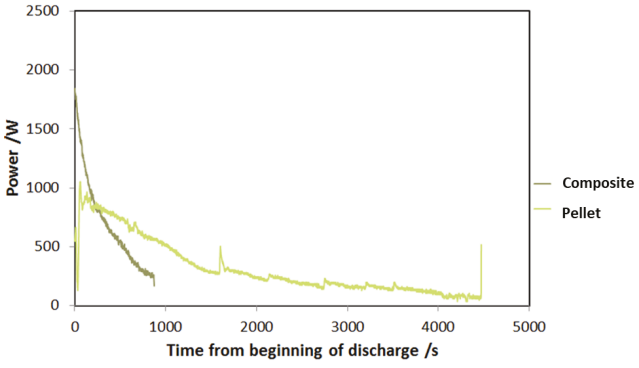


**Figure 14.** Dynamic curve of power during discharge for the two adsorbers tested.

A second step in the comparison between the two systems is reported in Figure 15a,b, wherein the discharge power and recovered energy for the two adsorbers are shown. The boundary conditions used are: 85 °C driving temperature; 15 °C evaporation temperature; and 3600 s charge/discharge time for the pellets adsorber and 900 s for the composite adsorber. Results are displayed as a function of condensation temperature. The results for the energy comparison make use of the specific energy; they are normalized for the masses of the adsorbent materials in the two exchangers. There is a relevant difference in the discharge power achievable with the two technologies: as previously stated, average power during each cycle is much higher in the case of the composite adsorber, about double that of the pellets heat exchanger. The results in terms of specific energy stored do not show the same marked difference; there is only a low increase for the composite technology. However, the results regarding composite heat exchanger probably should take into account the effect of the mass of aluminum composite inside the exchanger.

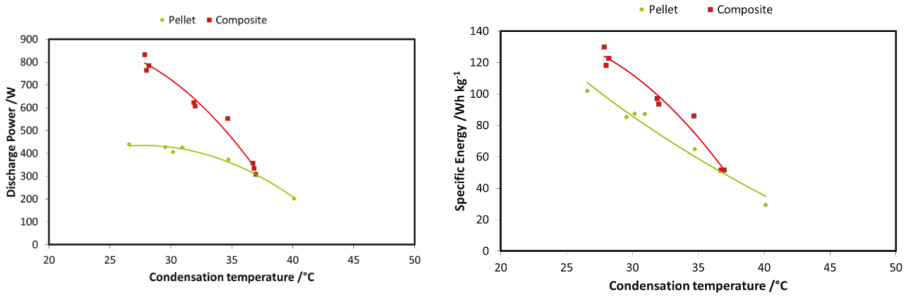


**Figure 15.** (**a**) Comparison of the adsorbers—power; (**b**) comparison of the adsorbers—energy.

Finally, Figures 16 and 17 show the comparison as a function of evaporation temperature, by considering the operation of the composite adsorber as well, in the best performing configuration, with four temperature levels. In addition, in this case, the results in terms of stored energy are normalized for the mass of adsorbent inside the storage. By considering these conditions, the effect of composite technology is to increase the achievable discharge power by about 60%, especially for higher evaporation temperatures. The maximum specific energy measured in both the pellet and composite adsorber was around 90 Wh/kg, but in the case of the composite adsorber, this result was achieved for an evaporation temperature of 15 °C, whereas for the pellet adsorber this was obtained for an evaporation temperature of 22 °C.

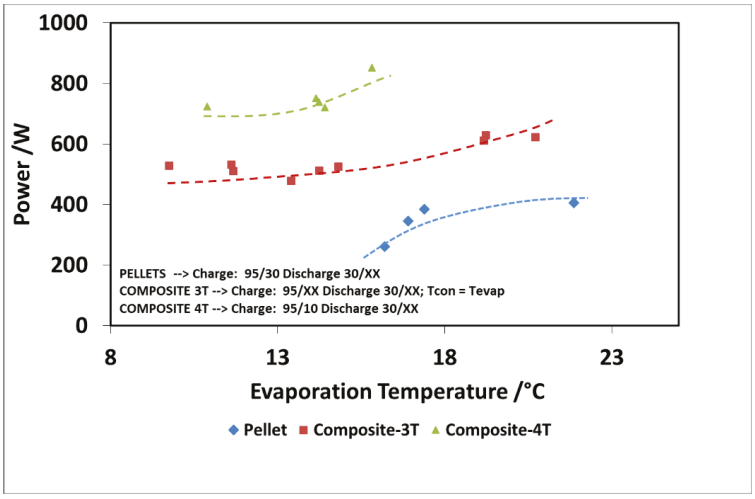


**Figure 16.** Comparison of discharge power for the adsorbers, considering the 4T operation as well (XX—must be read on the figure).

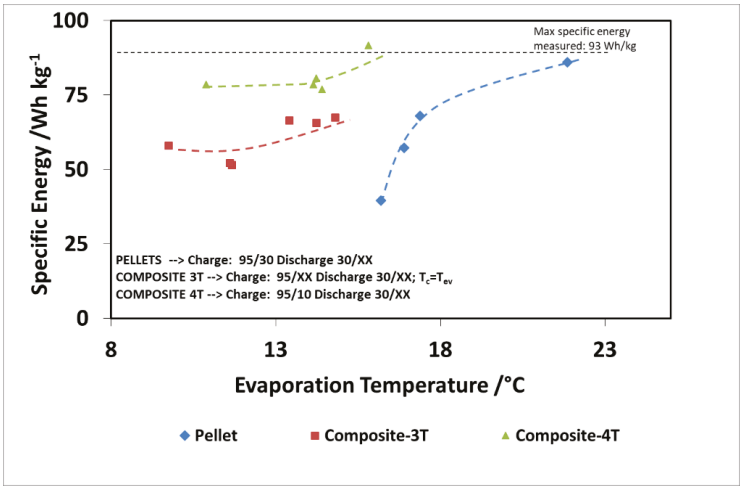


**Figure 17.** Comparison of recovered cold energy for the adsorbers, considering also, the 4T operation (XX—must be read on the figure).

## 4. Conclusions

In the present paper, the realization and testing of two different types of cold storage for mobile refrigeration applications based on two innovative adsorbent reactors was presented. The performances measured on a pelletized adsorber filled with commercial FAM Z02 zeolite, and a composite adsorber based on an aluminum, porous structure and a SAPO-34 coating were shown. Measurements were carried out thanks to an already existing testing bench specifically realized, and by applying a testing procedure previously developed and published by the authors. The main focus was on the more promising technology. Indeed, a composite adsorber based on an aluminum, porous structure and a SAPO-34 coating was tested by means of three main series of tests: a series of "mapping tests" for its characterization and two series of tests with different charging boundary conditions with respect to

traditional operation, with the aim of defining the optimum operating conditions. Finally, a comparison between the two adsorbers has been reported.

The test clearly showed that prototypes are able to store up to 580 Wh, with an average power during the discharging phase that ranges from 200 to 820 W and an energy efficiency of 0.3 for the operations in the selected conditions—revealing promising opportunities for future further developments and demonstrating the feasibility of their application to the refrigeration of the load compartments of small vans or cars.

**Author Contributions:** Conceptualization, S.V. and V.P.; methodology, S.V.; software, V.P.; validation, S.V., V.P. and D.L.R.; formal analysis, S.V. and V.P.; investigation, V.P. and D.L.R.; resources, S.V.; data curation, V.P.; writing—original draft preparation, A.B.; writing—review and editing, A.B.; visualization, A.B.; supervision, S.V. project administration, S.V.; funding acquisition, S.V. All authors have read and agreed to the published version of the manuscript.

**Funding:** This research received no external funding.

**Conflicts of Interest:** The authors declare no conflict of interest.

## Nomenclature

| | |
|---|---|
| $c_P$ | Specific heat, kJ/(kgK) |
| $\dot{m}$ | Mass flow rate, kg/s |
| $\dot{m}_{ev}$ | Mass flow rate to the evaporator, kg/s |
| $m_{adsorbent}$ | Adsorbent material mass, kg |
| $\dot{Q}_{ave}$ | Average Power, W |
| $E_{ev}$ | Stored energy into the evaporator, kJ |
| COP | Coefficient of Performance, - |
| $T_{in,ev}$ | Inlet temperature to the evaporator, K |
| $T_{out,ev}$ | Outlet temperature to the evaporator, K |
| $T_{in,ads}$ | Inlet temperature to the adsorber, K |
| $T_{out,ads}$ | Outlet temperature to the adsorber, K |
| $t_{\text{discharge}}$ | Discharge time, s |
| $t_{\text{charge}}$ | Charge time, s |

## References

1. Barberi, P.; Bossmann, T.F.; Laurent, F. *METIS Studies Study S6 Decentralised Heat Pumps: System Benefits under Different Technical Configurations*; European Commission, Directorate-General for Energy: Brussels, Belgium, 2019. [CrossRef]
2. Intergovernmental Panel on Climate Change; Groupe D'experts Intergouvernemental sur L'évolution du Climat. *IPCC/TEAP Special Report on Safeguarding the Ozone Layer and the Global Climate System: Issues Related to Hydrofluorocarbons and Perfluorocarbons*; Cambridge University Press: Cambridge, UK, 2005; 478p.
3. European Environment Agency. *ADEME (2003), ENERDATA, ISI-FhG, Energy Efficiency in the European Union 1990–2001*; SAVE-ODYSSEE Project on Energy Efficiency Indicators; EEA: Copenhagen, Denmark, 2003.
4. Tassou, S.A.; De-Lille, G.; Ge, Y.T. Food transport refrigeration—Approaches to reduce energy consumption and environmental impacts of road transport. *Appl. Therm. Eng.* **2009**, *29*, 1467–1477. [CrossRef]
5. Magnetto, D.; de Boer, R.; Vasta, S. TOPMACS: Thermally Operated Mobile Air Conditioning Systems. In *Vehicle Thermal Management Systems Conference and Exhibition*; Institution of Mechanical Engineers—VTMS 10; Elsevier: Amsterdam, The Netherlands, 2011; pp. 635–647.
6. Vasta, S.; Freni, A.; Sapienza, A.; Costa, F.; Restuccia, G. Development and lab-test of a mobile adsorption air-conditioner. *Int. J. Refrigeration* **2012**, *35*, 701–708. [CrossRef]
7. Guelpa, E.; Verda, V. Thermal energy storage in district heating and cooling systems: A review. *Appl. Energy* **2019**, *252*, 113474. [CrossRef]
8. Bataineh, K.; Taamneh, Y. Review and recent improvements of solar sorption cooling systems. *Energy Build.* **2016**, *128*, 22–37. [CrossRef]

9. Aydin, D.; Casey, S.P.; Riffat, S. The latest advancements on thermochemical heat storage systems. *Renew. Sustain. Energy Rev.* **2015**, *41*, 356–367. [CrossRef]
10. Engel, G. Sorption cold storage for thermal management of the battery of a hybrid vehicle. *Energy Procedia* **2018**, *155*, 149–155. [CrossRef]
11. Yu, N.; Wang, R.Z.; Wang, L.W. Theoretical and experimental investigation of a closed sorption thermal storage prototype using LiCl/water. *Energy* **2015**, *93*, 1523–1534. [CrossRef]
12. Jiang, L.; Roskilly, A.P.; Wang, R.Z.; Wang, L.W.; Lu, Y.J. Analysis on innovative modular sorption and resorption thermal cell for cold and heat cogeneration. *Appl. Energy* **2017**, *204*, 767–779. [CrossRef]
13. Vasta, S.; Brancato, V.; la Rosa, D.; Palomba, V.; Restuccia, G.; Sapienza, A.; Frazzica, A. Adsorption heat storage: State-of-the-art and future perspectives. *Nanomaterials* **2018**, *8*, 522. [CrossRef] [PubMed]
14. Sapienza, A.; Palomba, V.; Gullì, G.; Frazzica, A.; Vasta, S. A new management strategy based on the reallocation of ads-/desorption times: Experimental operation of a full-scale 3 beds adsorption chiller. *Appl. Energy* **2017**, 1081–1090. [CrossRef]


applied sciences

MDPI

Article

# Modified Silicone-SAPO34 Composite Materials for Adsorption Thermal Energy Storage Systems

**Luigi Calabrese [1,2], Stefano De Antonellis [3,*], Salvatore Vasta [4], Vincenza Brancato [4] and Angelo Freni [2]**

1 Department of Engineering, University of Messina, Contrada di Dio Sant'Agata, 98166 Messina, Italy; lcalabrese@unime.it
2 CNR ICCOM—Institute of Chemistry of Organometallic Compounds, Via G. Moruzzi, 1-56124 Pisa, Italy; angelo.freni@pi.iccom.cnr.it
3 Department of Energy, Politecnico di Milano, Via Lambruschini 4, 20156 Milano, Italy
4 Istituto per le Tecnologie Avanzate per l'Energia (ITAE-CNR), Via S. Lucia sopra Contesse n°5, 98126 Messina, Italy; salvatore.vasta@itae.cnr.it (S.V.); vincenza.brancato@itae.cnr.it (V.B.)
* Correspondence: stefano.deantonellis@polimi.it

Received: 30 October 2020; Accepted: 1 December 2020; Published: 5 December 2020

**Abstract:** In this work, novel silicone-SAPO34 composite materials are proposed for application in adsorption thermal energy storage systems. The innovative composite materials were obtained through a mold foaming process activated by a dehydrogenative coupling reaction between properly selected siloxane compounds. Morphology analysis by optical microscopy and measurement of the mechanical properties of the foamed materials at varying zeolite content demonstrated a quite homogeneous open-cell structure and good structural stability of the foam. Water adsorption isotherms of the adsorbent foams expanded in free space and inside paperboard were measured by a gravimetric adsorption apparatus, demonstrating that the presence of the polymeric fraction does not affect the adsorption capacity of the SAPO34 fraction added in the composite foam. Finally, main adsorption and thermodynamic properties of the proposed foam have been compared with those of other adsorbent materials, confirming the possible use of these new composite foams as adsorbent materials for adsorption thermal energy storage systems.

**Keywords:** adsorption; zeolite; SAPO34; foam; heat storage

## 1. Introduction

A major research topic in the field of adsorption systems for solar thermal energy storage, air-conditioning and dehumidification processes involves the development of new or modified adsorbent materials with enhanced adsorption and thermo-physical properties, low cost, high stability, and low regeneration temperature [1–5]. Possible adsorbent classes are zeolites, silica gels, activated carbons, metal organic frameworks (MOFs), and composite adsorbents made of a sorbent matrix embedding a hygroscopic salt [6]. Among them, silico-aluminophosphate zeotype materials (SAPO, ALPO) are very attractive due to the low regeneration temperature (<100 °C) and optimal shape of the water adsorption equilibrium curve [7–9]. In closed systems research on components optimization is mainly focused on the integration between heat exchanger and adsorbent material, to create the so called adsorber [10]. Two different approaches are currently under investigation: embedding a granular adsorbent in the heat exchanger [11]; coating the heat exchanger with the adsorbent material either using a binder [12] or by direct synthesis of the zeolite over the metallic surface of the heat exchanger [13]. The first approach allows good heat transfer efficiency without significantly affecting the vapor diffusion through the adsorber if a proper grain size and dispersion is selected [14]. The second approach is based on the reduction of the contact resistance between the heat exchanger and

a thin adsorbent coating (generally 0.05–0.2 mm), thus enhancing the heat transfer efficiency. However, a sufficiently high amount of adsorbent must be deposited over the heat exchanger, to avoid reduction of the achievable power density [15]. Similarly, in open systems the adsorption and desorption process is typically achieved through a honeycomb matrix impregnated with a desiccant material [16,17] or through a packed bed made of spherical beads of a sorption material [18]. In the first case, a high heat and mass exchange area between the air stream and the desiccant matrix is obtained and air pressure drop is low. Anyway, the manufacturing process of the honeycomb structure is quite complex and it requires the use of support materials (such as paper or glass fiber) and appropriate binders that partially limit the net sorption capacity of the desiccant. In the second case, packed bed can be easily realized by using beads of pure materials, without any need of binders. On the other side, this approach leads to a device with high water mass transfer resistance within desiccant beads and high air pressure drop, limiting the application of the system. Optimization of adsorber/desorber configuration in both open and closed systems is still an open issue, which heavily depends on the final application of the adsorption system [19].

Recently, an innovative silicone–zeolite foaming process has been developed in order to enhance the power density of the zeolite heat and mass exchanger in closed-cycle adsorption heat pumps and chillers [20,21]. Indeed, foamed materials, due to their intrinsic high surface area per unit mass, could allow to obtain a large amount of zeolite coating per unit of volume, and at the same time the foam porosity could act as a preferential pathway for the vapor diffusion. This approach allows improving the amount of active material embedded into the adsorbent heat exchanger and can be suitable for both open and closed systems. In a previous preliminary work, several samples of SAPO34 foams have been prepared and water adsorption isotherms have been measured by a gravimetric adsorption apparatus, demonstrating that they can adsorb a significant amount of water (up to 30 wt.%) under typical operating conditions of open-cycle adsorption systems [22]. Moreover, the tested foams exhibited sufficiently fast water sorption rate, as the silicone does not significantly reduce the transient adsorption capacity of pure zeolite.

Based on the promising results achieved in [22], in this work we assessed the feasibility of a SAPO34 foam-based innovative component for open and closed adsorption heat storage applications. Firstly, several samples with different foam formulations have been produced by varying the SAPO34 content in the range 20–60 wt.% and the corresponding water adsorption isotherms have been measured by a thermogravimetric method. Among the different tested formulations, Z60 foam (60 wt.% SAPO34 content) demonstrated the best adsorption properties, being suitable for the development of innovative components for heat storage applications. Accordingly, the Z60 foam preparation method has been further developed in order to allow the foam expansion in a partially closed environment (paperboard), to reproduce the constraints that would occur in a mold used to give the foam a specific geometry at the end of the solidification process. Morphological analysis of the Z60 foam expanded in the paperboard cavities has been carried out by optical microscopy, to evaluate the foam pores nature and size and study the interaction between foam microstructure and the paperboard support. Water vapor adsorption capacity of the obtained foam has been evaluated by thermogravimetric method and results have been compared with ones previously obtained for foams expanded in not constrained environment. Z60 foam adsorption data at equilibrium have been correlated considering the Dubinin–Asthakov approach, and the corresponding heat of adsorption has been calculated. Specific heat has been measured as a function of the SAPO34 amount by calorimetric technique. Finally, measured data of the proposed Z60 foam have been compared with properties of other available sorbent materials for heat storage purposes.

## 2. Materials and Methods

### *2.1. Sample Preparation*

The composite zeolite/siloxane foam was obtained by mold foaming process. Details of compounds used for the synthesis are summarized in Table 1. As zeolite filler, a SAPO34, (AQSOA-FAM Z02, supplied by Mitsubishi Chemicals, Tokyo, Japan) with average size in the range of 4–8 μm was used. The foaming matrix is constituted by two reactants (acquired by Gelest Inc., Morrisville, NY, USA) selected in order to have a dehydrogenative coupling reaction: a Methylhydrosiloxane—dimethylsiloxane copolymer, trimethylsiloxane terminated, PMHS (M.W. 1400–1800, viscosity 15–25 cSt), and a silanol terminated polydimethylsiloxane (PDMS—M.W. 110,000, viscosity 50,000 cSt). In order to activate the reaction between the two siloxane compounds, Tin(II) 2-ethylhexanoate (Sn(II)) (supplied by Sigma Aldrich, St. Louis, Missouri, NY, USA) was used as catalyst.

Two different types of samples have been prepared in this study. In the first case the slurry has been introduced in an open mold, in order to guarantee an almost free expansion of the foam. In the second case, the slurry has been forced inside channels of a paperboard, in order to constrain the foam expansion in a similar way to what would happen in the construction of real components. As shown in Figure 1, the foamed composite sample preparation can be summarized in five main steps:

(1) Filler dispersion. Preliminarily SAPO34 zeolite powder was gradually dispersed under vigorous magnetic stirring in the polydimethylsiloxane (PDMS) compound for about 60 s. In order to obtain a homogenous dispersion of the filler and to reduce the solution viscosity, water and ethanol solvents were added to the mixture.

(2) Composite slurry. Afterward, the polymethylhydrosiloxane (PMHS) compound was thoroughly added in the mixture obtained in point 1, always under vigorous magnetic stirring. The stirring was maintained for 60 s until a homogenous composite slurry is obtained.

(3) Reaction activation. The catalyst (diluted in ethanol) is gently added in the composite slurry. A vigorous mixing was applied for about 20 s.

(4) Molding. Immediately, the catalyst activated composite slurry was poured, by using a syringe tool:

- Into a cylindrical open mold (diameter 25 mm).
- Into the cavities of a corrugated cardboard (inner height and base of the cross section respectively equal to 5 mm and 10 mm, channel length equal to 5 cm).

The samples rest open to air at room temperature for about 30 s, to stabilize the mixture in the free surface area of the mold.

(5) Foaming. Finally, the foaming process was triggered putting the filled samples into an oven set at 60 °C for 24 h to allow the matrix curing. At the end of the curing process the obtained foams poured in a cylindrical mold were cut in order to get cubic samples with edge of about 20 mm.

The foamed structure is obtained during the last point 5 of the process thanks to the dehydrogenative coupling reaction between hydroxyl terminated polydimethylsiloxanes (PDMS) that react with hydride functional siloxane (PMHS) to produce foamed silicone materials, according to the following reaction:

$$\equiv Si - OH + H - Si \equiv \rightarrow \equiv Si - O - Si \equiv + H_2 \uparrow \quad (1)$$

The reaction of siloxane compounds leads to a polymer network in a silicone rubber [23]. As reaction product gaseous hydrogen is formed, acting as blowing agent [24]. This process is indicated as chemical blowing process. Furthermore, a physical blowing phenomenon occurs during the crosslinking reaction, due to the evaporation of the solvent during the curing stage. The combination of chemical and physical blowing allows to obtain a microporous structure with good foaming ration and well-interconnected bubbles.

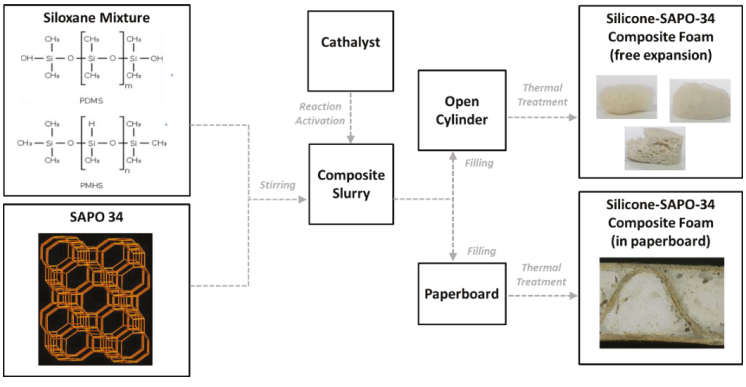


**Figure 1.** Preparation steps of the silicone-SAPO34 composite foam.

Three different foam formulations were produced by varying the SAPO34 filler content in the range 20–60 wt.% of the PDMS-PMHS siloxane matrix. All produced formulations with details of compound amounts are summarized in Table 1. The samples were codified by means a prefix "Z" coupled to a number. Z is referred to the zeolite based foam, instead the number indicates the amount (%) of the SAPO34 zeolite added to the siloxane matrix; i.e., Z20 code is referred to a composite foam filled by 20 wt.% of SAPO34. The term Z0 is used to refer to pure foam without zeolite. (The bold explanation)

**Table 1.** Siloxane solution compositions (wt.%) at varying zeolite content.

| Component | Z0 | Z20 | Z40 | Z60 |
|---|---|---|---|---|
| PDMS—Siloxane | 42.6% | 37.4% | 29.8% | 21.7% |
| PMHS—Siloxane | 21.3% | 18.7% | 14.9% | 10.9% |
| Ethanol—Solvent | 14.9% | 12.3% | 10.3% | 7.6% |
| Water—Solvent | 10.6% | 8.7% | 7.4% | 5.4% |
| Sn(II)—Catalyst | 10.6% | 8.7% | 7.4% | 5.4% |
| Zeolite—Filler | 0% | 14.2% | 30.2% | 48.9% |
| Zeolite/Foam | 0% | 20% | 40% | 60% |

### *2.2. Experimental Equipment and Methodology*

#### 2.2.1. Dynamic Water Vapor Adsorption Analyzer

Water adsorption isotherms of pure zeolite SAPO34 and of the adsorbent foams Z20, Z40, and Z60 have been measured by a gravimetric adsorption apparatus (Aquadyne DVS). The anhydrous reference state was obtained at 80 °C in nitrogen atmosphere and at ambient total pressure. Experimental uncertainty of temperature, relative humidity and mass of the apparatus are respectively: ±0.2 °C; from ±0.8% at 20 °C to ±1.8% at 70 °C; 1.0 μg plus 0.001% of measured mass.

The anhydrous reference state of pure zeolite or foams is obtained by drying each sample in the chamber of the equipment for several hours (around 8–10 h), until no weight variation is observed, at the aforementioned conditions. Then, the chamber is set at the desired temperature (30 °C, 50 °C, or 70 °C) and sorption curve is determined by evaluating the sample mass variation at different relative humidity. Each step is assumed in steady state conditions when mass variation is lower than 0.0001% in a minute.

#### 2.2.2. Differential Scanning Calorimetry

The specific heat was evaluated by means of calorimetric measurement performed by DSC1 METTLER TOLEDO. The instrument before all measurements was calibrated by pure indium sample.

The test was performed measuring the baseline of the empty crucible, the baseline of the sample, and the baseline of the reference material (sapphire). Subsequently, the difference between sample and empty crucible is defined as $H$, while the difference between reference and empty crucible is defined as $h$. Knowing these values, the specific heat of the sample under investigation can be calculated as

$$c_{p,\,sample} = \frac{H}{h}\,\frac{m_{ref}}{m_{sample}}\,c_{p,ref} \tag{2}$$

The used protocol for each measurement is as follows, consistent with the American Standard ASTM E1269-11:

- Drying of the foam sample up to 85 °C over night.
- Loading of the dry adsorbent material inside a crucible and sealing it to prevent humidity adsorption.
- Measurement of the specific heat in temperature interval between 30 °C and 70 °C, employing the standard specific heat method against a reference material (sapphire method). The heating rate for specific heat measurement is usually 2 °C $min^{-1}$.

#### 2.2.3. Other Equipment

Optical microscopy was carried out by using a three-dimensional digital microscope (Hirox HK-8700). Mechanical properties of the prepared foams were measured by using a universal testing machine (2.5 kN Zwick Line) equipped with a 2.5 kN load cell (sensitivity of 0.001 N).

## 3. Results

In this section physical properties of prepared samples of silicone–zeolite foams are reported and discussed. Results are shown first for samples obtained through a quasi-free expansion process and, then, for samples prepared inside paperboard channels. Tests have been carried out in the temperature range between 30 °C and 70 °C, which is of interest for low temperature heat storage applications.

### *3.1. Composite Foams Obtained through Almost Free Expansion Process*

#### 3.1.1. Morphology and Mechanical Properties

The macroporous morphology of the composite foams at varying zeolite content is reported in Figure 2. All specimens evidenced a micro-structure without macroscopic defects indicating a suitable foaming process. A quite homogeneous cell geometry and distribution can be also highlighted. Although, some differences among foams, at varying zeolite content can be observed. In particular, at low zeolite content (foam Z20), the foam morphology is characterized by well-interconnected bubbles, suggesting the presence of micro channels among the bubbles. In fact, these foams are characterized by an open/close cell structure. The bubble walls are structurally compact, thick and defect-free. This suggests that mechanically unstable regions in the foams were not recognized. During the foaming process, the expansion of the siloxane matrix takes place because of hydrogen gas evolution induced by dehydrogenative coupling reaction. This leads to an expansion of the structure with progressively larger macropores. This effect is more evident as higher is the zeolite content in the composite foam. At increasing filler content, the viscosity of slurry significantly increases, thus hindering the hydrogen induced bubbling growth. As a consequence, foams with high zeolite content (foam Z60) showed numerous small bubbles homogeneously distributed. Some small and local macropores were occasionally evidenced.

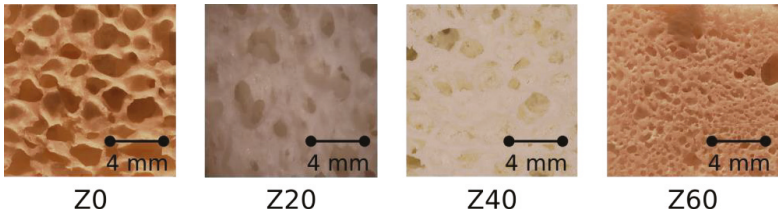


**Figure 2.** Macroporus morphology of composite foams at increasing zeolite content.

In order to better relate composite foam morphology and its mechanical performances, Table 2 summarizes apparent density (calculated as weight to volume ratio) and elastic properties for all composite zeolite foams. As reference, the not filled foam was also added. This information, can provide a direct practical information on the use and handling conditions of the material.

**Table 2.** Density and elastic properties for all composite zeolite foams.

| Component | | Z0 | Z20 | Z40 | Z60 |
|---|---|---|---|---|---|
| **Apparent Density (g cm$^3$)** | average | 0.27 | 0.30 | 0.37 | 0.91 |
| | Stand. Dev. | 0.021 | 0.033 | 0.058 | 0.127 |
| **Average diameter (mm)** | average | 1.21 | 1.07 | 0.66 | 0.26 |
| | Stand. Dev. | 0.97 | 0.85 | 0.55 | 0.18 |
| **Elastic Modulus (MPa)** | average | 0.031 | 0.050 | 0.055 | 1.552 |
| | Stand. Dev. | 0.005 | 0.006 | 0.009 | 0.274 |
| **Comp. Stress (30% Strain) (MPa)** | average | 0.005 | 0.006 | 0.014 | 0.340 |
| | Stand. Dev. | $5 \times 10^{-4}$ | $5 \times 10^{-4}$ | $5 \times 10^{-3}$ | 0.098 |

Due to the zeolite filler addition, a gradual increase of elastic modulus and compression stress can be observed. In particular, the Foam Z60 showed an elastic modulus of 1.552 MPa, about two orders of magnitude higher than the unfilled one (Foam Z0, 0.031 MPa).

As a consequence of the soft behavior of the microporous matrix, all composite foams exhibited a quite low compression stress. Although, as observed for the elastic modulus, a progressive increase at increasing the zeolite amount, was observed. However, although an increase in compressive stress takes place, the modulus increase limits the foam compressibility, representing a warning to pay attention during practical use and handling of the material.

This behavior can be ascribed to the foam microstructure. At increasing amount of adsorbent filler in the foam, apparent density of the foam increases due to a densification effect of the composite material induced by the filler addition. The foaming ratio is gradually reduced as evidenced by comparing the density of Foam Z60 that is three times higher than unfilled one (foam Z0). In particular, based on calculated apparent density, it is possible to identify the foam void content (Vc), defined as

$$\text{Vc} = 1 - \text{Apparent Density}/\text{Bulk Density} \quad (3)$$

where the bulk density can be calculated through the rule of the mixture of the composite constituents. The void content decreases at increasing filler content. In particular for Z0 and Z60 batches a Vc of 72.2% and 47.8% was obtained. This confirms the limited foaming for high zeolite content composite specimens.

The presence of the filler partially hinders the bubble growth during the foaming stage, mainly limiting the coalescence phenomena of the bubbles. In fact, the bubble dimension in the foams with higher amount of zeolite filler are characterized by quite lower average diameter size. The standard deviation is also reduced as confirmation of the less dispersed size distribution. However,

the composite foam structure preserves the presence of microchannels, which, considering also the high permeability of the silicone matrix to water vapor, could act as preferential paths for the water vapor diffusion, potentially preserving the effective adsorbing capacity of the zeolite.

#### 3.1.2. Adsorption Capacity

As shown in Figure 3, water adsorption isotherms of pure SAPO34 and of Z20, Z40, and Z60 have been measured at 30 °C and 70 °C. The sharp uptake rise at low relative humidity (RH < 15–20%) and, more generally, the isotherm shape of the pure material is similarly present also in the foams proposed in this work. At each step of relative humidity, sorption capacities of Z20, Z40, and Z60 are lower than one of pure SAPO34. This effect is related to the presence of silicone (included in the reference mass of each sample) that does not participate in the sorption process. As discussed in a previous research [22], the reduced adsorption capacity is in agreement with the zeolite mass fraction. In fact, if the adsorption capacity were referred only to the dry mass of zeolite of each sample, adsorption isotherm curves of pure desiccant and of foams would be very close (maximum reduction around 14%).

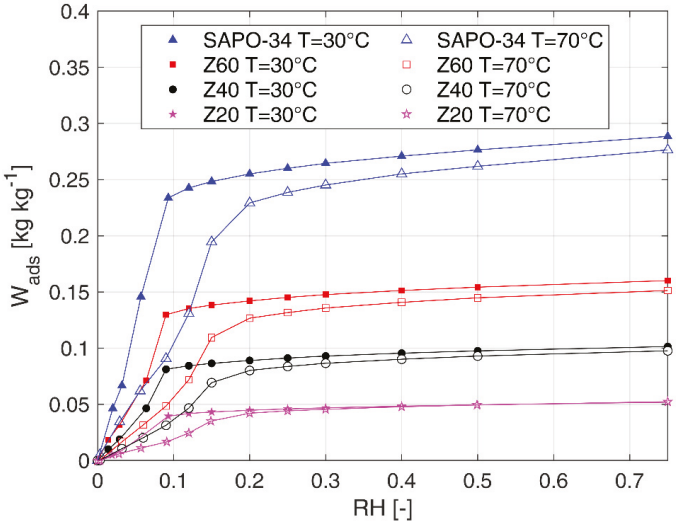


**Figure 3.** Adsorption capacity of pure SAPO34 and zeolite foams at different temperature.

Based on obtained results, Z60 foam keeps a high sorption capacity of the SAPO34 and, therefore, can be effectively used to develop innovative components for heat storage applications.

Experimental data at 30 °C and 70 °C and additional ones at 50 °C have been used to fit parameters of sorption isotherm curves proposed by Dubinin–Asthakov (D-A) [25]:

$$W_{ads} = W_0\, e^{-\left(\frac{A}{E}\right)^n} = W_0\, e^{-\left(\frac{-RT\ ln(RH)}{E}\right)^n} \quad (4)$$

where $W_0$ is the maximum sorption capacity, $A$ is the adsorption potential, $E$ is the characteristic D-A parameter and $n$ is an exponent describing the surface heterogeneity. The adopted fitting approach has already been used by other researchers [26,27] for SAPO34, with satisfactorily results. Parameters can be fitted by using entire data between minimum and maximum sorption capacity (obtaining one set of parameters) [26] or by dividing the uptake curve in different sections (obtaining multiple sets of parameters) [27]. Authors adopted the first approach because it is particularly simple and obtained correlation can be easily implemented in phenomenological models of the device, although the second one generally leads to a more accurate correlation. Obtained parameters of Z60 are $W_0$ = 0.1486 kg kg$^{-1}$,

E = 420 kJ kg$^{-1}$ and n = 4.01 with R-square equal to 0.9376. Measured adsorption equilibrium curves and numerical results obtained through Equation (4) are reported in Figure 4.

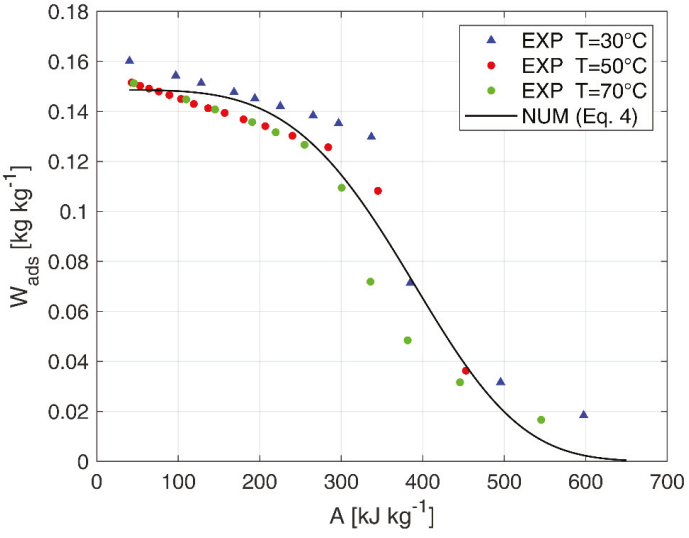


**Figure 4.** Adsorption capacity Z60 zeolite foam at different temperatures as a function of the adsorption potential.

Finally, according to the adopted D-A approach, it is worth specifying that the heat of adsorption can been calculated as:

$$Q_{ads} = \lambda + A \tag{5}$$

where λ is the enthalpy of evaporation of water at a given temperature and $A$ is the adsorption potential. In Figure 5, the heat of adsorption of Z60 is calculated and plotted against the sorption capacity for different temperatures (by using Equations (4) and (5)).

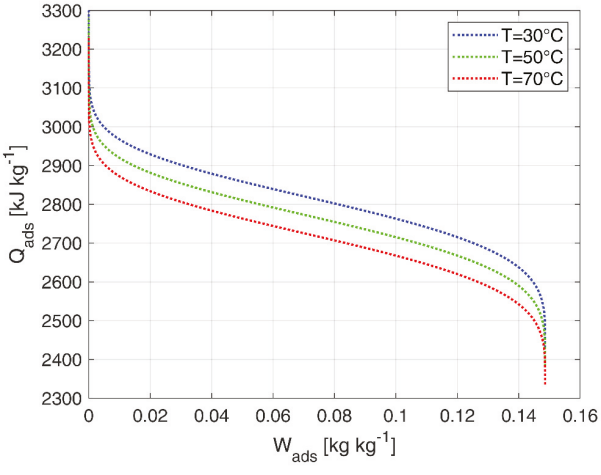


**Figure 5.** Z60 zeolite foam: heat of adsorption as a function of adsorption capacity at different temperatures.

Although the evaluation of the adsorption kinetics is not the scope of this work, it is worth specifying that silicone foam does not affect significantly adsorption kinetics. Sorption characteristic time of pure zeolite and foamed samples is of the same magnitude order.

#### 3.1.3. Specific Heat

Figure 6 reports the specific heat $c_p$ evaluated for Z20, Z40, and Z60 foams in anhydrous state and in the temperature range 30–70 °C. As expected, in all cases the specific heat increases as temperature increases. Moreover, the specific heat is higher in samples with lower SAPO34 loading, ranging from about 0.85 kJ kg$^{-1}$ °C$^{-1}$ (foam Z60) to about 1.6 kJ kg$^{-1}$ °C$^{-1}$ (foam Z20). This behavior is due to the higher specific heat of the polymeric phase with respect to the pure SAPO34 fraction, which is characterized by relatively low specific heat (0.82–0.94 kJ kg$^{-1}$ °C$^{-1}$ [28]). The low specific heat of the Z60 foam is a physical property of interest for the application of thermal energy storage. In fact, it leads to a decrease in the energy exchanged to vary the temperature of the material in the charging and discharging cycles.

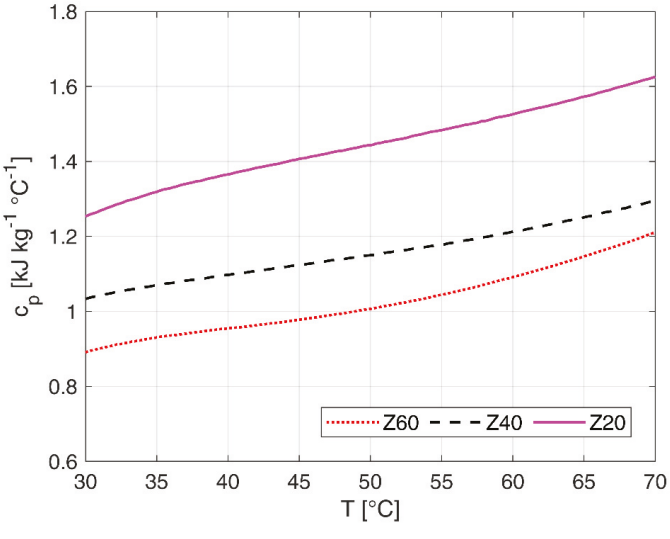


**Figure 6.** Zeolite foam: specific heat of Z20, Z40, and Z60 foams.

### *3.2. Paperboard Foamed Samples*

#### 3.2.1. Morphology

Preliminarily, optical images to assess the morphology of the foamed structure in the paperboard cavities were performed. In particular, the corrugated paperboard samples were cut in transversal and longitudinal direction to corrugation, *a* and *b* lines, respectively, as schemed in the drawing reported in Figure 7. No evidence of material loss after the cutting step was observed indicating a good structural stability of the foam filled in the cardboard cavities.

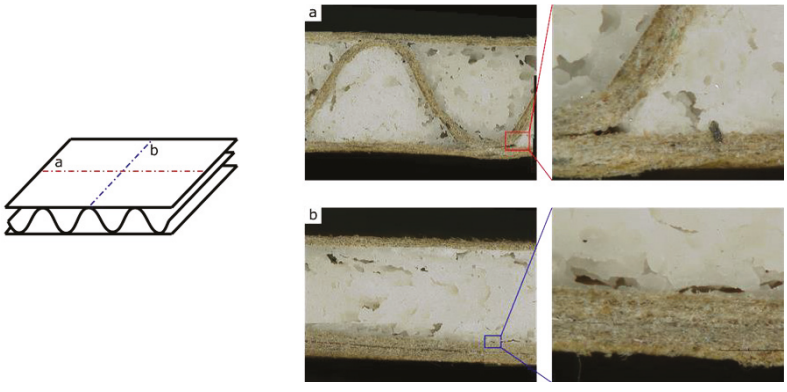


**Figure 7.** Optical images of cross-section corrugated paperboard filled with zeolite foam.

At first analyzing the transversal direction (Figure 7a), the foam morphology shows the clear presence of bubbles randomly distributed along the whole cross-section. The size and shape of the bubbles can be varied according to the coalescence phenomena that take place during foaming. This results in a heterogeneous distribution of bubble geometries [29]. However, the foam is homogeneously distributed. The adsorbent composite material is also present in the narrow cavities formed between the wave and plain sheets of the cardboard. This indicates that the filling process of the cardboard channels was effective and suitable for the viscosity of the composite slurry. However, it should be pointed out that small debonding area at the interface with the cardboard occurred, probably due to a non-optimal interaction of the composite with the surface of the cardboard. This aspect is much more evident by analyzing the longitudinal section (shown in Figure 7b). In this cross section direction, analyzing the foam/paperboard interface, some delamination lines alternate between large anchoring areas. This is imputable to the foaming process that takes place inside the cavity. The stress state induced by the increase in volume, during the bubble formation, entail the formation of shear stresses along the walls [30], that, considering the progressive solidification of the matrix during the curing, trigger cracks and delamination at the foam/paperboard interface. Although, these localized damages do not lead in the mechanical stability loss of the foam, which is always compact and not easily removable by the touch.

#### 3.2.2. Adsorption Capacity

Same samples of foam prepared in the paper board have been tested in dynamic vapor sorption analyzer in order to obtain equilibrium adsorption isotherms at 30 °C and 70 °C. It is worth specifying that only pure foam has been analyzed without any cardboard part. In Figure 8 sorption isotherms of foam expanded in the paperboard are compare with ones previously obtained through a quasi-free expansion in open cylinders, as reported in Section 3.1. It is possible to state that the constraint related to the presence of the paperboard does not affect the sorption capacity of the foam. Therefore, sorption capacity data and Dubinin–Asthakov coefficients discussed in Section 3.1.2 can be effectively used also for Z60 prepared in the paperboard.

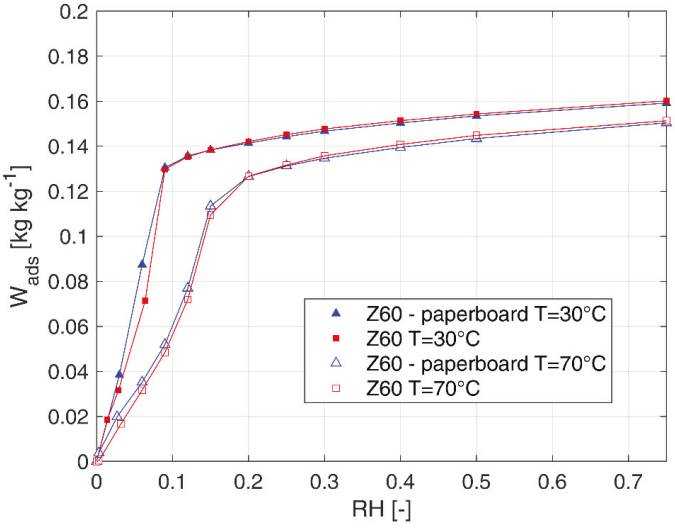


**Figure 8.** Adsorption capacity of pure Z60 zeolite foams expanded in free space (open cylinder) and inside paperboard at different temperatures.

## 4. Comparison with Other Storage Materials

As shown in [31], several classes of materials are available which can fit the requirements for heat storage applications. Table 3 reports the thermo-physical properties of sorbents suitable for application in thermal energy storage systems and compares them with the measured data for Z60.

**Table 3.** Comparison of Z60 properties with sorbent material classes for heat storage.

| | Silica Gels | Zeolites | AlPOs/SAPOs | Composites | MOFs | Activated Carbons | Z60 |
|---|---|---|---|---|---|---|---|
| **Adsorption heat (kJ/kg)** | 160/180 * | 50/300 * | 250/300 * | 50/250 * | 20/200 ** | 45/900 *** | 375/450 * |
| **Typical desorption temperatures (°C)** | 50/80 | 70/350 | 60/90 | 60/90 | 60/150 | 80/200 | 60/80 |
| **Density (kg/m$^3$)** | 650/700 | 650/900 | 800/900 | 300/600 | 1000/2000 | 700/750 | 780/1030 |
| **Specific heat (kJ/(kg °C))** | 0.8/0.9 | 0.85/0.95 | 0.85/0.95 | 0.95/1.05 | 0.8/1.2 | 0.8/1.5 | 0.8/1.5 |
| **Thermal conductivity (W/(m °C))** | 0.15/0.20 | 0.15/0.25 | 0.15/0.25 | 0.15/0.30 | 0.10/015 | 0.15/0.75 | 0.15/0.25 |
| **Possible refrigerants** | water | water | water | water, methanol, ethanol | water, methanol, ethanol | methanol, ethanol, ammonia | water |
| **Amount of uptake exchanged in a typical cycle (kg/kg)** | 0.03/0.10 | up to 0.2 | up to 0.25 | up to 0.8 | 0.16/0.40 | 015/0.60 | up to 0.25 |

* The heat of adsorption is calculated for a cycle with $T_{des}$ = 100 °C, $T_{cond}$ = 30 °C, $T_{ads}$ = 50 °C, $T_{ev}$ = 10 °C, with water as sorbate. ** The heat of adsorption is calculated from isotherms at 298 K, 303 K and 333 K, with water as sorbate. *** The range of heat of adsorption is calculated with methanol and ammonia as sorbates.

In particular, thermal conductivity for Z60 sample was experimentally measured by means of C-Therm TCi, a specific tool that allows the evaluation of the thermal conductivity and the effusiveness of the materials (solids, liquids, powders and slurries) using the technique defined "Modified Transient Plane Source (MTPS)", compliant with the ASTM D7984 standard.

The other data presented are, instead, taken from literature while the ones on heat of adsorption are based on the experimental measurements.

It is worth noticing that Z60 possesses enhanced properties for application in devices for heat storage, however the identification of the best material for heat storage is extremely application-related.

Indeed, the operating conditions under which the material is employed can strongly influence its overall performance.

As showed in the sections above, Z60 can be effectively regenerated at lower temperatures, significantly below 100 °C still having a higher uptake under the typical boundary conditions of thermal energy storage.

Table 3 also shows as newly developed materials, such as MOFs and composites, exhibit also good properties for heat storage applications, however such classes of materials are still expensive or not commercially available. Classical materials (silica-gels, activated carbons, and zeolites), instead, are cheap and easily available, but present the worst performances.

## 5. Conclusions

Novel silicone-SAPO34 composite materials have been proposed for application in adsorption thermal energy storage systems. Morphological aspects and mechanical properties at varying SAPO34 content (range 20–60 wt.%) were investigated, demonstrating homogeneous open-cell structure and good structural stability of the foam. Water adsorption measurement carried out by thermogravimetric system evidenced high adsorption capacity of the composite materials.

Based on aforementioned considerations, the foam can be used to develop scaled up prototypes of adsorbers for both open and closed systems for heat storage. Verification of the foam stability to aging cycles is another critical issue to be addressed in future activity.

**Author Contributions:** Conceptualization, L.C., S.D.A., and A.F.; methodology, S.D.A., L.C., and A.F.; investigation, L.C., S.D.A., S.V., V.B., and A.F.; data curation, L.C., S.D.A., S.V., and V.B.; writing—original draft preparation, S.D.A., L.C., S.V., and A.F.; writing—review and editing, S.D.A., L.C., S.V., and A.F.; supervision, S.D.A. and A.F. All authors have read and agreed to the published version of the manuscript.

**Funding:** This research received no external funding.

**Conflicts of Interest:** The authors declare no conflict of interest.

## References

1. Li, T.X.; Wang, R.Z.; Li, H. Progress in the development of solid–gas sorption refrigeration thermodynamic cycle driven by low-grade thermal energy. *Prog. Energy Combust. Sci.* **2014**, *40*, 1–58. [CrossRef]
2. Palomba, V.; Frazzica, A. Recent advancements in sorption technology for solar thermal energy storage applications. *Sol. Energy* **2019**, *192*, 69–105. [CrossRef]
3. Zouaoui, A.; Zili-Ghedira, L.; Nasrallah, S.B. Open solid desiccant cooling air systems: A review and comparative study. *Renew. Sustain. Energy Rev.* **2016**, *54*, 889–917. [CrossRef]
4. Jani, D.B.; Mishra, M.; Sahoo, P.K. Solid desiccant air conditioning—A state of the art review. *Renew. Sustain. Energy Rev.* **2016**, *60*, 1451–1469. [CrossRef]
5. Zheng, X.; Ge, T.S.; Wang, R.Z. Recent progress on desiccant materials for solid desiccant cooling systems. *Energy* **2014**, *74*, 280–294. [CrossRef]
6. Henninger, S.K.; Ernst, S.-J.; Gordeeva, L.G.; Bendix, P.; Fröhlich, D.; Grekova, A.D.; Bonaccorsi, L.; Aristov, Y.; Jaenchen, J. New materials for adsorption heat transformation and storage. *Renew. Energy* **2017**, *110*, 59–68. [CrossRef]
7. Zheng, X.; Wang, R.Z.; Ge, T.S.; Hu, L.M. Performance study of SAPO-34 and FAPO-34 desiccants for desiccant coated heat exchanger systems. *Energy* **2015**, *93*, 88–94. [CrossRef]
8. Freni, A.; Maggio, G.; Sapienza, A.; Frazzica, A.; Restuccia, G.; Vasta, S. Comparative analysis of promising adsorbent/adsorbate pairs for adsorptive heat pumping, air conditioning and refrigeration. *Appl. Therm. Eng.* **2016**, *104*, 85–95. [CrossRef]
9. Intini, M.; Goldsworthy, M.; White, S.; Joppolo, C.M. Experimental analysis and numerical modelling of an AQSOA zeolite desiccant wheel. *Appl. Therm. Eng.* **2015**, *80*, 20–30. [CrossRef]
10. Li, X.H.; Hou, X.H.; Zhang, X.; Yuan, Z.X. A review on development of adsorption cooling—Novel beds and advanced cycles. *Energy Convers. Manag.* **2015**, *94*, 221–232. [CrossRef]

11. Santamaria, S.; Sapienza, A.; Frazzica, A.; Freni, A.; Girnik, I.S.; Aristov, Y.I. Water adsorption dynamics on representative pieces of real adsorbers for adsorptive chillers. *Appl. Energy* **2014**, *134*, 11–19. [CrossRef]
12. Freni, A.; Bonaccorsi, L.; Calabrese, L.; Caprì, A.; Frazzica, A.; Sapienza, A. SAPO-34 coated adsorbent heat exchanger for adsorption chillers. *Appl. Therm. Eng.* **2015**, *82*, 1–7. [CrossRef]
13. Bonaccorsi, L.; Calabrese, L.; Freni, A.; Proverbio, E.; Restuccia, G. Zeolites direct synthesis on heat exchangers for adsorption heat pumps. *Appl. Therm. Eng.* **2013**, *50*, 1590–1595. [CrossRef]
14. Girnik, I.S.; Aristov, Y.I. Making adsorptive chillers more fast and efficient: The effect of bi-dispersed adsorbent bed. *Appl. Therm. Eng.* **2016**, *106*, 254–256. [CrossRef]
15. Bauer, J.; Herrmann, R.; Mittelbach, W.; Schwieger, W. Zeolite/aluminum composite adsorbents for application in adsorption refrigeration. *Int. J. Energy Res.* **2009**, *33*, 1233–1249. [CrossRef]
16. De Antonellis, S.; Joppolo, C.M.; Molinaroli, L. Simulation, performance analysis and optimization of desiccant wheels. *Energy Build.* **2010**, *42*, 1386–1393. [CrossRef]
17. Zhang, Y.; Wang, R. Sorption thermal energy storage: Concept, process, applications and perspectives. *Energy Storage Mater.* **2020**, *27*, 352–369. [CrossRef]
18. De Antonellis, S.; Colombo, L.; Freni, A.; Joppolo, C. Feasibility study of a desiccant packed bed system for air humidification. *Energy* **2021**, *214*. [CrossRef]
19. Aristov, Y.I. Concept of adsorbent optimal for adsorptive cooling/heating. *Appl. Therm. Eng.* **2014**, *72*, 166–175. [CrossRef]
20. Calabrese, L.; Bonaccorsi, L.; Bruzzaniti, P.; Frazzica, A.; Freni, A.; Proverbio, E. Adsorption performances of SAPO34 silicone composite foams for adsorption heat pump applications. *Mater. Renew. Sustain. Energy* **2018**, *7*, 24. [CrossRef]
21. Calabrese, L.; Bonaccorsi, L.; Freni, A.; Proverbio, E. Silicone composite foams for adsorption heat pump applications. *Sustain. Mater. Technol.* **2017**, *12*, 27–34. [CrossRef]
22. Bonaccorsi, L.; Calabrese, L.; De Antonellis, S.; Freni, A.; Joppolo, C.; Motta, M. Composite silicone-SAPO-34 foams: Experimental characterization for open cycle applications. In Proceedings of the 13th REHVA World Congress, CLIMA 2019, Bucharest, Romania, 26–29 May 2019; Volume 111, pp. 1–4.
23. Chruściel, J.J.; Leśniak, E. Preparation of flexible, self-extinguishing silicone foams. *J. Appl. Polym. Sci.* **2011**, *119*, 1696–1703. [CrossRef]
24. Jawhar, M.-C.D.; Blanc, D.; Chaumont, P.; Cassagnau, P. Study of the Coalescence Mechanisms During Silicone Foaming. *Macromol. Mater. Eng.* **2013**, *299*, 336–343. [CrossRef]
25. Ruthven, D.M. *Principles of Adsorption and Adsorption Processes*; John Wiley & Sons: Hoboken, NJ, USA, 1984.
26. Nienborg, B.; Helling, T.; Fröhlich, D.; Horn, R.; Munz, G.; Schossig, P. Closed Adsorption Heat Storage—A Life Cycle Assessment on Material and Component Levels. *Energies* **2018**, *11*, 3421. [CrossRef]
27. Brancato, V.; Frazzica, A. Characterisation and comparative analysis of zeotype water adsorbents for heat transformation applications. *Sol. Energy Mater. Sol. Cells* **2018**, *180*, 91–102. [CrossRef]
28. Kakiuchi, H.; Shimooka, S.; Iwade, M.; Oshima, K.; Yamazaki, M.; Terada, S.; Watanabe, H.; Takewaki, T. Novel Water Vapor Adsorbent FAM-Z01 and its Applicability to an Adsorption Heat Pump. *Kagaku Kogaku Ronbunshu* **2005**, *31*, 361–364. [CrossRef]
29. Calabrese, L.; Brancato, V.; Palomba, V.; Frazzica, A.; Cabeza, L.F. Assessment of the hydration/dehydration behaviour of MgSO4·7H2O filled cellular foams for sorption storage applications through morphological and thermo-gravimetric analyses. *Sustain. Mater. Technol.* **2018**, *17*, 00073. [CrossRef]
30. Calabrese, L.; Bonaccorsi, L.; Bruzzaniti, P.; Freni, A.; Proverbio, E. Morphological and functional aspects of zeolite filled siloxane composite foams. *J. Appl. Polym. Sci.* **2018**, *135*, 45683. [CrossRef]
31. Vasta, S.; Brancato, V.; La Rosa, D.; Palomba, V.; Restuccia, G.; Sapienza, A.; Frazzica, A. Adsorption Heat Storage: State-of-the-Art and Future Perspectives. *Nanomaterials* **2018**, *8*, 522. [CrossRef]

applied sciences

MDPI

Article

# Thermodynamic Efficiency of Water Vapor/Solid Chemical Sorption Heat Storage for Buildings: Theoretical Limits and Integration Considerations

**Frédéric Kuznik [1,*] and Kévyn Johannes [2]**

[1] INSA–Lyon, Université de Lyon, CETHIL UMR5008 F–69621 Villeurbanne, France
[2] UCBL, Université de Lyon, CETHIL UMR5008 F–69621 Villeurbanne, France; kevyn.johannes@insa-lyon.fr
* Correspondence: frederic.kuznik@insa-lyon.fr; Tel.: +33-472-438-461

Received: 6 April 2019; Accepted: 6 January 2020; Published: 9 January 2020

**Featured Application: The paper provides theoretical limits of chemisorption heat storage in buildings and discusses solutions for an efficient system integration.**

**Abstract:** The theoretical limits of water sorbate-based chemical sorption heat storage are investigated in this study. First, a classification of thermochemical heat storage is proposed based on bonding typology. Then, thermodynamics of chemical solid/gas sorption is introduced. The analysis of the reaction enthalpy from the literature indicates that this value is only slightly varying for one mole of water. Using this observation, and with the help of thermodynamic considerations, it is possible to derive conclusions on energy efficiency of closed and open heat storage systems. Whatever the salt, the main results are (1) the energy required for evaporation of water is, at least, 65% of the available energy of reaction, and (2) the maximum theoretical energy efficiency of the system, defined as the ratio of the heat released to the building over the heat provided to the storage, is about 1.8. Considering the data from literature, it is also possible to show that perfectly working prototypes have an energy efficiency about 49 %. Based on those results, it is possible to imagine that for the best available material, a perfect thermochemical heat storage system would correspond to 12 times water with a temperature difference about 50 °C. Such solution is definitely competitive, provided that some difficult issues are solved—issues that are discussed throughout this paper.

**Keywords:** chemical sorption; heat storage; system efficiency; reaction enthalpy; theoretical limits

## 1. Introduction

It is obvious that everything has a limit. However, it is better to know its value to avoid wasting effort, time and money to find means of going beyond that limit. Chemical solid/gas reaction, i.e., thermochemical, can reach high thermal energy density. The first studies dealing with chemical heat storage are from the 1980s but it has become a real subject of interest during the last 10 years [1–8]. Among possible reactions, those using water are the most studied because of its availability and non-toxicity. Whatever the system, closed or open reactor, one of the main design criteria is the energy efficiency of the thermal storage system: this is the purpose of the present article.

Basically, thermal energy storage can be used for a wide range of applications [9]: for temperatures ranging from 600 °C in concentrated solar power to −20 °C for cooling; and for dimensions ranging from thousands of cubic meters to cubic millimeters. However, the most studied application remains building as it is an important leverage of energy consumption reduction. In buildings, the available heat can mainly come from solar energy or electrical energy. Therefore, the charging temperature of the storage system remains below 150 °C: only materials with a dehydration temperature below this limit will be considered. During the discharge, the system must provide the heat required for heating

and/or domestic hot water production: these constraints will drive the power and temperature during the release of heat. The two main objectives of heat storage in buildings are 1) to store heat during the summer and release heat during cold days: interseasonal storage or 2) to store heat during electricity off-peak period and release heat during peak load: peak load shaving.

Now, let us have a look at the literature dealing with chemical reaction system efficiency. $MgCl_2 \cdot 6\,H_2O$ was selected by [10] to be tested in a 17 L open reactor. Under realistic operating condition, the energy storage capacity of the reactor reached about 139 kWh $m^{-3}$. The energy efficiency was characterized by the instantaneous electrical *COP* of the system evaluated via:

$$COP_{el} = \frac{P_{heating}}{P_{fan}} \quad (1)$$

where $P_{heating}$ is the heat released and $P_{fan}$ the fan electrical energy. A maximum electrical coefficient of performance of 12 was found, but the authors expected to reach up to 30 with by optimizing the heat recovery and decreasing the pressure drop in the storage. Of course this high *COP* value is a direct consequence of the "home-made" definition. For the sake of clarity and generalizability, the present study will only deal with thermodynamic efficiency of the system.

A laboratory scale closed chemical heat storage system was developed in [11], capable of holding about 974 g of material. The storage material used was $SrBr_2 \cdot 6\,H_2O$ and 13 dehydration and hydration cycles were conducted. The energy storage capacity of the reactor was about 65 kWh. The reactor thermal energy efficiency was 0.77 meaning a global heat loss of 23%.

It is worth mentioning that other reactors have been experimentally tested but no data are available concerning the energy efficiency:

- $SrBr_2 \cdot 6\,H_2O$ in an open reactor—[12],
- $Na_2S \cdot 5\,H_2O$ in a closed reactor—[13],
- $SrBr_2 \cdot 6\,H_2O$ in an open reactor—[14,15],
- $CaCl_2 \cdot 2\,H_2O$ in a closed reactor—[16],
- $CaCl_2 \cdot 2\,H_2O$ in an open reactor—[17].

The experimental investigation was focused on the reactor alone and the storage capacity and efficiency were based on a perfect system integration. For example, heat required for water vapor generation is never evaluated nor discussed. Further discussion on protype efficiency is discussed in Section 4 of the paper.

On the other side, the theoretical *COP* of chemical heat pump, i.e., closed system, was studied in [18]. The calculated standard enthalpy of reaction of 34 salts was used to evaluate the influence of thermophysical properties on energy and exergy efficiency of a perfect system with recovery of condensation heat and "energy–free" heat of vaporization. The main results were (1) the maximum *COP* is about 1.84 for $CaSO_4 \cdot 2\,H_2O$ and (2) the behavior of the energetic efficiency and the exegetic efficiency is opposite. The calculations were based on the evaluation of the perfect thermodynamic cycle.

The originality of the paper is the evaluation of the theoretical limits of the thermodynamic efficiency of water sorbate/salt chemical sorption heat storage system. To our knowledge, it is the first attempt to evaluate such limits. The starting point of our work is simple: examining data from the literature, the enthalpy of reaction of one mole of water varies little from one reaction to the other. Then, with the help of chemical thermodynamics, it is possible to derive general considerations concerning the efficiency of open and closed heat storage systems integrated in a building. Moreover, also considering the existing prototype data, more expanded conclusions are derived.

## 2. Heat Storage Classification

In the literature, *thermochemical heat storage* is employed for a family of reactions involving both physical and chemical processes. A tentative of classification is given in [19] and is presented in

Figure 1. However, in this classification, sorption is used to aggregate different physical phenomena and can lead to misunderstandings. Then, we propose, in this section, to derive a classification of thermochemical heat storage based on physical phenomena typology. We deliberately limit the classification development to heterogeneous Involving components of two or more phases) reactions as homogeneous reactions are seldom used for thermal energy storage.

Let us first define sorption: according to [20], sorption is *the process by which a substance (sorbate) is sorbed (adsorbed or absorbed) on or in another substance (sorbent)*. The process can be caused by physical bonding, i.e., physical sorption, or chemical bonding, i.e., chemical sorption. The main difference between physical and chemical sorption lies in the nature of created bonds. Physical sorption is weak, long range bonding mostly Van der Walls interactions and hydrogen bonding. Chemical sorption is strong, short range bonding involving orbital overlap and charge transfer. Another main difference between physical and chemical sorption is that the latter requires activation energy whereas it is not the case for the first process.

Sorption can be absorption or adsorption. Definitions of both processes can be found in [20]:

- Absorption is *the process of one material (absorbate) being retained by another (absorbent); this may be the physical solution of a gas, liquid, or solid in a liquid, attachment of molecules of a gas, vapor, liquid, or dissolved substance to a solid surface by physical forces, etc.*.
- Adsorption is *an increase in the concentration of a dissolved substance at the interface of a condensed and a liquid phase due to the operation of surface forces. Adsorption can also occur at the interface of a condensed and a gaseous phase*.

While molecule undergoing absorption are taken up through the bulk of the absorbent (for example by diffusion), adsorption is a surface process. It is sometimes difficult to find the difference between adsorption and absorption. Taking for example the dehydration of lithium sulphate monohydrate [21] (i.e., chemical sorption), nucleation is supposed to occur at the surface of the grain (adsorption) and then the growth proceeds towards the center of the grains by diffusion (absorption).

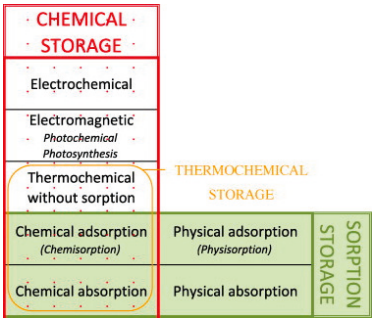


**Figure 1.** Chemical storage and sorption storage classification—reproduced from [19], copyright permission: Elsevier, 2019.

Physical sorption can be split into absorption and adsorption (also called physisorption). As with physical sorption, chemical sorption can be split into absorption and adsorption:

- Chemical absorption or reactive absorption is a chemical reaction between the absorbed and the absorbing substances. Sometimes it combines with physical absorption. This type of absorption depends upon the stoichiometry of the reaction and the concentration of its reactants.
- Chemical adsorption is called chemisorption. Chemisorption is *Adsorption which results from chemical bond formation (strong interaction) between the adsorbent and the adsorbate in a monolayer on the surface* [20].

From the previous definition, we propose in Figure 2 a classification of heat storage systems based on the physical/chemical phenomena involved. For heat storage, the split between physical and chemical sorption is important as the heat related to the two phenomena is quite different. For example, heat of adsorption is different for physisorption and chemisorption:

- Physisorption: 5–45 kJ $mol^{-1}$ in [22]; 2–29 kJ $mol^{-1}$ in [23]
- Chemisorption: 80–400 kJ $mol^{-1}$ in [22]; >30 kJ $mol^{-1}$ in [23]

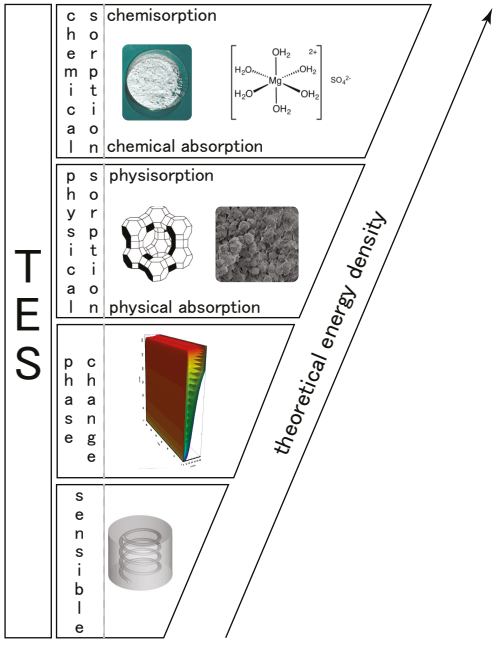


**Figure 2.** Classification of heat storage by physical phenomena.

## 3. Basics of Chemical Thermodynamics

### *3.1. Energy Change in Chemical Sorption*

Let us consider the water sorbate heterogeneous chemical sorption reaction process expressed under the following general form:

$$A_{solid} + \nu H_2O_{gas} \rightleftharpoons (A\nu H_2O)_{solid} \quad (2)$$

The first law of thermodynamics states that the change in the internal energy of a system $\Delta U$ is equal to the sum of the heat gained/lost by the system $Q$ and the work done by/on the system $W$:

$$\Delta U = Q + W \quad (3)$$

The amount of work of expansion done by the reaction during any transformation is given by:

$$W = -\int P \times dV \quad (4)$$

At constant volume (i.e., $W = 0$), the heat released or absorbed by the reaction is equal to the change in the internal energy that occurs during the reaction:

$$\Delta U = Q_V \tag{5}$$

Such configuration is close to **closed chemical sorption heat storage systems**.

At constant pressure, the change in the internal energy during the reaction is given by:

$$\Delta U = Q_P + W = Q_P - P \times \Delta V \tag{6}$$

Let us introduce the enthalpy of the system $H$ related to the internal energy by:

$$H = U + P \times V \tag{7}$$

Then, the heat released or absorbed during a chemical reaction at constant pressure is equal to the change in the enthalpy of the system:

$$\Delta H = Q_P \tag{8}$$

Such configuration is close to **open chemical sorption heat storage systems**.

The relationship between the change in internal energy and the change in enthalpy, assuming an ideal gas, is given by:

$$\Delta H = \Delta U - \nu \times R \times T \tag{9}$$

where $R = 8.31$ J K$^{-1}$ mol$^{-1}$ is the gas constant and $\nu$ the stoichiometric coefficient defined in Equation (2). For a temperature of 273.15 K, $R \times T = 2.27$ kJ mol$^{-1}$. This value is very low compared to the heat of reaction given per mole of water Values of enthalpies of reaction are given in Table 1), less than 4%, and then can be neglected. Consequently, it is possible to assume that the change in internal energy is more or less equal to the change in enthalpy.

### *3.2. Enthalpy of Reaction*

For the reaction given in Equation (2), $dn_{H_2O}$, $dn_A$ and $dn_{A\nu H_2O}$ are respectively the mole variation of water, solid $A$ (i.e., dehydrated salt) and solid $A\nu H_2O$ (i.e., hydrated salt). Then, the degree of advancement of the reaction $\xi$ is given by:

$$d\xi = \frac{dn_{H_2O}}{\nu} = dn_A = dn_{A\nu H_2O} \tag{10}$$

The variation of enthalpy can be written under the following form:

$$dH = \left(\frac{\partial H}{\partial P}\right)_{T,\xi} \times dP + \left(\frac{\partial H}{\partial T}\right)_{P,\xi} \times dT + \Delta_r H \times d\xi \tag{11}$$

where $\Delta_r H$ is the enthalpy of reaction at constant temperature and pressure. Of course, for a transformation at constant pressure and temperature (Constant temperature or neglected variation of enthalpy due to temperature change), the variation of enthalpy is given by $\Delta H = \Delta_r H \times \xi = Q_P$

The standard enthalpy of reaction (denoted $\Delta_r H^0$) is the enthalpy change that occurs in a system when one mole of matter is transformed by a chemical reaction under standard conditions, i.e., a temperature of 273.15 K and a pressure of 100,000 Pa. The standard enthalpy of reaction can be measured or computed using the standard enthalpy of formation of the reactants and products.

The enthalpy of reaction for a temperature $T$ is related to the standard enthalpy of reaction via:

$$\Delta_r H^0{}_T = \Delta_r H^0{}_{273.15} + \int_{273.15}^{T} (C_{A\nu H_2O} - C_A - \nu \times C_{H_2O}) \times dT \tag{12}$$

where $C$ is the specific heat of $A\nu H_2O$, $A$ or $H_2O$. It is worth mentioning that usually, the quantity $\int_{273.15}^{T} (C_{A\nu H_2O} - C_A - \nu \times C_{H_2O}) \times dt$ is small compared to $\Delta_r H^0{}_{273.15}$.

Moreover, the chemical sorption reaction being monovariant, the equilibrium is given by the Clausius–Clapeyron relation:

$$\ln\left(\frac{P_e}{P_0}\right) = -\frac{\Delta_r H^0}{\nu \times R \times T_e} + \frac{\Delta_r S^0}{\nu \times R} \tag{13}$$

where $P_e$ is the equilibrium water vapor pressure [Pa] and $T_e$ the equilibrium temperature [K].

## 4. Material Considerations

In the remaining of the study, we will consider only reactions involving temperatures below 150 °C which corresponds to a building application [1]. However, the ideas developed in the present paper can be straightforwardly adapted to other applications or other sorbates.

The dehydration of cobalt(II) chloride–6–hydrate (CoCl2.6H2O) was investigated in [24]. The enthalpy of formation was calculated using thermodynamic values. The results show that one mole of water corresponds to a variation of the reaction enthalpy about 55.2 kJ mol$^{-1}$. It is worth mentioning that the latter value is very close to the enthalpy of vaporization of ice at 25 °C i.e., 52 kJ mol$^{-1}$. This conclusion is also validated by [25].

Enthalpy of reaction given in the literature are summarized in Table 1. The enthalpy of reaction of one mole of water is only varying between 55.1 kJ mol$^{-1}$ and 67.8 kJ mol$^{-1}$. Of course, this value is close to the observations made in the literature and given above. This observation is the starting point of our demonstration concerning the maximum efficiency of a chemical sorption heat storage integrated in a building.

**Table 1.** Measured enthalpy of reaction extracted from the literature.

| Hydrated Salt | Dehydrated Salt | $\Delta_r H$ [kJ mol$^{-1}$] | $\Delta_r H/\nu$ [kJ mol$^{-1}$] | Reference |
|---|---|---|---|---|
| $MgSO_4 \cdot 6\,H_2O$ | $MgSO_4 \cdot H_2O$ | 275.7 | 55.1 | [26] |
| $LiNO_3 \cdot 3\,H_2O$ | $LiNO_3$ | 165.8 | 55.3 | [27] |
| $Al_2(SO_4)_3 \cdot 18\,H_2O$ | $Al_2(SO_4)_3 \cdot 8\,H_2O$ | 554.5 | 55.4 | [27] |
| $CaCl_2 \cdot 6\,H_2O$ | $CaCl_2 \cdot H_2O$ | 277.0 | 55.4 | [27] |
| $CuSO_4 \cdot 5\,H_2O$ | $CuSO_4 \cdot 3\,H_2O$ | 111.7 | 55.8 | [26] |
| $SrCl_2 \cdot 6\,H_2O$ | $SrCl_2$ | 342.0 | 57.0 | [27] |
| $LiSO_4 \cdot H_2O$ | $LiSO_4$ | 57.2 | 57.2 | [26] |
| $CuSO_4 \cdot 3\,H_2O$ | $CuSO_4 \cdot H_2O$ | 114.8 | 57.4 | [26] |
| $La(NO_3)_3 \cdot 6\,H_2O$ | $La(NO_3)_3 \cdot 1.5\,H_2O$ | 260.4 | 57.9 | [27] |
| $MgCl_2 \cdot 6\,H_2O$ | $MgCl_2 \cdot 4\,H_2O$ | 116.4 | 58.2 | [26] |
| $LaCl_3 \cdot 7\,H_2O$ | $LaCl_3 \cdot H_2O$ | 355.5 | 59.3 | [27] |
| $Na_2S_2O_3 \cdot 5\,H_2O$ | $Na_2S_2O_3$ | 279.9 | 56.0 | [27] |
| $MgSO_4 \cdot 7\,H_2O$ | $MgSO_4 \cdot H_2O$ | 335.7 | 56.0 | [27] |
| $CaCl_2 \cdot 2\,H_2O$ | $CaCl_2 \cdot 0.3\,H_2O$ | 101.0 | 59.4 | [28] |
| $MgCl_2 \cdot 6\,H_2O$ | $MgCl_2$ | 361.2 | 60.2 | [29] |
| $KOH \cdot 2\,H_2O$ | $KOH \cdot 1.2\,H_2O$ | 48.2 | 60.3 | [27] |
| $Zn(NO_3)_2 \cdot 6\,H_2O$ | $Zn(NO_3)_2$ | 372.0 | 62.0 | [27] |
| $Na_2S \cdot 5\,H_2O$ | $Na_2S$ | 310.0 | 62.0 | [30] |
| $CaBr_2 \cdot 6\,H_2O$ | $CaBr_2 \cdot 0.3\,H_2O$ | 353.9 | 62.1 | [27] |
| $LiCl \cdot H_2O$ | $LiCl$ | 62.2 | 62.2 | [27] |
| $K_2CO_3 \cdot 1.5\,H_2O$ | $K_2CO_3$ | 95.5 | 63.7 | [27] |
| $SrBr_2 \cdot 6\,H_2O$ | $SrBr_2 \cdot H_2O$ | 337.0 | 67.4 | [27] |
| $MgCl_2 \cdot 4\,H_2O$ | $MgCl_2 \cdot 2\,H_2O$ | 135.6 | 67.8 | [26] |

## 5. Efficiency: from Material to System

### *5.1. Concepts*

The principle diagram of a perfect sorption heat storage system using solid–water vapor chemisorption is presented in Figure 3. The 2 curves present the solid/water vapor equilibrium of the sorbent and the vapor/liquid equilibrium of the water sorbate. Under the solid/water vapor line, the sorbent is under the $A_{solid}$ form. Above the solid/water vapor line, the sorbent is under the $(Av\mathrm{H_2O})_{solid}$ form. Basically, the two main concepts of system design are closed and open.

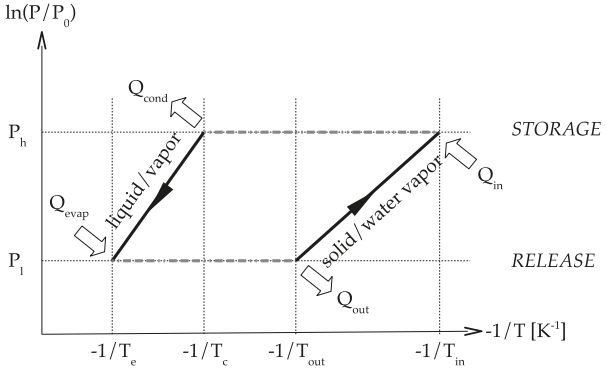


**Figure 3.** Theoretical Clausius–Clapeyron chemical sorption cycle – reproduced from [1], copyright permission: Elsevier, 2019.

The concept of closed chemical sorption thermal energy storage system is given in Figure 4. At the beginning, sorbent is under the $(Av\mathrm{H_2O})_{solid}$ form. During the storage step, $Q_{in}$ heat is transferred to the solid at the temperature $T_{in}$. Therefore, dehydration occurs, and water vapor pressure is increasing. Consequently, the gas moves from the material to the condenser where the pressure is $P_h$. The vapor condensates (in the condenser) and heat of condensation is released, $Q_{cond}$. During the release step, liquid is evaporated (in the evaporator) at temperature $T_e$, requiring energy, $Q_{evap}$. The pressure in the evaporator is higher than in the solid and a vapor flow stands. Thermal energy $Q_{out}$ is then released during the sorption reaction in the solid.

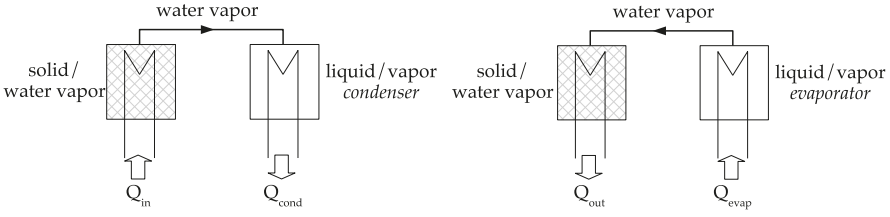


**Figure 4.** Closed heat storage system—quantities refer to Figure 3—reproduced from [1], copyright permission: Elsevier, 2019.

The other option consists of using an open system; a principle diagram of such system is given in Figure 5. The concept consists of using dry air (inert from the reaction point of view) and water vapor (i.e., humid air). During the storage step, the humid air is passing through the material under the $(Av\mathrm{H_2O})_{solid}$ form. $Q_{in}$ thermal energy is then transferred to the solid at the temperature $T_{in}$, resulting

in the dehydration process and a potential heat of condensation in the carrier, $Q_{cond}$. During the release step, humid air is passing through the material under the $A_{solid}$ form and may requires a quantity of heat to evaporate liquid water, $Q_{evap}$. The water vapor is sorbed and a quantity of thermal energy $Q_{out}$ is transferred to the humid air.

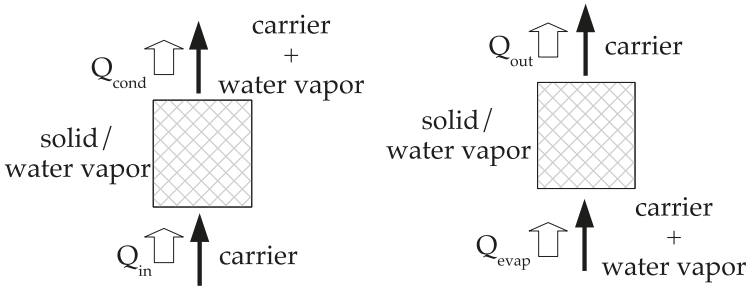


(**a**) storage – desorption (**b**) release – sorption

**Figure 5.** Open heat storage system—quantities refer to Figure 3—reproduced from [1], copyright permission: Elsevier, 2019.

In a closed system, a water tank with a heat exchanger is necessary. It behaves either like a condenser, or like an evaporator, depending on the storage or release step. In an open system, it is necessary to find the water vapor. In most of the publications, it is stated that this humidity can come from inside the building. However, calculations show that it is not enough water vapor, especially in wintertime when outside specific humidity is very low.

### *5.2. Literature Review*

#### 5.2.1. Closed Systems

A thermochemical heat pump based on the $SrBr_2$ salt was developed for the aim of both heating and cooling in [12]. The prototype is able to store 60 kWh $m^{-3}$ and 40 kWh $m^{-3}$ respectively for heating and cooling. The specific powers for heating and cooling is in the range 2.5 kW $m^{-3}$ to 4 kW $m^{-3}$. The main limitation identified by the authors was the low heat transfer at the interface between the reactive layer and the exchanger wall.

$Na_2S$ was the salt used in [31] to develop a modular heat storage system. The average heating power is 3.79 kW and energy released about 0.5 kWh. The calculations do not take into account the energy required for water vaporization during adsorption.

A closed system using $MgCl_2$ has been numerically studied in [29]. In this work, the material with the heat exchanger is modeled using Comsol Multiphysics 4.3a to evaluate the thermal and mass transport behavior of salt-hydrate during charging process. From the model, it is also possible to evaluate the temperature field in the reactor and possible problems of melting.

#### 5.2.2. Open Systems

Pure salt thermochemical heat storage has been studied in laboratory with the design and test of a prototype using the hydration of the strontium bromide $SrBr_2$ [15,32]. They report in their study that hydration specific powers up to 4.3 kW $m^{-3}$ and an energy density of 190 kWh $m^{-3}$ has been reached for a theoretical bed salt energy density of 388 kWh $m^{-3}$.

$KAI(SO_4)_2$ has been tested in a reactor of 25 kg of salt [33]. The results are an energy density of 0.2 kW kg and a power density of 4 W kg.

In [10], a selection procedure was realized to select the material tested $MgCl_2$. A prototype of 17 $dm^3$ has been tested in laboratory conditions. The prototype was able to provide 50 W heating

power at 60 °C, with an instantaneous *COP* of 12, i.e., a density about 3 kW $m^{-3}$. The authors also highlighted that the improvement of heat recovery and pressure drop could increase the performance.

A composite $MgSO_4$ salt inside zeolite reactor of 7.1 $dm^3$ was monitored during hydration and dehydration in [34]. The results are a released power of 64 W for an energy of 636 kWh meaning a released power density of 9 kW $m^{-3}$ and an energy density of 90 kWh $m^{-3}$.

### *5.3. Discussion*

Figure 6 is summarizing the results under the form of the prototype energy density versus the material energy density, of course for the available data. The main result is that whatever the material, the perfect laboratory scale reactor energy density is about 49 % of the material alone! Improvements are necessary to increase this efficiency, based on heat and mass transfers. Of course, those measurements are realized under perfect boundary conditions without considering the reactor integration in the building. In particular, the way the water vapor is produced and the way the water condensation energy is recovered has a high impact on the final maximum energy efficiency. This is the purpose of the next section.

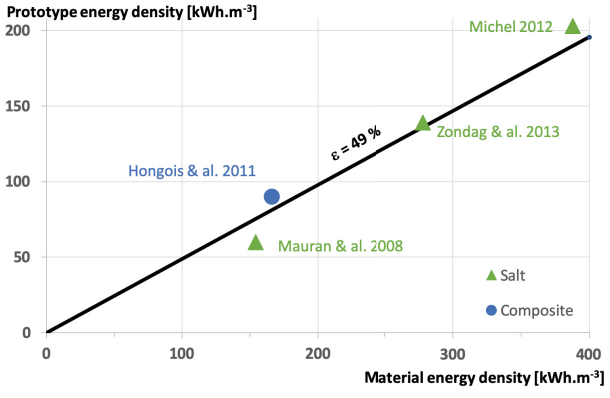


**Figure 6.** Prototype energy density versus material energy density.

## 6. Thermodynamic Efficiency: From System to Integration in Buildings

Whatever the system, open or closed, it is important to answer the issue related to the thermodynamic efficiency limit of the heat storage. Basically, the designer of such system must know the thermodynamics limit to evaluate the enhancement possibilities of its prototype.

Let us first define $Q^+$ as the supplied energy per mole of salt to the storage system and $Q^-$ as the recovered energy per mole of salt. For the sake of universality, the efficiency of the system $\eta$ is defined as:

$$\eta = \frac{Q^-}{Q^+} \tag{14}$$

This efficiency can also be found as *COP* in the literature [3]. However, the definition of *COP* may vary from one author to the other: an example is the definition of *COP* given by [10] which is completely different from the one given by [18].

The maximum reachable efficiency $\eta_{max}$ is calculated with the maximum $Q^-$, called $Q^-_{max}$, and, of course, the minimum $Q^+_{min}$.

The assumptions used to evaluate the **theoretical limits** of the energy efficiency are:

- Heat losses in the system are not taken into account.
- Sensible heat of materials and parts of the reactor are neglected.

- The energy released or absorbed by the reaction is approximated by the standard enthalpy of reaction.
- The equilibrium drop influence is neglected (see [18]).
- Only total hydration/dehydration processes are under investigation.

Given the previous assumptions, if the heat of condensation is not recovered and if the heat of evaporation is energy–free (Energy–free means that no additional energy is required for producing water vapor), the trivial efficiency is $\eta_{max} = 1$ (see Figure 7—$Q^{-}_{max} = Q^{+}_{min} = \Delta_r H^0$).

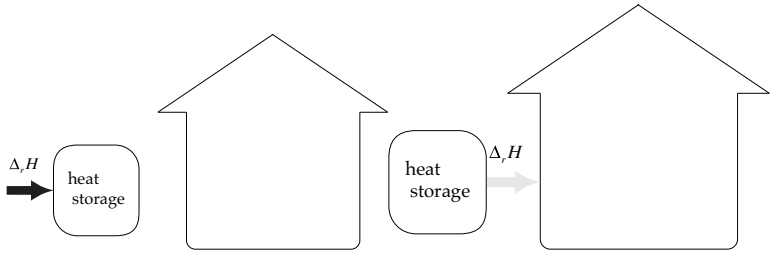


**Figure 7.** System integration: heat of condensation is not recovered, and heat of evaporation is energy–free: $\eta_{max} = 1$.

Considering the previous assumptions, if non-free heat of evaporation, the maximum efficiency becomes (see Figure 8):

$$\eta_{max} = \frac{Q^{-}_{max}}{Q^{+}_{min}} = \frac{\Delta_r H^0}{\Delta_r H^0 + Q_{evap}} = \frac{1}{1 + \frac{Q_{evap}}{\Delta_r H^0}} \tag{15}$$

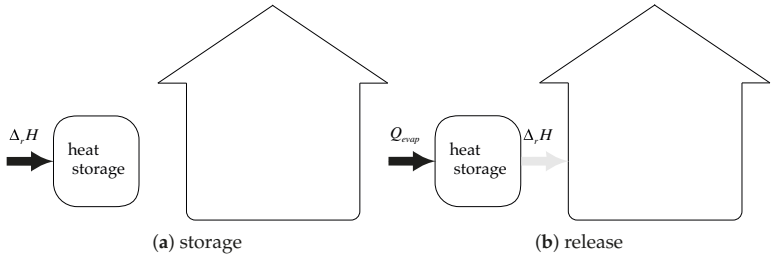


**Figure 8.** System integration: heat of condensation is not recovered and heat of evaporation is not free: $\eta_{max} = \frac{1}{1+\frac{Q_{evap}}{\Delta_r H^0}}$.

The quantity of energy required to evaporate liquid water per mole of salt is evaluated with:

$$Q_{evap} = \nu \times M_{H_2O} \times L_v \tag{16}$$

where $L_v$ is the water heat of vaporization in standard conditions taken as 2456 kJ kg$^{-1}$ and $M_{H_2O}$ the molar mass of water equal to 18 g mol$^{-1}$. Considering data from Table 1, and considering that $\Delta_r H^0/\nu$ is varying between 55.1 kJ mol$^{-1}$ and 67.8 kJ mol$^{-1}$, the ratio $Q_{evap}/\Delta_r H^0$ can be straightforwardly evaluated as:

$$0.65 \leq \frac{Q_{evap}}{\Delta_r H^0} \leq 0.80 \tag{17}$$

Introducing Equation (17) into Equation (15), the energy efficiency of the system becomes:

$$0.55 \leq \eta_{max} \leq 0.6 \tag{18}$$

The previous equations also show that energy required for evaporation is, at least, 65% **of the available energy of reaction**! And the maximum energy efficiency of the integrated system $\eta_{max}$ is 60% only!

Let us now consider the case with a total recover of condensation heat and energy–free heat of evaporation. Then, the energy efficiency becomes (see Figure 9):

$$\eta_{max} = \frac{Q^-_{max}}{Q^+_{min}} = \frac{\Delta_r H^0 + Q_{cond}}{\Delta_r H^0} = 1 + \frac{Q_{cond}}{\Delta_r H^0} \tag{19}$$

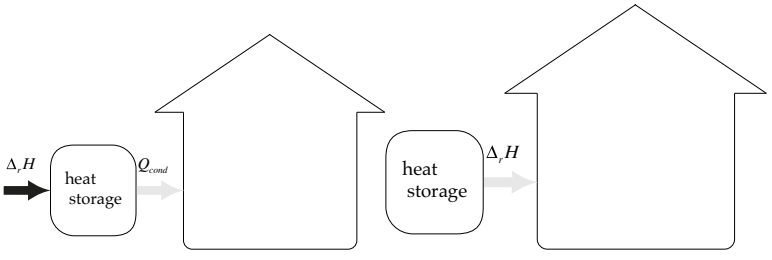


(**a**) storage (**b**) release

**Figure 9.** System integration: heat of condensation is recovered and heat of evaporation is energy–free: $\eta_{max} = 1 + \frac{Q_{cond}}{\Delta_r H^0}$.

The quantity of energy (per mole of salt) recoverable from condensation is evaluated by:

$$Q_{cond} = \nu \times M_{H_2O} \times L_v \tag{20}$$

Starting from Equation (19) and introducing Equation (20), the energy efficiency of the system becomes:

$$1.6 \leq \eta_{max} \leq 1.8 \tag{21}$$

The maximum theoretical energy efficiency of the system is about 1.8, whatever the salt! This conclusion is clearly in accordance with the results of [18] where the maximum value is 1.84. However, our study extends these results to the integration of an open system. Our study also highlights the necessity to work on the system integration as the conclusions are valid whatever the salt.

## 7. Conclusions

Chemical materials are available for heat storage in buildings with reaction temperatures in agreement with the available heat. For safety reasons, those materials are non-toxic and use water for reacting. From a selection of available data, the most promising material is magnesium sulphate with an energy density of 780 kWh $m^{-3}$.

From material to reactor, perfect reactor, the efficiency is 49 %, meaning that for magnesium sulphate, the maximum reactor prototype energy density would be 382 kWh $m^{-3}$. Of course, there still some development to realize to increase the ratio between perfect reactor and material energy densities. Another issue that is not under consideration presently in scientific literature, would be to pass from the lab scale prototype to large, or real, scale reactor.

Regarding data from the literature, the reaction enthalpy of one mole of water only varies between 55.1 kJ $mol^{-1}$ and 67.4 kJ $mol^{-1}$. Considering an open or closed single-stage system, the two main conclusions are:

- Energy required for evaporation of water is, at least, 65% of the available energy of reaction.
- For a perfect system, the maximum theoretical energy efficiency of the system is about 1.8.

Dealing with the integration of the system in a building, two main issues appear, related to the water vapor origin and the heat of condensation. If the water vapor is not energy-free and if the heat of condensation is not used, then the maximum efficiency is 65%. For a perfect magnesium sulphate reactor, the maximum energy density becomes 229 kJ $mol^{-1}$. It corresponds to 4 times water with a temperature difference about 50 °C. In that case, the difference is too low for magnesium sulphate to be competitive. However, if water vapor is energy-free and if the heat of condensation is recovered, then the maximum energy efficiency becomes 180 %. For a perfect magnesium sulphate reactor, the maximum energy density becomes 688 kJ $mol^{-1}$. It corresponds to 12 times water with a temperature difference about 50 °C. Such solution can definitely be competitive!
The previous conclusions do not depend on the adsorbent material considered. Then, a special attention must be paid on the system for:

- Developing water evaporation system "energy–free" or low–energy for the discharging phase.
- Developing or using water condensation recovery systems: examples of such recovery systems are the cascaded thermal battery [35,36] or the integration of a heat–pump.

Of course, these theoretical limits remain valid for the operating conditions given in this work and further studies must be carried to extend the conclusions to higher temperature storage. Moreover, numerical modeling is also under investigation to evaluate the potential improvement of the system integrated in the building.

**Author Contributions:** State of the art, F.K., K.J.; writing–original draft preparation, F.K.; writing–review and editing, K.J., F.K. All authors have read and agreed to the published version of the manuscript.

**Funding:** This project was funded by the DECARTH 2016 project ANR-16-CE22-0006-01 of the French National Research Agency.

**Conflicts of Interest:** The author declares no conflict of interest.

## Abbreviations

*List of Symbols*

| | | |
|---|---|---|
| $C$ | specific heat capacity | J $kg^{-1}$ $K^{-1}$ |
| $H$ | enthalpy | J |
| $L_v$ | vaporization heat of water | J $kg^{-1}$ |
| $P$ | pressure | Pa |
| $Q$ | heat energy per mole of salt | J$mol^{-1}$ |
| $R$ | gas constant | J $K^{-1}$ $mol^{-1}$ |
| $S$ | entropy | J |
| $T$ | temperature | K |
| $U$ | internal energy | J |
| $V$ | volume | $m^3$ |
| $W$ | work | J |

*Greek letters*

| | |
|---|---|
| $\nu$ | stoechiometric coefficient |
| $\eta$ | efficiency |
| $\xi$ | advancement of reaction |

*Subscript*

| | |
|---|---|
| $e$ | equilibrium |
| $evap$ | evaporation |
| $max$ | maximum |
| $min$ | minimum |
| $r$ | reaction |
| 0 | standard |

*Superscript*

| | |
|---|---|
| 0 | standard |
| $-$ | recovered energy |
| $+$ | supplied energy |

## References


1. Kuznik, F.; Johannes, K.; Obrecht, C. Chemisorption heat storage in buildings: State–of–the–art and outlook. *Energy Build.* **2015**, *106*, 183–191. [CrossRef]
2. Prieto, C.; Cooper, P.; Fernandez, A.I.; Cabeza, L. Review of technology: Thermochemical energy storage for concentrated solar power plants. *Renew. Sustain. Energy Rev.* **2016**, *60*, 909–929. [CrossRef]
3. Sole, A.; Martorell, I.; Cabeza, L. State of the art on gas–solid thermochemical energy storage systems and reactors for building applications. *Renew. Sustain. Energy Rev.* **2015**, *47*, 386–398. [CrossRef]
4. Cot-Gores, J.; Castell, A.; Cabeza, L. Thermochemical energy storage and conversion: A–state–of–the–art review of the experimental research under practical conditions. *Renew. Sustain. Energy Rev.* **2012**, *16*, 5207–5224. [CrossRef]
5. Andre, L.; Abanades, S.; Flamant, G. Screening of thermochemical systems based on solid-gas reversible reactions for high temperature solar thermal energy storage. *Renew. Sustain. Energy Rev.* **2016**, *64*, 703–715. [CrossRef]
6. Aydin, D.; Casey, S.P.; Riffat, S. The latest advancements on thermochemical heat storage systems. *Renew. Sustain. Energy Rev.* **2015**, *41*, 356–367. [CrossRef]
7. Cabeza, L.; Sole, A.; Barreneche, C. Review on sorption materials and technologies for heat pumps and thermal energy storage. *Renew. Energy* **2017**, *110*, 3–39. [CrossRef]
8. Kuznik, F. Chemisorption heat storage for solar low-energy buildings. In *Advances in Solar Heating and Cooling*; Wang, R.Z., Ge, T.S., Eds.; Woodhead Publishing: Cambridge, UK, 2016; pp. 467–487.
9. Dincer, I.; Rosen, M. *Thermal Energy Storage: Systems and Applications*; Wiley: Hoboken, NJ, USA, 2010; 620p.
10. Zondag, H.; Rikkert, B.; Smeding, S.; de Boer, R.; Bakker, M. Prototype thermochemical heat storage with open reactor system. *Appl. Energy* **2013**, *109*, 360–365. [CrossRef]
11. Fopah-Lele, A.; Rohde, C.; Neumann, K.; Tiejen, T.; Ronnebeck, T.; N'Tsoukpoe, K.E.; Osterl, T.; Opel, O.; Ruck, W.K. Lab-scale experiment of a closed thermochemical heat storage system including honeycomb heat exchanger. *Energy* **2016**, *114*, 225–238. [CrossRef]
12. Mauran, S.; Lahmidi, H.; Goetz, V. Solar heating and cooling by a thermochemical process. First experiments of a prototype storing 60 kW h by a solid/gas reaction. *Sol. Energy* **2008**, *82*, 623–636. [CrossRef]
13. De Jong, A.J.; van Vliet, L.; Hoegaerts, C.; Roel, S.M.; Cuypers, R. Thermochemical Heat Storage—From Reaction Storage Density to System Storage Density. *Energy Proc.* **2016**, *91*, 128–137. [CrossRef]
14. Michel, B.; Mazet, N.; Neveu, P. Experimental investigation of an open thermochemical process operating with a hydrate salt for thermal storage of solar energy: Local reactive bed evolution. *Appl. Energy* **2016**, *180*, 234–244. [CrossRef]
15. Michel, B.; Mazet, N.; Neveu, P. Experimental investigation of an innovative thermochemical process operating with a hydrate salt and moist air for thermal storage of solar energy: Global performance. *Appl. Energy* **2014**, *129*, 177–186. [CrossRef]
16. Richter, M.; Bouche, M.; Linder, M. Heat transformation based on CaCl2/H2O—Part A: Closed operation principle. *Appl. Therm. Eng.* **2016**, *102*, 615–621. [CrossRef]

17. Bouche, M.; Richter, M.; Linder, M. Heat transformation based on CaCl2/H2O—Part B: Open operation principle. *Appl. Therm. Eng.* **2016**, *102*, 641–647. [CrossRef]
18. Obermeier, J.; Muller, K.; Arlt, W. Thermodynamic analysis of chemical heat pumps. *Energy* **2015**, *88*, 489–496. [CrossRef]
19. N'Tsoukpoe, K.E.; Liu, H.; Le Pierres, N.; Luo, L. A review on long-term sorption solar energy storage. *Renew. Sustain. Energy Rev.* **2009**, *13*, 2385–2396. [CrossRef]
20. McNaught, A.D.; Wilkinson, A. *IUPAC Compendium of Chemical Terminology*, 2nd ed.; Wiley Blackwell: Hoboken, NJ, USA, 1997.
21. Valdivieso, F.; Bouineau, V.; Pijolat, M.; Soustelle, M. Kinetic study of the dehydration of lithium sulphate monohydrate. *Renew. Solid State Ionics* **1997**, *101–103*, 1299–1303. [CrossRef]
22. Bolis, V. Fundamentals in Adsorption at the Solid-Gas Interface. Concepts and Thermodynamics. In *Calorimetry and Thermal Methods in Catalysis*; Auroux, A., Ed.; Springer: Berlin/Heidelberg, Germany, 2013; pp. 3–50.
23. Gottfried, J.M. CO Oxidation Over Gold. Ph.D. Thesis, Freien Universitat Berlin, Berlin, Germany, 2003.
24. Grindstaff, W.K.; Fogel, N. Thermochemistry of cobalt(II) chloride hydrates. *J. Chem. Soc. Dalton Trans.* **1972**, 1476–1481. [CrossRef]
25. Mishra, S.K.; Kanungo, S.B. Thermal dehydration and decomposition of nickel chloride hydrate $NiCl_2 \cdot H_2O$. *J. Therm. Anal.* **1992**, *38*, 2417–2436. [CrossRef]
26. Ferchaud, C.J.; Zondag, H.A.; de Boer, R.; Rindt, C. Characterization of the sorption process in thermochemical materials for seasonal solar heat storage application. In Proceedings of the 12th International Conference on Energy Storage, Lleida, Spain, 16–18 May 2012.
27. N'Tsoukpoe, K.E.; Schmidt, T.; Rammelberger, H.U.; Watts, B.A.; Rick, W.K. A systematic multi–step screening of numerous salt hydrates for low temperature thermochemical energy storage. *Appl Energy* **2014**, *124*, 1–16. [CrossRef]
28. Molenda, M.; Stengler, J.; Linder, M. Reversible hydration behavior of CaCl2 at high H2O partial pressures for thermochemical energy storage. *Thermochim. Acta* **2013**, *560*, 76–81. [CrossRef]
29. Fopah-Lele, A.; Kuznik, F.; Rammelberger, H.U.; Schmidt, T.; Ruck, W.K. Thermal decomposition kinetic of salt hydrates for heat storage systems. *Appl. Energy* **2015**, *154*, 447–458. [CrossRef]
30. De Boer, R.; Haije, W.; Veldhuis, J. Determination of structural, thermodynamic and phase properties in the $Na_2S$–$H_2O$ system for application in a chemical heat pump. *Thermochim. Acta* **2002**, *395*, 3–19. [CrossRef]
31. Iammak, K.; Wongsuwan, W.; Kiatsiroroi, W. Investigation of Modular Chemical Energy Storage Performance. In Proceeding of the Joint International Conference on Sustainable Energy and Environment, Hua Hin, Thailand, 1–3 December 2004; pp. 504–507.
32. Michel, B.; Mazet, N.; Mauran, S.; Stitou, D. Thermochemical process for seasonal storage of solar energy: Characterization and modeling of a high density reactive bed. *Energy* **2012**, *47*, 553–563. [CrossRef]
33. Marias, F.; Tanguy, G.; Wyttenbach, J.; Rouge, S.; Papillon, P. Thermochemical storage: First results of pilot storage with moist air. In Proceedings of ISES 2011, Kassel, Germany, 28 August–2 September 2011.
34. Hongois, S.; Kuznik, F.; Steven, P.; Roux, J.J. Development and characterisation of a new MgSO4/zeolite composite for long-term thermal energy storage. *Sol. Energy Mater. Sol. Cells* **2011**, *95*, 1831–1837. [CrossRef]
35. Li, T.; Wu, S.; Yan, T.; X.U.; J.; Wang, R. A novel solid-gas thermochemical multilevel sorption thermal battery for cascaded solar thermal energy storage. *Appl. Energy* **2016**, *161*, 1–10. [CrossRef]
36. N'Tsoukpoe, K.E.; Mazet, N.; Neveu, P. The concept of cascade thermochemical storage based on multimaterial system for household applications. *Renew. Energy* **2016**, *129*, 138–149.


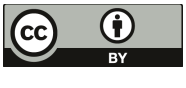

applied sciences

MDPI

Article

# Performance Analysis of a Solar DHW System with Adsorption Module Operating in Different World Locations

**Marco S. Fernandes [1,*], Vítor A. F. Costa [2], Gonçalo J. V. N. Brites [1], Adélio R. Gaspar [1] and José J. Costa [1]**

[1] ADAI-LAETA, Department of Mechanical Engineering, University of Coimbra, P-3030 788 Coimbra, Portugal; goncalo.brites@uc.pt (G.J.V.N.B.); adelio.gaspar@dem.uc.pt (A.R.G.); jose.costa@dem.uc.pt (J.J.C.)

[2] TEMA (Center for Mechanical Technology and Automation), Department of Mechanical Engineering, University of Aveiro, P-3810 193 Aveiro, Portugal; v.costa@ua.pt

* Correspondence: marco.fernandes@adai.pt; Tel.: +351-239-790-714; Fax: +351-239-790-701

Received: 18 November 2019; Accepted: 11 December 2019; Published: 13 December 2019

**Abstract:** A numerical study was conducted on the performance of a solar domestic hot water storage system with an adsorption module operating in seven different world locations. The base system was optimized for Portuguese conditions and, without changing the system itself and the water consumption profile, its performance was investigated by altering local installation and operating conditions and solar collector inclination angles. The overall dynamical model of the system was used for numerical simulations. The improved performance of the system was assessed by the reduction achieved on the annual energy consumption of a backup water heater when compared with a similar conventional energy storage system (without an adsorption module). The results showed that the best performances were obtained in locations where winter and summer are clearly defined, especially locations where winters are colder, and with solar collectors' inclination angles larger than the local latitude, except for locations with low latitudes, where solar collectors' inclination angles are not so relevant to the system performance. It was also discussed how the performance results must be carefully analyzed, as for low-latitude locations the absolute savings are in fact smaller even if their relative values are of the same order or even higher than for higher-latitude locations.

**Keywords:** solar DWH; adsorption; heat storage; energy efficiency; climate conditions; numerical simulation

## 1. Introduction

Currently, the main environmental challenges worldwide are to increase the share of renewable energy sources in final energy use and achieve an increase of energy efficiency in order to contribute to reducing greenhouse gas emissions. One of the most promising measures is to increase the utilization of solar energy. However, due to its intermittent nature, there is a need for thermal energy storage technologies in most of areas where solar energy is utilized [1,2]. This is especially relevant to domestic hot water (DHW) systems. Water heating is still a large share of the total energy consumption of households worldwide [3]. For example, it represents 19% of the total energy consumption of households in the United States [4] and 14.8% of the total energy consumption of households in the European Union [5]. Therefore, if this energy demand is fulfilled with the help of solar water heater systems, it will help to increase energy efficiency, decrease fossil fuels dependency and reduce greenhouse gas emissions. Actually, the energy efficiency in the water heating sector has increased by 25% worldwide since 2000, and it is estimated to increase by 43% until 2040 [6], for which developing more efficient solar thermal energy storage solutions that also increase the share of renewable heating systems is a necessity.

In general, thermal energy storage can be accomplished through sensible, latent, or thermochemical (e.g., sorption) processes. Compared with conventional sensible and latent thermal energy storage processes, adsorption can deal with the temporary thermal energy storage in an easier, more compact and efficient way, even for long periods, with high energy densities and low or even null heat losses. In addition, adsorption thermal energy storage systems are able to use a wide range of heat sources, e.g., solar thermal, biomass, geothermal, thermal surplus, or available waste heat. It is thus a promising alternative to conventional heat storage systems and also to integrating or partially or fully replacing heating from fossil fuels or electric systems [2,7–10]. This technology is still under development, since different issues need to be solved at both material and system levels, to become a feasible technology for commercial applications. However, adsorption heat storage is gaining more and more attention in the scientific community as an emerging technology; its viability has already been demonstrated, and different adsorption cycles have already been applied for thermal energy storage in several research works [1,8,11–15].

In this context, a new adsorption thermal energy storage system was presented and optimized in previous works [16–19], trying to reduce some limitations of conventional sensible DHW heat storage systems. It is especially appropriate for solar energy systems, where energy supply does not typically coincide with hot water demands and is not possible to control. The system combines the main features of the adsorption thermal energy storage with a conventional hot water storage tank. It is composed of a hot water tank, an adsorber (filled with silica gel) located inside the hot water tank, a condenser, and an evaporator. Water is the working fluid in the adsorption system. The adsorber stores the thermal energy received from the hot water in the storage tank (desorption heat) and releases it later to heat up the water in the tank (adsorption heat). The condensation of the operating fluid in the condenser releases heat into the storage tank, and the evaporation of the operating fluid in the evaporator extracts heat from the ambient.

This work aimed to evaluate the performance of the DHW storage system with an adsorption module, previously optimized for the Portuguese climate conditions, when operating in some representative locations around the world. It was thus an assessment on how a given product behaves in distinct world locations without further modifications of the system itself. However, the particular characteristics of each location were taken into consideration regarding the system's installation (solar collectors' inclination), the weather data, and the mains water temperature entering the system.

## 2. Materials and Methods

### *2.1. Description and Operation of the Adsorption Storage System*

The main purpose of the thermal energy storage system with an adsorption module is to take advantage of the adsorption process to store part of the thermal energy obtained from solar collectors in an effective and compact way. The thermal energy is firstly used to regenerate the adsorbent material (desorption) and retrieved later to heat up the water in the storage tank, when the previously desorbed working fluid is adsorbed by the adsorbent (adsorption). Additionally, the adsorption module works like a heat pump, capturing low-temperature heat from the surrounding ambient air and releasing it at higher temperatures to heat up the water in the storage tank. The considered system with the adsorption module has the following specificities: (i) the adsorber is immersed in the DHW tank; (ii) during the desorption phase, the cold intake water is preheated by the recovered condensation heat of the desorbed vapor; and (iii) during the evaporation phase, heat is captured from the surrounding ambient air. The system's main objective is to reduce the backup heating needs (usually electric heating) and likewise to reduce the nonrenewable energy consumption.

The system, presented in Figure 1, consists of a conventional hot water storage reservoir with an adsorber unit immersed inside. The adsorber is filled with an adsorbent material and is connected to a condenser. This heat exchanger is immersed in a secondary water tank to preheat the intake of cold mains water and is connected to an evaporator exposed to the ambient air. These main components

(adsorber, condenser, and evaporator) form a closed airtight circuit operating under moderate vacuum conditions. A first valve (V1 in Figure 1) separates the adsorber unit from the condenser, a second valve (V2 in Figure 1) separates the condenser from the evaporator, and a third valve (V3 in Figure 1) separates the evaporator from the adsorber. A backup electric heater is used at the DHW reservoir outlet to heat up the water, when the temperature setpoint for hot water consumption is not reached in the storage tank. The adsorption working pair in the system is silica gel/water.

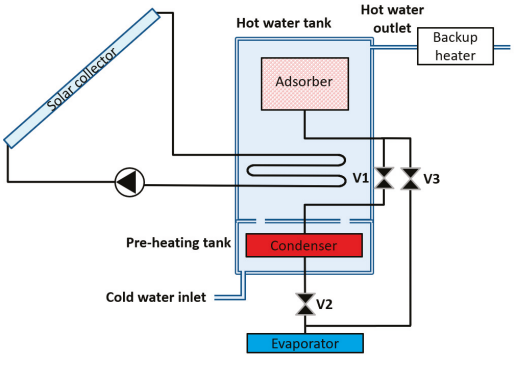


**Figure 1.** Solar thermal domestic hot water system with an adsorption module.

The adsorber, filled with silica gel, is horizontally immersed in the top section of the DHW tank, to take advantage of the thermal stratification effect. The desorbed water vapor is condensed in the condenser during the desorption phase. The condenser is immersed in the secondary water reservoir, where the cold mains water is preheated before entering the main storage tank. The evaporator receives and stores the condensed water coming from the condenser. This water is later vaporized at low pressure, during the adsorption phase, extracting low-temperature heat from the surrounding ambient air (similarly to what happens in a heat pump).

The detailed description and operation of the system can be found in Reference [16], while a study regarding its optimization is presented in Reference [18]. The three phases of the system's operation are briefly described as follows:

(a) Charging

At the beginning of the charging phase, all valves remain closed, and heat (solar energy) enters the storage tank. Afterward, when the water temperature in the main tank surpasses a specified value, V1 opens (this setpoint prevents the solar heat input to be used for desorption, while the water in the main reservoir is still not warm enough). The adsorber receives the thermal energy from the hot water in the main tank, and the water vapor is released from the silica gel bed (desorption). The desorbed vapor is subsequently condensed in the condenser, and the resultant condensation heat is recovered to preheat the cold water in the secondary tank.

When the charging phase ends, V1 closes, while V2 allows, before it closes, the drainage of the condensate water to the evaporator, where it is stored until the discharge phase starts.

(b) Storage

After the adsorber is energy-charged (after desorption) and the condensate water is in the evaporator, all valves remain closed. Hence, the adsorption process does not take place, since the silica gel (in the adsorber) and the water (in the evaporator) are kept separate. Therefore, the adsorption module remains charged as an adsorption potential with no energy losses, even for long periods.

(c) Discharging

Once the adsorber is energy-charged and the evaporator–adsorber connection is allowed (by opening V3, when the water temperature of the main tank drops below a specified value—V3 setpoint), it promotes the adsorption of the water vapor produced in the evaporator at low temperature and low pressure. While adsorbing this vapor and as long as the water in the main tank is colder than the adsorber, the adsorption heat is released from the adsorber to heat up the water in the main tank. During the evaporation phase, low-temperature heat is extracted from the ambient air. Afterwards, when the adsorption process ends, all valves are closed again, and the adsorption module is ready to initiate a new energy-charging phase.

### *2.2. Dynamic Modeling of the DHW Adsorption System*

The solar thermal system was modeled using TRNSYS® 17 (Figure 2), a type of simulation software with a modular structure, where the system is divided into a set of components (types), modeled using mathematical equations programmed in FORTRAN [20]. Since TRNSYS® does not present any components to model/simulate the adsorption process, the model for the adsorption module (adsorber, condenser, evaporator, and preheating water tank) was elaborated in MATLAB®, and the original TRNSYS® hot water storage reservoir was altered in order to integrate it, taking advantage of the interaction capabilities between both programs.

The detailed description of the dynamic model of the adsorption storage module and its interaction with the solar thermal system are presented in References [16,17].

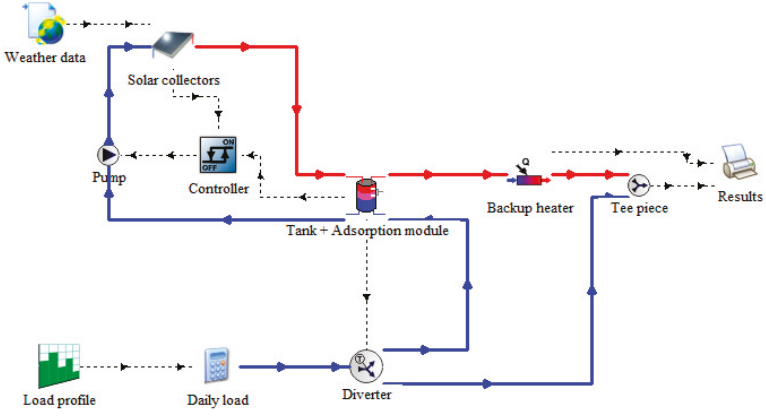


**Figure 2.** TRNSYS® diagram of a solar thermal system with an adsorption module. Solid lines represent water flow, while dashed lines represent information flow.

### *2.3. Methodology*

The operation of a system designed and optimized for the Portuguese conditions was simulated for different world locations. Seven capital cities, each taken as representative of different continents in both the Northern and Southern Hemispheres, were considered: Beijing, China (39.9° N, 116.4° E), Baltimore (Baltimore was selected instead of Washington D.C., since there were no available climate data for the latter. Therefore, the data from the closest main city were used in this study.), USA (39.3° N, 76.6° W), Lisbon, Portugal (38.7° N, 9.1° W), New Delhi, India (28.6° N, 77.2° E), Brasília, Brazil (15.8° S, 47.9° W), Cape Town, South Africa (33.9° S, 18.4° E), and Canberra, Australia (35.3° S, 149.1° E). These locations were chosen, since they represent the capital cities of important countries located in different continents and hemispheres, where the system's operation can be of interest. On the other hand, most of these countries also have high energy savings concerns and represent high potential of worldwide science readers interested in exploring and testing the present system. The weather data for these locations were downloaded from the EnergyPlus website [21]. For each location, the effect of the solar

collectors' inclination was also investigated, considering a variation of ±10° in relation to the location's latitude, with steps of 5°, i.e., analyzing 5 different collectors' slopes per location.

The adsorption system's performance was evaluated by the difference between the yearly energy consumption of the backup water heater using a conventional energy storage system (i.e., without an adsorption module) and that using a system with an adsorption module, which is written as:

$$Q_{saving} = Q_{backup,conv,year} - Q_{backup,ads,year}, \quad (1)$$

where $Q_{saving}$ is the annual backup energy saving, i.e., the annual adsorption system's performance. $Q_{backup,conv,year}$ is the yearly energy consumption of the backup water heater using a conventional energy storage system, and $Q_{backup,ads,year}$ represents the yearly energy consumption of the backup water heater using a system with the adsorption module.

The main parameters considered in this study are presented in Table 1 and Figure 3. The adsorber, the condenser and evaporator dimensions, and the valves' setpoints corresponded to its optimal configuration for Portuguese conditions, defined in Reference [18]. These parameters were similar for all the assessed locations. On the other hand, the mains water temperature entering the system varied according to the weather data for each location.

The dataset with the results of the solar DHW system with adsorption module performances operating in the seven world locations and the respective climate data is publicly available online (see Supplementary Materials, hosted at Figshare [22]).

**Table 1.** Parameters considered in the study.

| Parameter | Value |
|---|---|
| Simulation time step | 300 s |
| Simulation period | 1 year |
| Main tank volume | 250 L |
| Main tank height | 0.8 m |
| Preheating tank volume | 62.5 L |
| Solar heat exchanger length | 10.1 m |
| Solar heat exchanger surface area | 0.805 $m^2$ |
| Consumption setpoint | 45 °C |
| Pump mass flow rate | 186.2 kg/h |
| Solar collector area | 3.68 $m^2$ |
| Solar collector circuit upper thermostat dead band | 6 °C |
| Solar collector circuit lower thermostat dead band | 2 °C |
| Adsorption module components material | Copper |
| Silica gel type | A |

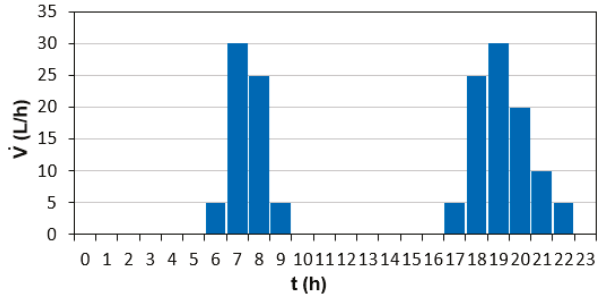


**Figure 3.** Hourly water consumption profile considered in the study [23].

## 3. Results and Discussion

Figure 4 presents a comparison between the annual energy consumption of the backup water heater in a conventional DHW solar system and that in a DHW solar system with an adsorption module for five solar collector slopes in the seven assessed locations. The locations were sorted in descending order of latitude. For each collector inclination, the annual backup energy saving ($Q_{saving}$) is presented on top of the respective bars in Figure 4, in both absolute (MJ) and percentual values. It should be noted that the scales of the ordinates are not the same for all the locations.

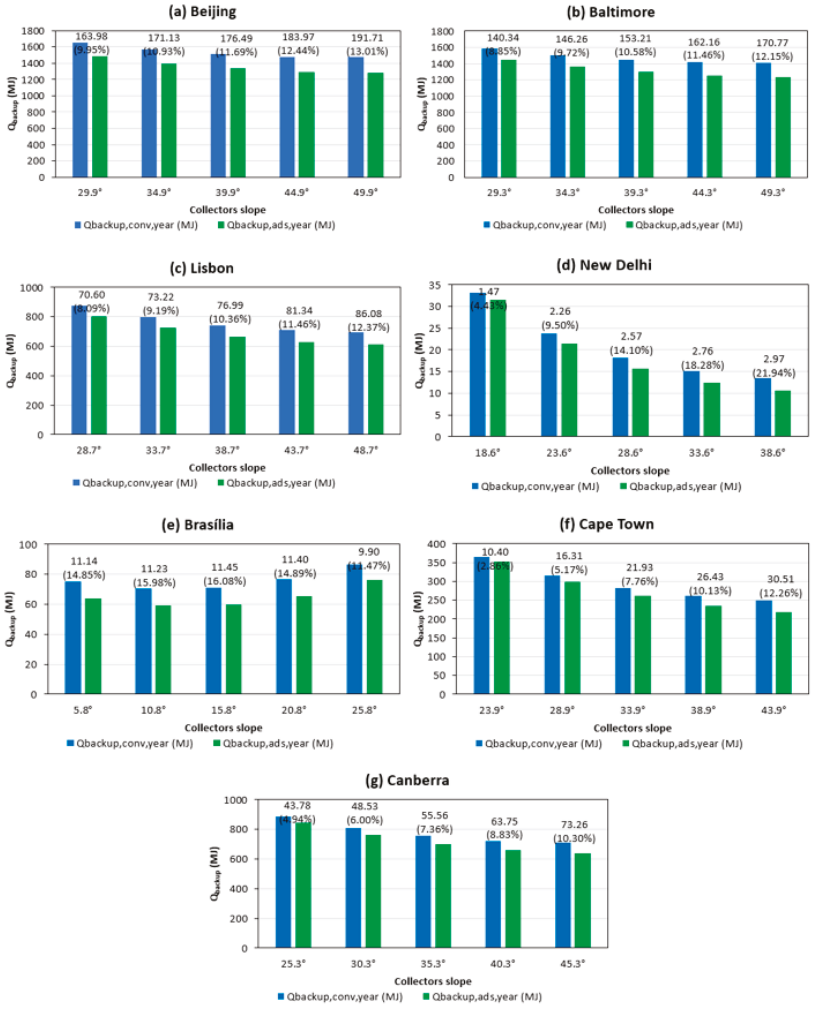


**Figure 4.** Comparison of yearly energy consumption of the backup water heater ($Q_{backup}$) using a conventional DHW solar system (blue bars) and that using a DHW solar system with an adsorption module (green bars) for different solar collector slopes in the seven assessed locations: (**a**) Beijing; (**b**) Baltimore; (**c**) Lisbon; (**d**) New Delhi; (**e**) Brasília; (**f**) Cape Town; (**g**) Canberra. The annual backup energy saving $Q_{saving}$ is presented on top of the bars in both absolute (MJ) and percentual (%) values (taking $Q_{backup,conv,year}$ as a reference).

A similar evolution is observable in most of the locations: higher collector slopes lead to lower energy consumptions for both the conventional system and the one with an adsorption module and result in higher energy savings ($Q_{saving}$). Therefore, the best results were obtained for large solar collector inclinations, thus favoring the system's operation during winter, when the heating needs are higher. The exception is Brasília (see Figure 4e), where this behavior was only noticed until the collector slope was increased to the intermediate level and was then inverted with further increase of the collector slope. This seems to be related with Brasília's latitude—15.8° S, which is lower than that of the remaining locations and between the Tropics (±23.5°). There, the solar zenith angle is always high, leading to higher solar radiation throughout the year (see Figure A1 in Appendix A). Therefore, there is little gain by varying the solar collectors' slope, as opposed to what happens for locations at higher latitudes (the remaining assessed locations), where the solar zenith angle is considerably lower in winter.

It is noticeable that at the warmer locations (New Delhi, Brasília, and Cape Town), despite the fact that the percentual energy savings are of the same order of magnitude, the absolute values of $Q_{saving}$ are much lower than in the remaining locations. Therefore, considering a similar investment cost for the adsorption system, there seems to be little advantage in installing such a system at these warmer locations, since the effective energy savings are much lower, within the corresponding massive payback periods.

The yearly solar radiation available at different locations and the corresponding minimum values of $Q_{backup}$ (with and without the adsorption module) and maximum values of $Q_{saving}$ are displayed in Figure 5. The $Q_{backup}$ and $Q_{saving}$ values can present significant differences for locations at similar latitudes: these values are clearly smaller in Lisbon in relation to those in other locations at similar latitudes—Beijing and Baltimore. This is due to the solar radiation availability in Lisbon (5880 MJ/year/m$^2$ in the horizontal plane), which is higher than in the other locations—5025 MJ/year/m$^2$ in Beijing and 5358 MJ/year/m$^2$ in Baltimore—, thus leading to lowering backup energy consumptions. Accordingly, locations with less available solar radiation tend to present higher $Q_{backup}$ and $Q_{saving}$ values, i.e., the system with an adsorption module operates with higher performance in these locations. This renders a very strong Pearson correlation coefficient ($\rho$) of −0.94 between the maximum absolute value of $Q_{saving}$ ($Q_{saving,max}$) and the available horizontal solar radiation (Table 2). The exception to this trend is Brasília, seemingly due to its low latitude, with similar solar radiations in the horizontal plane and in a plane with an inclination equal to the location's latitude, and a constant mains water temperature throughout the year (see Figure A1 in Appendix A).

**Table 2.** Pearson correlation coefficient ($\rho$) between the maximum absolute value of $Q_{saving}$ ($Q_{saving,max}$) and different locations and climates parameters.

| Parameter | $\rho$ |
|---|---|
| Latitude | 0.73 |
| Horizontal solar radiation | −0.94 |
| Solar radiation in a plane with an inclination equal to a location's latitude | −0.85 |
| $T_{min,year}$ | −0.89 |
| $\Delta T_{year}$ | 0.81 |

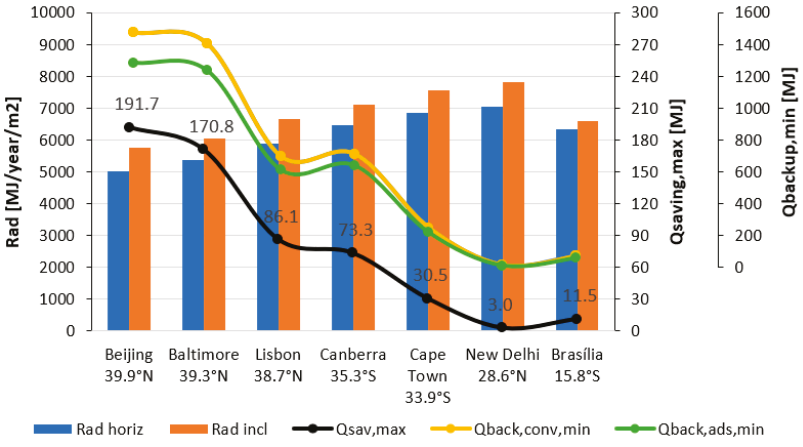


**Figure 5.** Yearly solar radiation values for both the conventional and adsorption systems, with the corresponding maximum values of $Q_{saving}$ presented for each location.

Overall, the system with an adsorption module presents higher performances in locations where winter and summer are clearly defined, and especially in locations, where winters are colder (higher latitudes), like Beijing and Baltimore and, in a smaller scale, Lisbon and Canberra, as can be seen in Figures 4, 5 and A1 (Appendix A). Additionally, the solar collectors of the system operating at these high latitudes must be oriented with inclinations higher than local latitudes, in order to present the highest performance. In other words, the system's performance is lower for lower latitudes and tends to increase for higher latitudes—locations with a low minimum annual temperature, $T_{min,year}$, and a large yearly temperature amplitude, $\Delta T_{year}$. This is noticeable given the strong ρ coefficients between $Q_{saving,max}$ and (a) the latitude (0.73, which indicates a better performance for higher latitudes), (b) $T_{min,year}$ (−0.89, which represents a better performance for lower minimum yearly temperatures), and (c) $\Delta T_{year}$ (0.81, pointing to a better performance for higher annual temperature amplitudes), as presented in Table 2.

Additionally, a detailed yearly evolution of the best $Q_{saving}$ for each location (corresponding to the best solar collector slope) is presented in Figure A2 (Appendix A). These results allow one to observe when and in which way the system with an adsorption module is more or less effective than its conventional counterpart. It can be seen that, for locations at higher latitudes, $Q_{saving}$ tends to increase gradually throughout the year, thus leading to an advantage over the conventional system during all, or at least most of, the year and resulting in higher annual (final) values. In contrast, the rising evolution of $Q_{saving}$ is much less distinct for locations at lower latitudes, sometimes adding up only during limited periods/seasons, thus leading to lower annual energy savings. In the case of New Delhi, the fact that it presents the highest yearly solar radiation (both in the horizontal and inclined planes), combined with a higher mains water inlet temperature (see Figure A1 in Appendix A), leads to a situation for which the proposed system is not an advantage: very low $Q_{backup}$ and almost null $Q_{saving}$. On the other hand, in Brasília, the mains water temperature is not so high, which combined with median solar radiation values leads to a more distinct evolution of $Q_{saving}$, especially in the periods of decreasing solar radiation (Figure A2 in Appendix A) and thus to a higher annual $Q_{saving}$ than in the case of New Delhi.

It is also noticeable that in the locations where the system with an adsorption module is more effective (i.e., all the locations except New Delhi and Brasília), $Q_{saving}$ tends to rise more distinctively during winter. The exception is Beijing, where $Q_{saving}$ adds up steadily throughout the year, given the lowest yearly solar radiation and the comparatively lower inlet temperature of the mains water (see Figure A1 in Appendix A). Compared to Beijing, Baltimore presents similar ambient and mains

water temperature evolutions and only slightly higher solar radiation values. However, the fact that the solar radiation is higher during the summer months leads to a lesser difference between $Q_{backup,conv}$ and $Q_{backup,ads}$, thus resulting in a less prominent $Q_{saving}$ evolution during that period. The evolution for Lisbon is identical to that in Baltimore (Figure A2 in Appendix A), except for the lower $Q_{saving}$ values at each timestep (and thus the resultant annual savings—170.8 MJ in Baltimore versus 86.1 MJ in Lisbon), since the solar radiation and mains water temperature values tend to be higher in the Portugal's capital throughout the year. On the other hand, the temperatures and the solar radiation evolutions are very similar between Cape Town and Canberra (Figure A1 in Appendix A); however, the solar radiation is slightly higher in the summer months in Cape Town (especially between November and February), and the mains water temperature is also higher. This leads to a higher yearly solar radiation (Figure 5) and a less prominent (or even nonexistent) $Q_{saving}$ evolution during the summer period (Figure A2 in Appendix A), which accounts for a smaller annual value of $Q_{saving}$—30.5 MJ in Cape Town compared to that of 73.3 MJ in Canberra.

In order to further improve the system performance in the colder regions, where the energy savings are higher, one would need to modify the system configuration (which is out of the scope of the present study). In this regard, considering the parameters listed in Table 1, the system efficiency would possibly improve by increasing the solar collector area, since more solar energy would be gathered and stored during the periods with higher availability of solar radiation. However, additional care must be taken, since the adsorption module dimensions would probably need to follow this increment to be able to store the thermal energy surplus. This could also lead to the need of increasing both tanks' volumes, in order to fit the adsorption module. Therefore, this assessment may not be straightforward as it would seem to be, and further studies are required to properly analyze this effect.

## 4. Conclusions

The inclusion of an adsorption module into a solar DWH system is an effective way to improve its performance. Although such systems are usually developed and optimized to operate under certain specific conditions, they can effectively operate in different locations, provided that the installation conditions are suitably adapted. In this case, the easiest installation parameter that can be changed is the solar collector's inclination angle. Thus, the best solar collector's inclination angle for each location and how the system performs when operating under each location particular conditions remain to be determined.

A solar DWH system previously optimized to operate in the Portuguese conditions was analyzed when installed and operated in seven different locations around the world, representative of the locations with similar latitudes and climatic conditions, and its performance was evaluated by numerical simulation. For each particular location, the best solar collector's inclination was assessed.

The results indicated that the best solar collector's inclination angle is not the local latitude and that some deviation must be considered for better performances. It was observed that, in general, the best performances were obtained for the solar collector's inclination angles larger than the local latitude. This favors the system's operation under winter conditions, when heating needs are higher. However, for low latitudes, the solar collector's inclination angle deviation relative to the latitude is not so relevant. Locations with less available solar radiation require higher yearly energy consumptions of the backup water heater, but present also higher $Q_{saving}$, thus indicating that the system with an adsorption module operates with a higher performance there.

It should also be retained that, for the warmer locations with low latitudes, care must be taken when assessing the system's performance improvement associated to the use of the adsorption module only in terms of the percentual increase of $Q_{saving}$. This percentual increase can be relatively high for these locations, even if the absolute value of this reduction is in fact low. However, it is the absolute value of the obtained energy consumption reduction that is relevant to investment decisions.

These results allow for a deeper understanding on the system's performance under different local installation and operating conditions by considering a limited number of representative locations.

The results can thus serve as a starting point for further studies aiming to extend this work to other locations, in order to statistically assess the system's performance throughout the world. In this line, if the system configuration is altered (as opposed to the present assumption of "as is" system), further studies are required to properly evaluate the optimal system configuration for each location.

**Supplementary Materials:** The performance dataset of a solar DHW system with an adsorption module operating in seven world locations and respective climate data are available online at URL https://doi.org/10.6084/m9.figshare.10048961, hosted at Figshare [22].

**Author Contributions:** Conceptualization, V.A.F.C., M.S.F., J.J.C., and A.R.G.; methodology, M.S.F. and G.J.V.N.B.; software, M.S.F.; formal analysis, M.S.F. and G.J.V.N.B.; investigation, M.S.F.; writing of the original draft preparation, M.S.F.; writing of review and editing, M.S.F., V.A.F.C., J.J.C., A.R.G., and G.J.V.N.B.; visualization, M.S.F.; supervision, V.A.F.C.; project administration, V.A.F.C., J.J.C., and A.R.G.; funding acquisition, A.R.G. and V.A.F.C.

**Funding:** This research work was funded by the Portuguese Foundation for Science and Technology (FCT) and by the European Regional Development Fund (FEDER) through COMPETE 2020—Operational Program for Competitiveness and Internationalization (POCI) in the framework of the research project Ren4EEnIEQ (grant numbers: PTDC/EMS-ENE/3238/2014, POCI-01-0145-FEDER-016760, and LISBOA-01-0145-FEDER-016760). Vítor A.F. Costa acknowledges the FCT for the financial support provided through the projects (grant numbers: UID/EMS/00481/2013-FCT and CENTRO-01-0145-FEDER-022083).


**Conflicts of Interest:** The authors declare no conflicts of interest.

## Appendix A

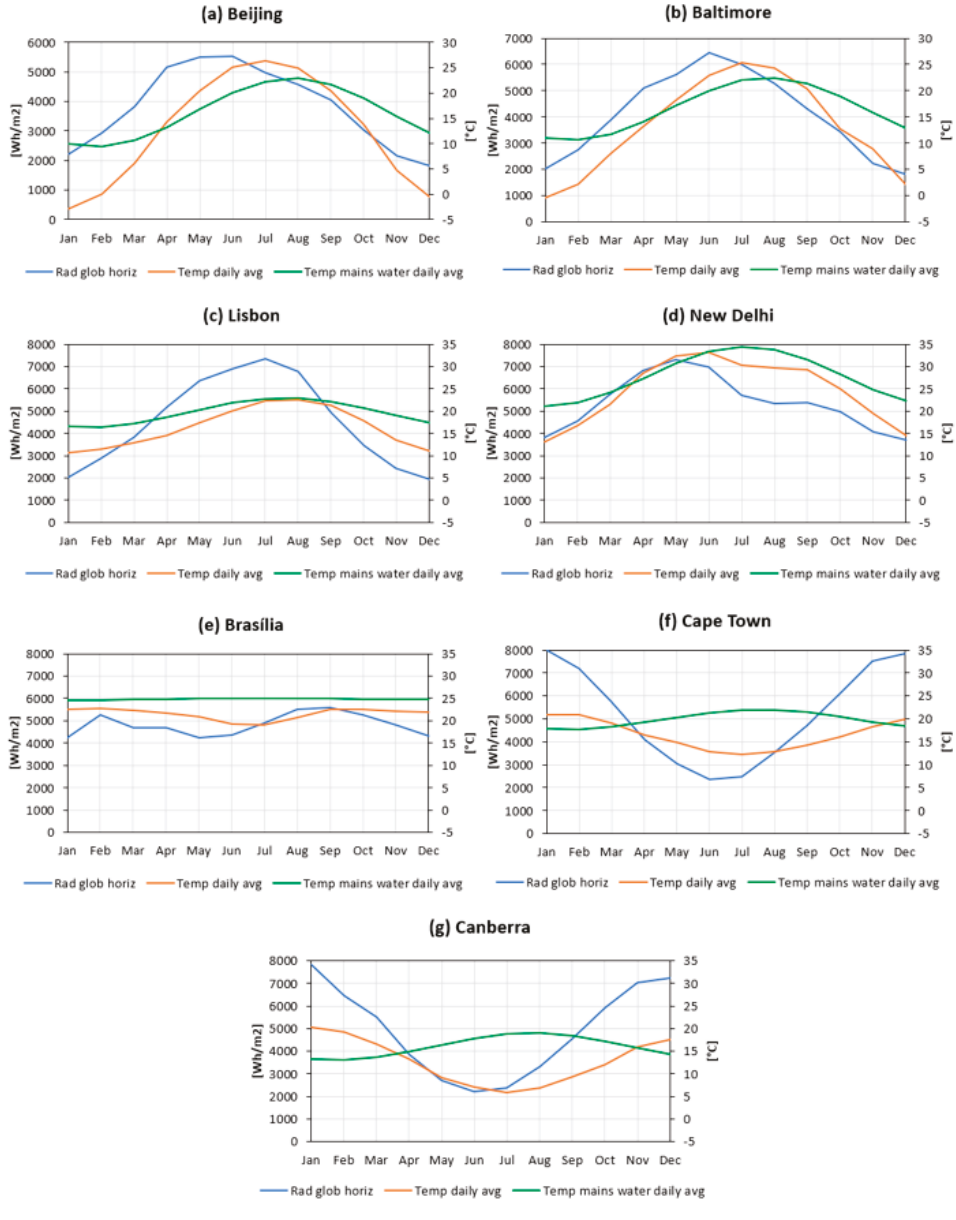


**Figure A1.** Evolutions of the average global horizontal solar radiation, the average daily ambient temperature, and the average daily mains water temperature throughout the year at the seven assessed locations: (**a**) Beijing; (**b**) Baltimore; (**c**) Lisbon; (**d**) New Delhi; (**e**) Brasília; (**f**) Cape Town; (**g**) Canberra.

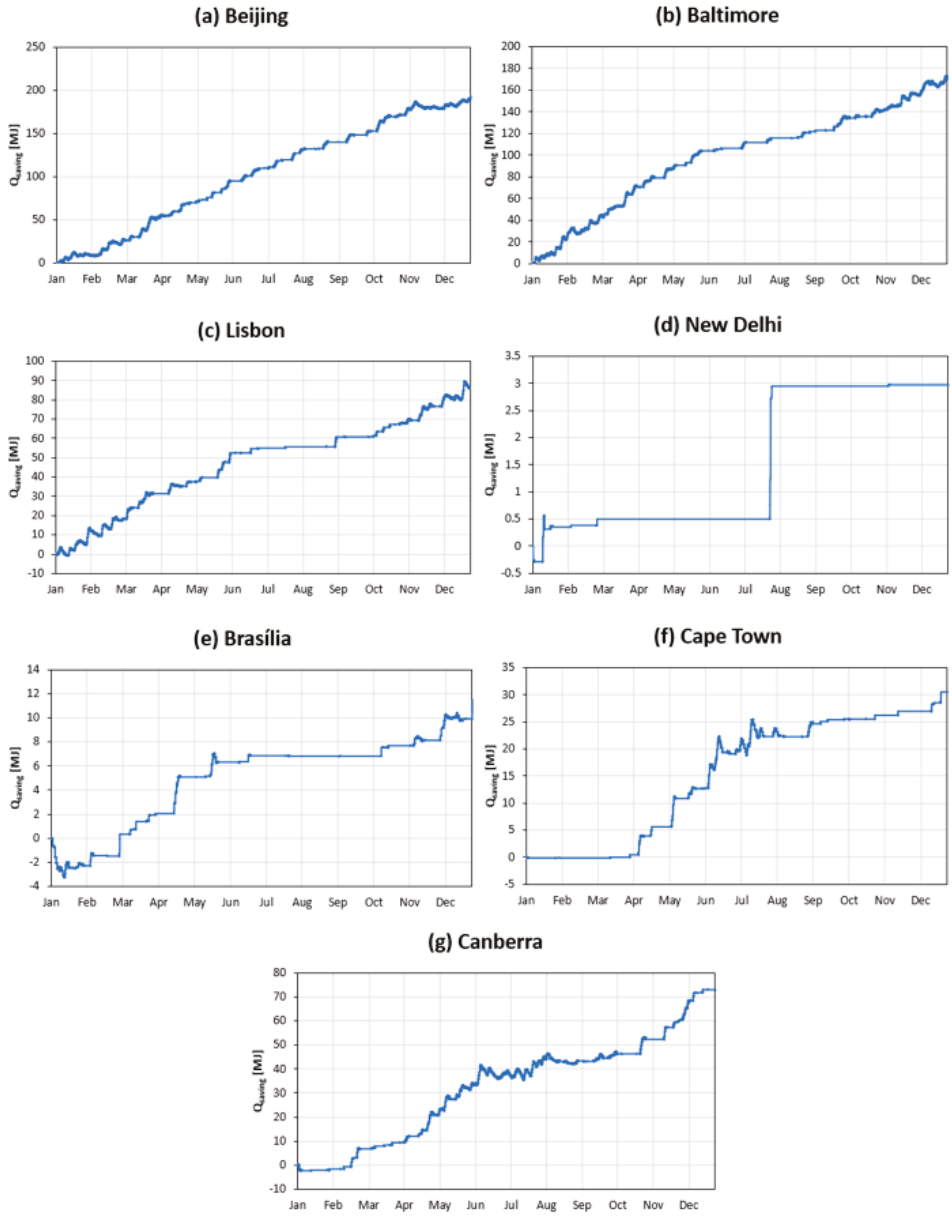


**Figure A2.** Evolutions of the best annual $Q_{saving}$ throughout the year for the locations considered: (**a**) Beijing; (**b**) Baltimore; (**c**) Lisbon; (**d**) New Delhi; (**e**) Brasília; (**f**) Cape Town; (**g**) Canberra.

## References

1. Krese, G.; Koželj, R.; Butala, V.; Stritih, U. Thermochemical seasonal solar energy storage for heating and cooling of buildings. *Energy Build.* **2018**, *164*, 239–253. [CrossRef]
2. Alva, G.; Liu, L.; Huang, X.; Fang, G. Thermal energy storage materials and systems for solar energy applications. *Renew. Sustain. Energy Rev.* **2017**, *68*, 693–706. [CrossRef]

3. Gautam, A.; Chamoli, S.; Kumar, A.; Singh, S. A review on technical improvements, economic feasibility and world scenario of solar water heating system. *Renew. Sustain. Energy Rev.* **2017**, *68*, 541–562. [CrossRef]
4. EIA—U.S. Energy Information Administration. Use of Energy Explained. Energy Use in Homes. Available online: https://www.eia.gov/energyexplained/use-of-energy/homes.php (accessed on 24 October 2019).
5. Eurostat—Statistics Explained. Energy Consumption in Households. Available online: https://ec.europa.eu/eurostat/statistics-explained/index.php/Energy_consumption_in_households (accessed on 24 October 2019).
6. IEA. Energy Efficiency: Buildings. Available online: https://www.iea.org/topics/energyefficiency/buildings/ (accessed on 24 October 2019).
7. Gordeeva, L.G.; Aristov, Y.I. Adsorptive heat storage and amplification: New cycles and adsorbents. *Energy* **2019**, 440–453. [CrossRef]
8. Fernandes, M.S.; Brites, G.J.V.N.; Costa, J.J.; Gaspar, A.R.; Costa, V.A.F. Review and future trends of solar adsorption refrigeration systems. *Renew. Sustain. Energy Rev.* **2014**, *39*, 102–123. [CrossRef]
9. Xu, J.; Wang, R.Z.; Li, Y. A review of available technologies for seasonal thermal energy storage. *Sol. Energy* **2014**, *103*, 610–638. [CrossRef]
10. Aydin, D.; Casey, S.P.; Riffat, S. The latest advancements on thermochemical heat storage systems. *Renew. Sustain. Energy Rev.* **2015**, *41*, 356–367. [CrossRef]
11. Palomba, V.; Frazzica, A. Recent advancements in sorption technology for solar thermal energy storage applications. *Sol. Energy* **2019**, *192*, 69–105. [CrossRef]
12. Fumey, B.; Weber, R.; Baldini, L. Sorption based long-term thermal energy storage—Process classification and analysis of performance limitations: A review. *Renew. Sustain. Energy Rev.* **2019**, *111*, 57–74. [CrossRef]
13. Sarbu, I.; Sebarchievici, C. A Comprehensive Review of Thermal Energy Storage. *Sustainability* **2018**, *10*, 191. [CrossRef]
14. Kuznik, F.; Johannes, K.; Obrecht, C.; David, D. A review on recent developments in physisorption thermal energy storage for building applications. *Renew. Sustain. Energy Rev.* **2018**, *94*, 576–586. [CrossRef]
15. Lefebvre, D.; Tezel, F.H. A review of energy storage technologies with a focus on adsorption thermal energy storage processes for heating applications. *Renew. Sustain. Energy Rev.* **2017**, *67*, 116–125. [CrossRef]
16. Fernandes, M.S.; Brites, G.J.V.N.; Costa, J.J.; Gaspar, A.R.; Costa, V.A.F. A thermal energy storage system provided with an adsorption module—Dynamic modeling and viability study. *Energy Convers. Manag.* **2016**, *126*, 548–560. [CrossRef]
17. Fernandes, M.S.; Brites, G.J.V.N.; Costa, J.J.; Gaspar, A.R.; Costa, V.A.F. Modeling and parametric analysis of an adsorber unit for thermal energy storage. *Energy* **2016**, *102*, 83–94. [CrossRef]
18. Fernandes, M.S.; Gaspar, A.R.; Costa, V.A.F.; Costa, J.J.; Brites, G.J.V.N. Optimization of a thermal energy storage system provided with an adsorption module—A GenOpt application in a TRNSYS/MATLAB model. *Energy Convers. Manag.* **2018**, *162*, 90–97. [CrossRef]
19. Fernandes, M.S.; Brites, G.J.V.N.; Costa, J.J.; Gaspar, A.R.; Costa, V.A.F. Numerical recipes for successfully modeling the phase transitions in thermal energy storage adsorption systems. *Energy Storage* **2019**, 1–10. [CrossRef]
20. Solar Energy Laboratory. Mathematical Reference. In *TRNSYS 17—A Transient System Simulation Program*; University of Wisconsin—Madison: Madison, WI, USA, 2012; Volume 4.
21. EnergyPlus. Available online: https://energyplus.net (accessed on 24 October 2019).
22. Fernandes, M.S. Dataset of a Solar DHW System with Adsorption Module Performance Operating in Seven World Locations. Available online: https://doi.org/10.6084/m9.figshare.10048961 (accessed on 18 November 2019).
23. LNEG—Laboratório Nacional de Energia e Geologia. SolTerm—Análise de desempenho de sistemas solares. Version 5.0. Available online: https://www.lneg.pt/iedt/projectos/370/ (accessed on 18 November 2019).


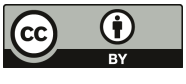

MDPI
St. Alban-Anlage 66
4052 Basel
Switzerland
Tel. +41 61 683 77 34
Fax +41 61 302 89 18
www.mdpi.com

*Applied Sciences* Editorial Office
E-mail: applsci@mdpi.com
www.mdpi.com/journal/applsci

MDPI
St. Alban-Anlage 66
4052 Basel
Switzerland

Tel: +41 61 683 77 34
Fax: +41 61 302 89 18

www.mdpi.com


ISBN 978-3-0365-1374-4